THE HYDRODYNAMIC FORCES AND THE HIGH FREQUENCY NOISE RESULTING FROM CAVITATION ON UNDERWATER BODIES

Thesis

by

James W. Daily

In Partial Fulfilment of the Requirements for
the Degree of Doctor of Philosophy

California Institute of Technology
Pasadena, California

1945

INDEX

ABSTRACT

Water Tunnel measurements were made of the hydrodynamic forces and moments, and of the high frequency noise resulting from cavitation on underwater bodies. All stages of cavitation from incipient to the full cavity were covered by the investigations.

The main findings of the force measurements are:

1. There is no sudden increase in drag with inception of cavitation. The sharp rise occurs only after the normal flow pattern is completely altered by an appreciable amount of visible cavitation.
2. A qualitative comparison of cavitation and separation indicates that they have the same basic effect on the flow in the boundary layer, and hence on the skin friction drag. For blunt bodies with severe separation for noncavitating conditions, the first appearance of cavitation does not immediately alter the flow pattern nor the drag.
3. Cavity drag measurements agree closely with values calculated from measured pressure distributions and for a given value of the cavitation parameter, K, are proportional to the bubble size relative to the diameter of the body.
4. Cavity cross force and moment depend on the cavity shape, and hence on the shape of the body at the point where cavity separation occurs. With spherical tipped noses so proportioned that the cavity separates on the spherical segment, not only at zero but at the maximum yaw, the cross force is zero independent of yaw, and the moment is caused by the drag only. Other shapes produce asymmetrical cavities and definite cross forces and moments.
5. With complete projectiles the conditions for cavity flow with tail sticking through the side of the cavity are reproduced. A low cross force with a zero or stabilizing moment is obtained.

Measurements of the sound emitted in the 20 to 100 KC frequency range with the beginning and growth of cavitation show:

1. With appearance of the slightest trace of cavitation, the acoustic pressure increases to several times the value of the background noise.
2. The maximum noise is measured when the zone of cavitation is limited to a very narrow band of small bubbles. With further growth the measured sound drops off.
3. The main source of sound is in the region of the trailing edge of the cavitation zone where the vapor bubbles are collapsing. If, as at advanced stages, the vapor bubbles are entrained and swept downstream before collapsing, the noise level drops.

ACKNOWLEDGEMENTS

The experiments described in this thesis were performed in the High Speed Water Tunnel at the California Institute of Technology (1). The Water Tunnel is operated under contract OEMsr-207 with the Office of Scientific Research and Development, and is sponsored by Division 6, Section 6.1 of the National Defense Research Committee.

The investigations were performed by the Water Tunnel staff with the writer responsible for organizing and supervising the experimental program, and for analyzing the results. The material included in the section on Hydrodynamic Forces and Moments Acting During Cavitation is an enlargement of preliminary results reported by the writer at the Second Conference on Underwater Ballistics in January, 1945 (2). The material on Cavitation Noise from Underwater Bodies is taken from a recent Water Tunnel report (3) of which the writer was senior author.

This thesis must be prefaced with an expression of sincere appreciation to Professor Robert T. Knapp for all the encouragement, advice and assistance which it has been the writer's good fortune to receive over several years of personal and professional contact. To him goes full credit for making this thesis possible.

Throughout the course of these experiments the writer has become indebted to all the several groups in the Water Tunnel organization for their willing assistance. Particular credit is due the test crews for their cooperation in making the special measurements required. During the actual writing of the thesis, Alrae McDonald, Ruth Kemp, and Doris Straten were most helpful in preparing figures and manuscript. Special thanks are due to Althea Pease and the other members of the photographic department for handling the countless photographs used for illustrations, and to my wife, Sarah Daily, for typing the final manuscript.

(1) Figures in parentheses refer to Bibliography in Appendix

THE HYDRODYNAMIC FORCES AND THE HIGH FREQUENCY NOISE RESULTING FROM CAVITATION ON UNDERWATER BODIES

The phenomenon known as cavitation was first recognized about fifty years ago when the recurrent damage experienced by ship's propellers was associated with the peculiar noise and loss of thrust arising for certain cases of excess speed or too little submergence. The basic physical conception of the phenomenon as the formation of vapor filled cavities when the local pressure at some point in the fluid drops to the vapor pressure, and the rapid "implosive" collapse of these cavities when they are carried into high pressure zones, was recognized early. But in spite of the contributions of many subsequent investigations, a complete physical picture of all phases of the phenomenon and its hydrodynamic effects is not yet available. The primary purpose of this report is to provide additional information about the physical characteristics of cavitation through a discussion of the results of measurements of the hydrodynamic forces and the high frequency noise resulting from cavitation on underwater bodies.

I THE PHYSICAL CHARACTERISTICS OF CAVITATION

The Factors Affecting the Inception of Cavitation

It is generally agreed that the conditions necessary for cavitation occur when the pressure at some point in the fluid is reduced to the vapor pressure. Assuming that the fluid will not support a tension (4), local boiling or vaporization will occur when the vapor pressure is reached. The cavities or bubbles thus formed are known as cavitation. Actually, if fluids will support a tension (5), it is possible that cavitation does not occur until the pressure drops somewhat below the vapor pressure. If gases such as air are dissolved in the liquid (5) (6), they will tend to come out of solution when the pressure is lowered. It has been observed that this produces a

(4) Figures in parentheses refer to Bibliography in Appendix

condition similar to cavitation at pressures above the vapor pressure. With much air it seems probable that the phenomenon will have a different appearance, since the dissolved air probably provides a source of gas for feeding the cavitation bubbles to insure early growth of large cavities. The effect of impurities and foreign materials such as small particles of solids has been discussed (5), (7), but no definite experimental information has been introduced to show that this has an important effect on cavitation, even though it is known that such particles form nuclei for the initial formation of bubbles during boiling of still water. Similarly, the effect of surface tension on the formation and collapse of cavities has been discussed (5), but no definite experimental correlation has been made.

Some relationship between the flow conditions and the pressure in the fluid body is necessary in order to determine the point in the flow where conditions will be such as to permit the inception of cavitation. Considering the simplest case of irrotational motion for an incompressible fluid, the equation of motion (8)(9) can be put in the following form:

$$\rho \frac{\partial \phi}{\partial t} + \rho \frac{V^2}{2} + P = \text{Constant} \qquad (1)$$

where

ρ = the density of the fluid

ϕ = the velocity potential describing the motion

t = time

V = the velocity at a given point

P = the pressure at a given point

This equation is for the general case of steady or unsteady motion. Cavitation will be caused by any characteristic of the flow that will reduce P to the vapor pressure. In the case of steady motion, $\frac{\partial \phi}{\partial t} = 0$, and P is reduced because of changes in velocity arising from the geometry imposed by the boundary conditions. For unsteady motion $\frac{\partial \phi}{\partial t}$ can be very large and cavitation can occur without much change in velocity. Conversely, of course, $\frac{\partial \phi}{\partial t}$ can be negative and tend to inhibit pressure reductions and cavitation.

The above equation applies only to areas where there is no vorticity. If vorticity exists, very low pressures can occur at the centers of rotation and cavitation is obtained readily, as has been observed in trailing vortices from various shaped objects. Turbulent motion also will produce local low pressure points, but these have been estimated to be of the order of one percent or less of the dynamic pressure.

The Effect of Body Shape on Inception

For vortex free motion, the lowest pressures in a system must occur at the boundary.(8)(10) The equation of motion shows that those bodies causing the largest accelerations and, hence, velocity changes and pressure reductions on the body surface will be the first to cavitate. The pressure distributions on some of the fundamental simple shapes can be readily calculated and, if the motion is steady, the maximum pressure reduction from the value in the undisturbed flow away from the body can be expressed as a fraction of the dynamic pressure and evaluated numerically. Comparison of this fraction shows the relative sensitivity of different shapes to cavitation. For example, a comparison of the effects of two- and three-dimensional bodies can be examined by using the cylinder and the sphere. For the cylinder

$$\left.\frac{P - P_o}{\rho \frac{V^2}{2}}\right|_{max} = -3$$

while for the sphere

$$\left.\frac{P - P_o}{\rho \frac{V^2}{2}}\right|_{max} = -1.25$$

where P_o is the pressure in the undisturbed flow. The greater tendency for cavitation to occur on two-dimensional objects is clearly illustrated. For bodies with lower surface curvatures, this fraction is numerically smaller with a corresponding higher resistance to cavitation. Calculation of the pressure distribution in this manner is not possible for bodies with discontinuities in the surface which

are sharply convex, because infinite accelerations are obtained for irrotational flow in such cases.

For motion of viscous fluids the flow is modified, of course, so that the above conclusions will be altered somewhat. For most shapes, however, the pressure distributions as calculated for irrotational flow hold reasonably well over the forward part of the body and the agreement over the body in general improves as Reynolds number increases. Thus, for the sphere, the cylinder, air foil shapes and the like, the theoretical values are very useful. Greatest deviations occur in the case of the bodies with the sharp edges just mentioned. Infinite accelerations do not occur because the flow separates from the body at these points. The result is that the effective shape of the body is changed to conform to the surface of the separating sheet of flow. On the other hand, rotation in the form of vortices are introduced so that pressure reductions below that calculated for this modified "body" are obtained. Furthermore, rotation in the flow means that Kirchhoff's law is invalid and the lowest pressures are no longer necessarily on the boundary of the fluis field. Indeed, the first visual evidence of cavitation in the case of such discontinuities is in the cores of the vortices away from the surface of the body. Actually, on many bodies there are zones of local separation in the boundary layer next to the surface. This separation is also a source of minute vortices with low pressure cores in which cavitation can appear.

The Cavitation Parameter and the Degree of Cavitation

Clearly the maximum value of dimensionless fraction $\frac{P - P_o}{\rho \frac{V^2}{2}}$ for a given body is a characteristic of that body. If $P = P_V$, the vapor pressure, it assumes the special significance of indicating the minimum hydrostatic pressure, P_o, which can be imposed on the system without cavitation occurring. As used for describing cavitation characteristics, it is normally given with the opposite sign and designated by the symbol K, so that

$$K = \frac{P_o - P_v}{\rho \frac{V^2}{2}} \qquad (2)$$

The usefulness of the cavitation parameter is not limited to indicating the conditions for inception of cavitation, but is equally useful in describing the conditions of velocity and pressure necessary for more advanced stages of cavitation. In order for cavitation to develop beyond the inception point, it is necessary that K be reduced numerically from its value at inception. Experiment has shown that for the more developed stages the degree of cavitation on a particular body and its general appearance can be reproduced for various combinations of P and V as long as the same K is obtained. If instead of P_V, P_B is used to indicate the pressure in the cavity generally, K will describe the conditions in gas as well as vapor filled bubbles. With reduction in K, the rate of vapor formation is increased and the cavity will grow until it envelops the body. For the terminal condition of K = 0, the maximum cavity will be obtained. This latter condition is difficult to reproduce experimentally with pure cavitation, but is obtained automatically in the case of the entry of projectiles from air into water.

Theoretical and Experimental Determination of Inception Points

The agreement between the theoretical and experimental determinations of the inception of cavitation is not thoroughly proven. The lack of refinements in measuring techniques can easily cause margins of error that mask the effects of air or impurities or the ability of water to withstand tension. In one set of Water Tunnel measurements (11) the first visual evidence of cavitation was observed to occur at K = 0.66, whereas the measured pressure distribution indicated K = 0.78. This difference is regarded as outside the possible experimental error. In another set (12) on a finer nose on which a different type of cavitation appeared, inception was variably observed at K = 0.34 to 0.43, whereas pressure measurements indicated K = 0.34. It has been reported by Rouse (13) that pressure distributions made during actual cavitation show deviations in the pressure reduction obtained even before any visual evidence of cavitation. Compared with the first mentioned result from the Water Tunnel tests, this indicates that inception may occur on a

microscopic scale at the K obtained from the noncavitating pressure distribution.

The Physical Appearance of Cavitation

The mechanism by which cavitation bubbles form initially and are continuously fed with vapor at some advanced stages has been the subject of speculation and experiment (5)(7)(14). It is known that a large amount of energy must be added to cause liquids to boil, and this energy must go into overcoming large internal pressures associated with the formation of vapor bubbles. In the case of flow the location of the initial vaporization and its subsequent growth and the collapse is dependent on the velocity and pressure field, and hence on the body shape. The type of formations obtained with various bodies have been examined visually in the Water Tunnel and have been mentioned in several previous reports (14)(15)(16)(3). There are, roughly, three classifications. In Figure 1 is shown photographs of the three types on two- and three-dimensional bodies. The first type occurs on bodies with convex surfaces of relatively sharp curvature and is made up of very small bubbles which give a "fine grained" or sudsy appearance. The second type obtained on shapes with surfaces less sharply convex is somposed of relatively large "coarse grained" bubbles that form intermittently on the surface. The third type is obtained on bodies with sharp discontinuities in surface and appears in the form of detached wisps in the fluid away from the body proper. These three types are associated with the kind of pressure distribution over the surface of the particular shape. Typical distributions for several of the examples illustrated are shown in Figure 2. It is seen that the "fine grained" type is associated with a pressure curve that shows a sudden reduction and equally sudden recovery, giving a narrow zone of low pressure. This sharp pressure gradient provides a clear cut front across which the fluid moves. All the particles of fluid are subject to the same conditions at the same time, and the result is the sharp line of bubble formation. Since formation occurs at every point along this line and because the gradient is steep, a single bubble does not

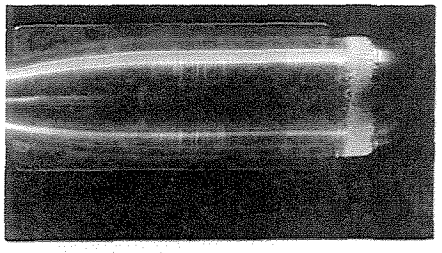

(A) Fine Grained Cavitation

Hemisphere
K = 0.60

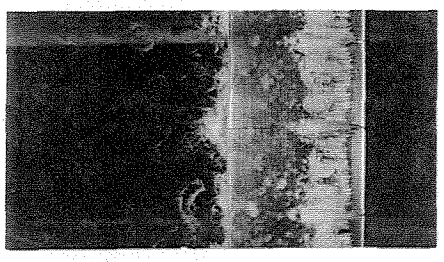

NACA 4412 Hydrofoil
Lower Surface $\alpha = 0^\circ$
K = 0.34

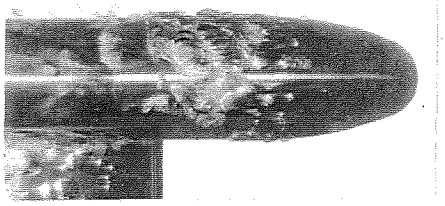

(B) Coarse Grained Cavitation

2 Cal. x 65 1/2° Spherogive
K = 0.24

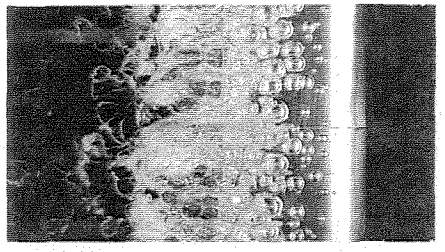

NACA 4412 Hydrofoil
Upper Surface $\alpha = 0^\circ$
K = 0.30

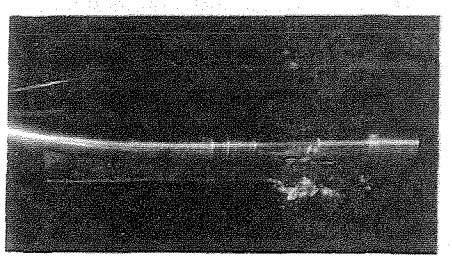

(C) Detached Cavitation

Square Ended Cylinder
K = 1.6

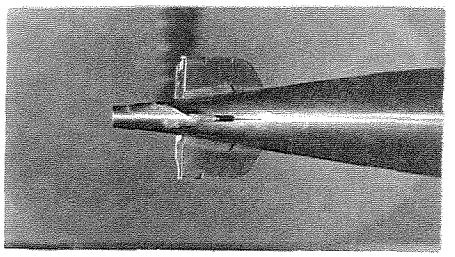

Upturned Tail Rudder
K = 0.95

TYPES OF CAVITATION

Figure 1

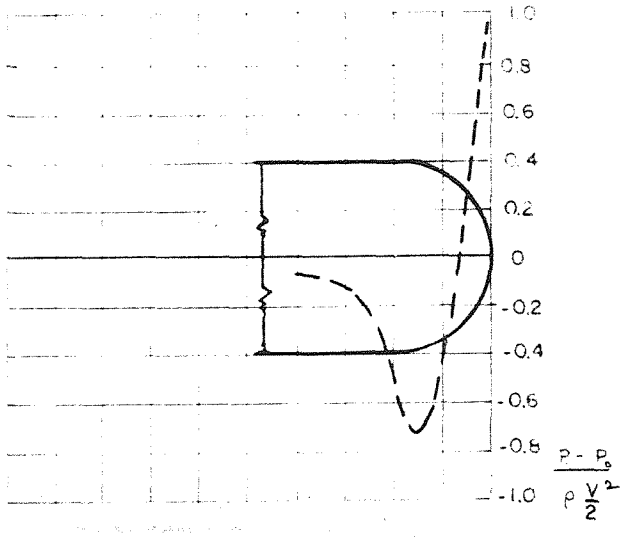

HEMISPHERE NOSE"

FINE GRAINED CAVITATION

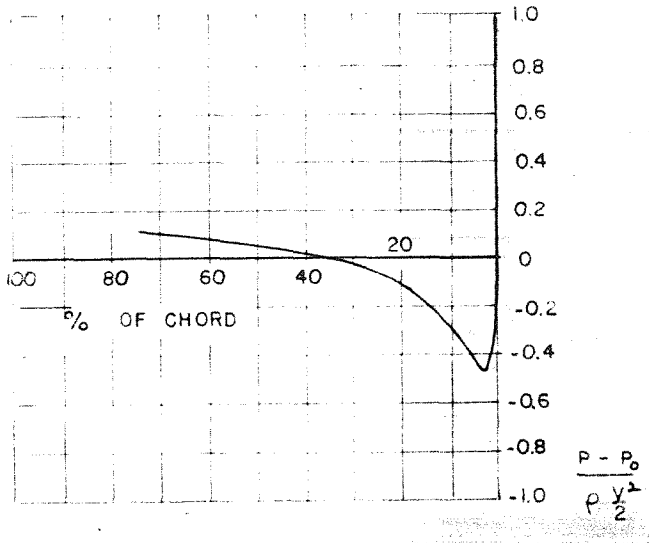

NACA 4412 HYDROFOIL °

LOWER SURFACE $\alpha = 0°$

FINE GRAINED CAVITATION

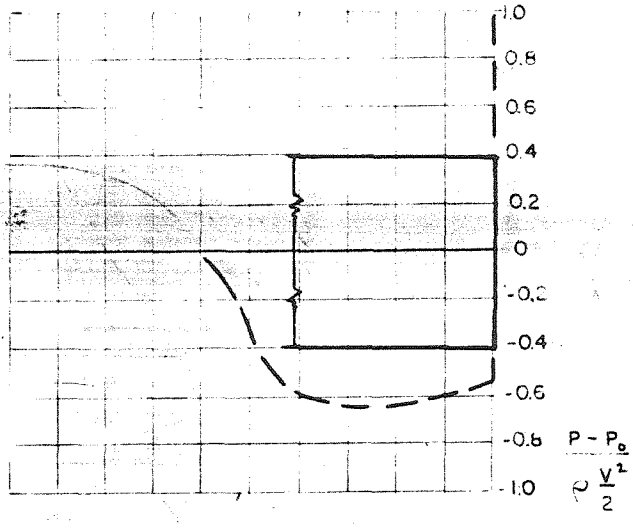

SQUARE END CYLINDER "

DETACHED CAVITATION

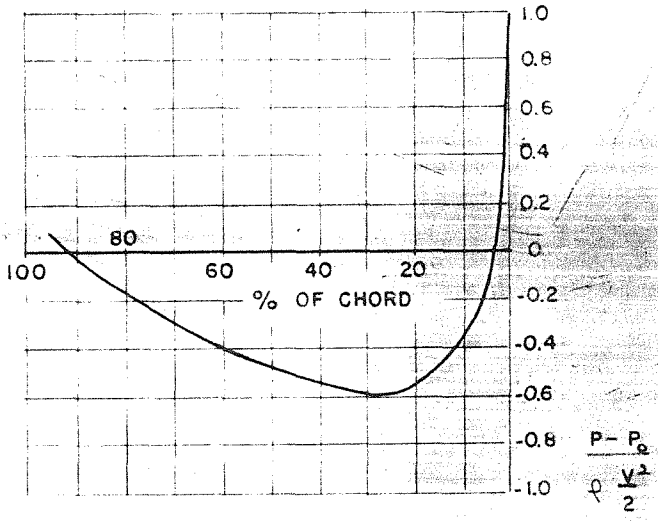

NACA 4412 HYDROFOIL °

UPPER SURFACE $\alpha = 0°$

COARSE GRAINED CAVITATION

" PRESS. DISTR. FROM REF. 13

° " " " REF. 17

PRESSURE DISTRIBUTION

FOR NON - CAVITATING FLOW

FIGURE 2

grow sufficiently to affect conditions appreciably on either side of it. This results in the fine grained appearance illustrated. With the second type the pressure gradient is less steep and the recovery is also gradual. Apparently a bubble which forms at a given point has time to grow and effectively distort the flow, and hence the pressure on either side of it. This results in an intermittent formation along a band in the reduced pressure zone instead of along a sharp line. For the third type, the sharp edge causes separation in the normal flow without cavitation. This results in eddies and vortices with resultant low pressures. Initial cavitation apparently occurs in these local points of low pressure.

As will be seen in the succeeding sections, the kind of bubble formation in the initial stages and the type of cavity obtained for the fully developed stages will affect the forces acting on a given body because the resultant change in momentum of the passing fluid will be different in each case. Also, the kind of bubble formation, and more particularly the type of collapse associated with each bubble type will affect the high frequency noise produced.

The Location of Incipient Cavitation

It has been thought that the point on the surface at which cavitation first appears should coincide with the point of minimum pressure as obtained from measurements without cavitation. As the illustrations in Figure 1 and the pressure curves in Figure 2 show, however, cavitation does not occur at this point, but some small distance farther downsteam. This is attributed to the face that a finite time is necessary for the vapor bubbles to form once they are subjected to the low pressure environment. Since the fluid is travelling at a high rate of flow, this means they are carried past the minimum pressure point. This might also be considered as an indication that the fluid can support some negative pressures. As cavitation is formed, of course, the velocity distribution is altered slightly so that the new conditions correspond to a changed pressure distribution (13).

II THE HYDRODYNAMIC FORCES AND MOMENTS ACTING DURING CAVITATION

A. The Effects of Cavitation on Drag

At the present time most interest is centered on the hydrodynamic forces obtained with cavitation for two extreme conditions; the initial stages immediately after the onset of cavitation, and the fully developed stage when a large portion of the cavitating body is enclosed in a vapor cavity. For the incipient stages the question of how far cavitation can develop before affecting the forces and moments appreciably is important, as well as the question of the magnitude of the resulting forces. This phase is important for all sorts of underwater bodies and hydraulic machines. For the fully developed condition, a knowledge of the forces and moments acting and the physical conditions of flow affecting these forces are important. One immediate application of this information is to the air-water entry problems arising for projectiles where the air cavity obtained at entry is similar if not identical to the vapor pocket obtained with cavitation.

In order to investigate these different aspects measurements of the forces and moments were made for a variety of bodies subjected to cavitating conditions in the High Speed Water Tunnel. Brief descriptions of the Water Tunnel and of the testing procedures are given in Appendix I. A more complete description of the Water Tunnel facilities is given in reference (1). Complete projectiles with different noses and tail structures were tested to determine the total performance for the incipient and more developed stages of cavitation. Short "bullet" shaped models with different noses were tested to obtain the effect of the nose shape alone, primarily for completely developed cavitation.

In addition to the measurements on three-dimensional bodies, tests were made of the drag of a cylinder aligned normal to direction of motion for cavitating and noncavitating flow. The drag of this two-dimensional case and of two of the three-dimensional shapes are compared with theoretical values calculated from the pressure distributions on the body surface.

Physical Growth Necessary to Change the Drag

The amount of cavitation necessary to cause a measurable change in drag is dependent somewhat on the shape of the body, the kind of cavitation that is formed, and the magnitude of the drag without cavitation. The results of measurements on several different bodies, and photographs of the cavitation at various stages of development are shown in Figures 3 to 13. The pictures were obtained with exposures of the order of 20 microseconds so that the flow was effectively "stopped". The drag measurements are presented as curves of the drag coefficient C_D plotted against the cavitation parameter, K. On this diagram, decreasing values of K represent conditions for increased cavitation. The methods of evaluating and correcting the test data is described in Appendix II, and a list of symbols and definitions is given in Appendix III.

The first two sets of data were obtained with a cylindrical body having an ogival tail or afterbody and tipped with a hemisphere nose in one case and left with a square end in the second. With this simple form a good comparison of the effect of nose shape should be obtained. Data for the hemisphere are shown in Figures 3 and 4. "Fine grained" type of cavitation is obtained with this nose while the drag of the entire body is low. The outline of the projectile can be seen in the first photograph of Figure 3. In the second photograph, a small band of cavitation is seen just aft of the junction between the hemisphere and the cylinder. In the bottom two photographs, the entire body is enveloped in a cavitation cavity. Examination of the drag curve shows that there is no sudden increase in drag with the onset of cavitation. Instead, the resistance increases very slowly until a K of about 0.5 is reached, when the cavitation zone on the nose is about 1/2 caliber long, as can be visualized by interpolation between photographs. With further development of cavitation, however, C_D rises rapidly to several times its initial value.

In Figures 5 and 6, data are shown for the cylinder with the square end. This "nose" produces the wispy type of cavitation at inception which develops into a fine grained white plume and

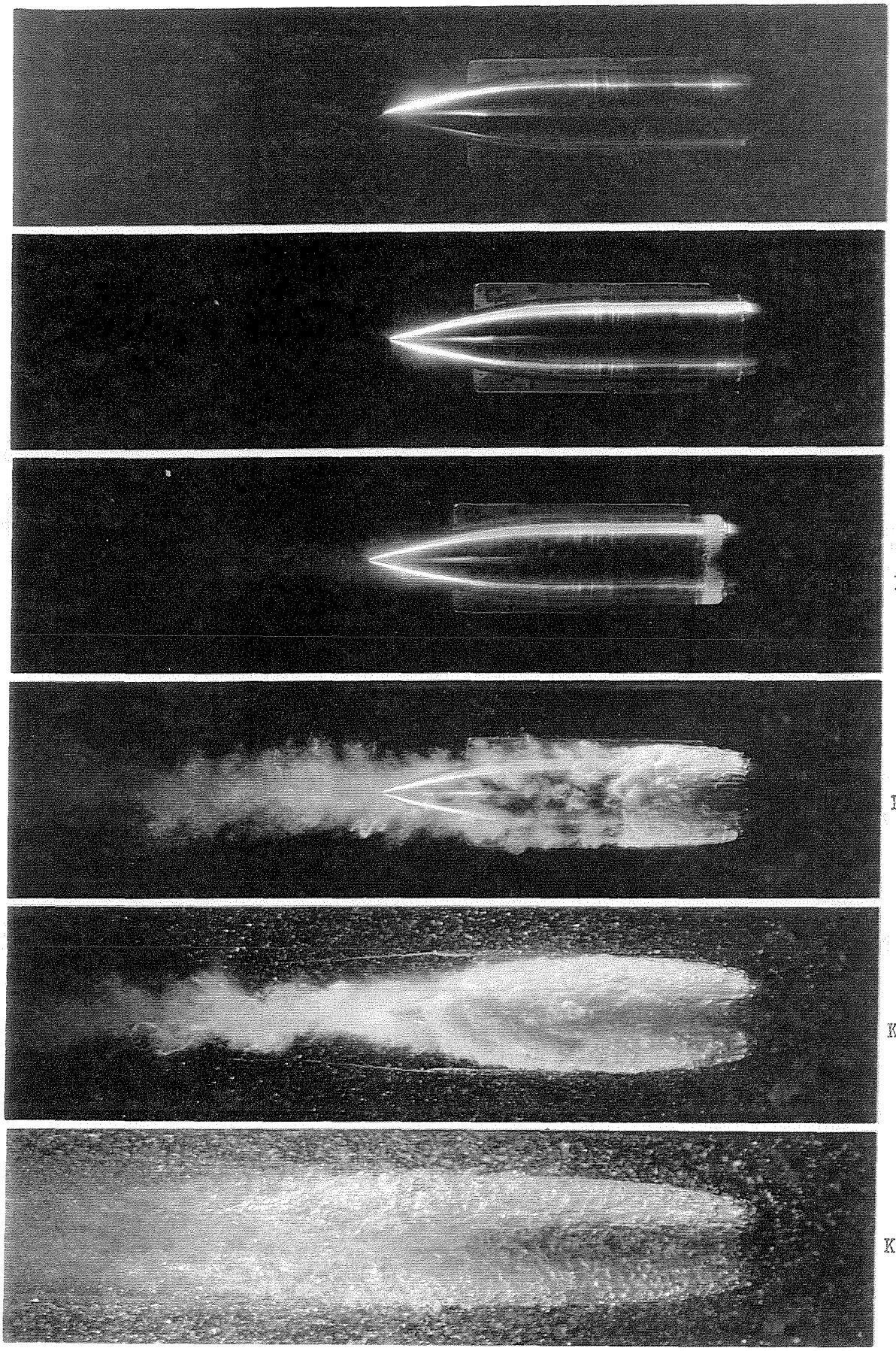

CAVITATION ON BODY WITH HEMISPHERE NOSE

$\psi = 0°$

Figure 3

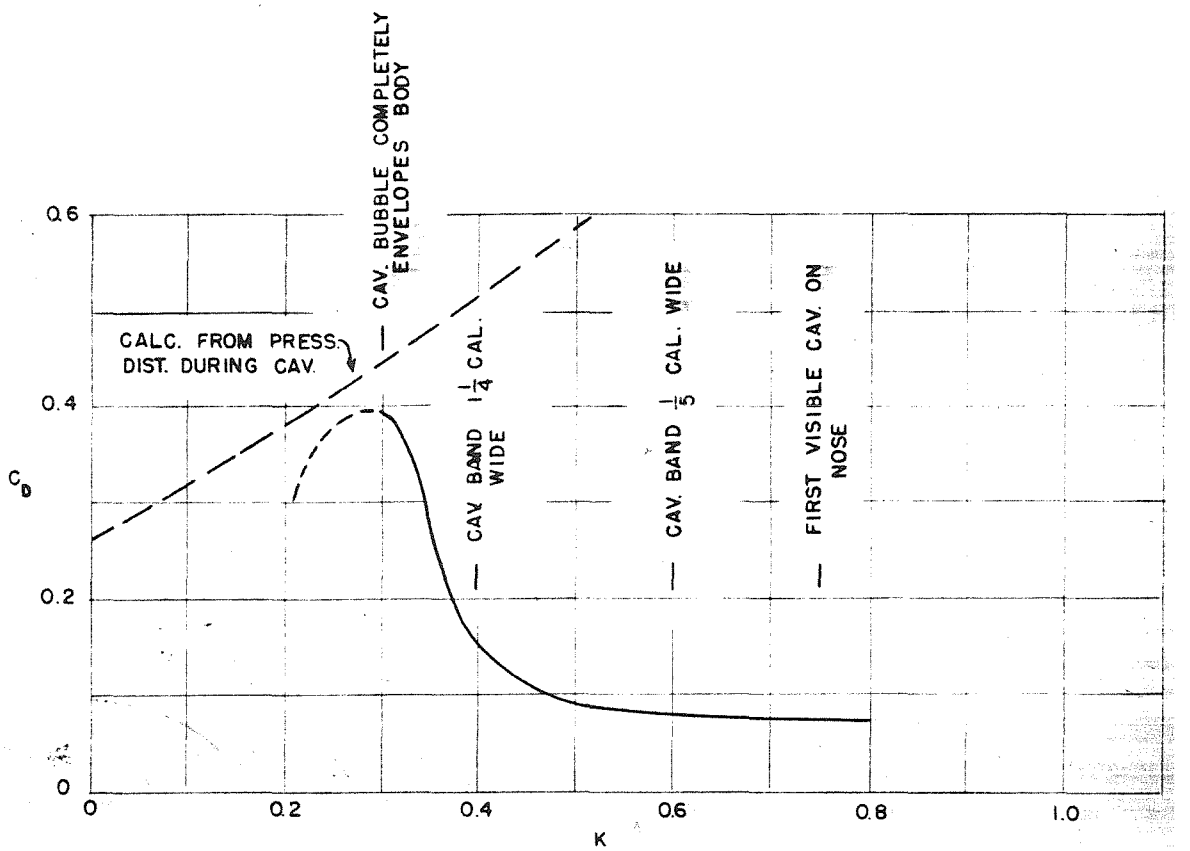

EFFECT OF CAVITATION ON DRAG
OF CYLINDER WITH HEMISPHERICAL NOSE
& TAPERED TAIL
$\psi = 0°$

FIGURE 4

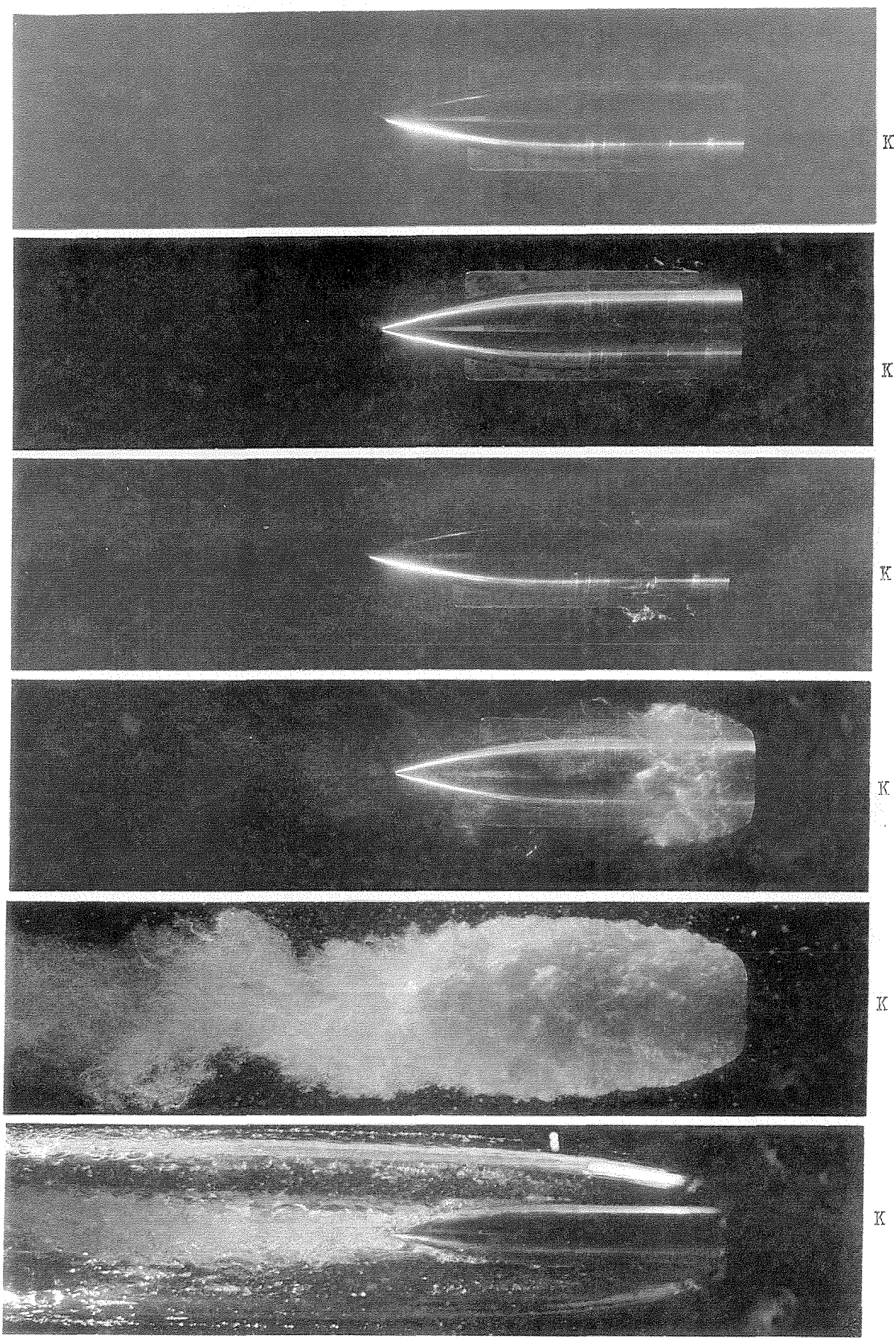

CAVITATION ON SQUARE END CYLINDER

$\psi = 0^\circ$

Figure 5

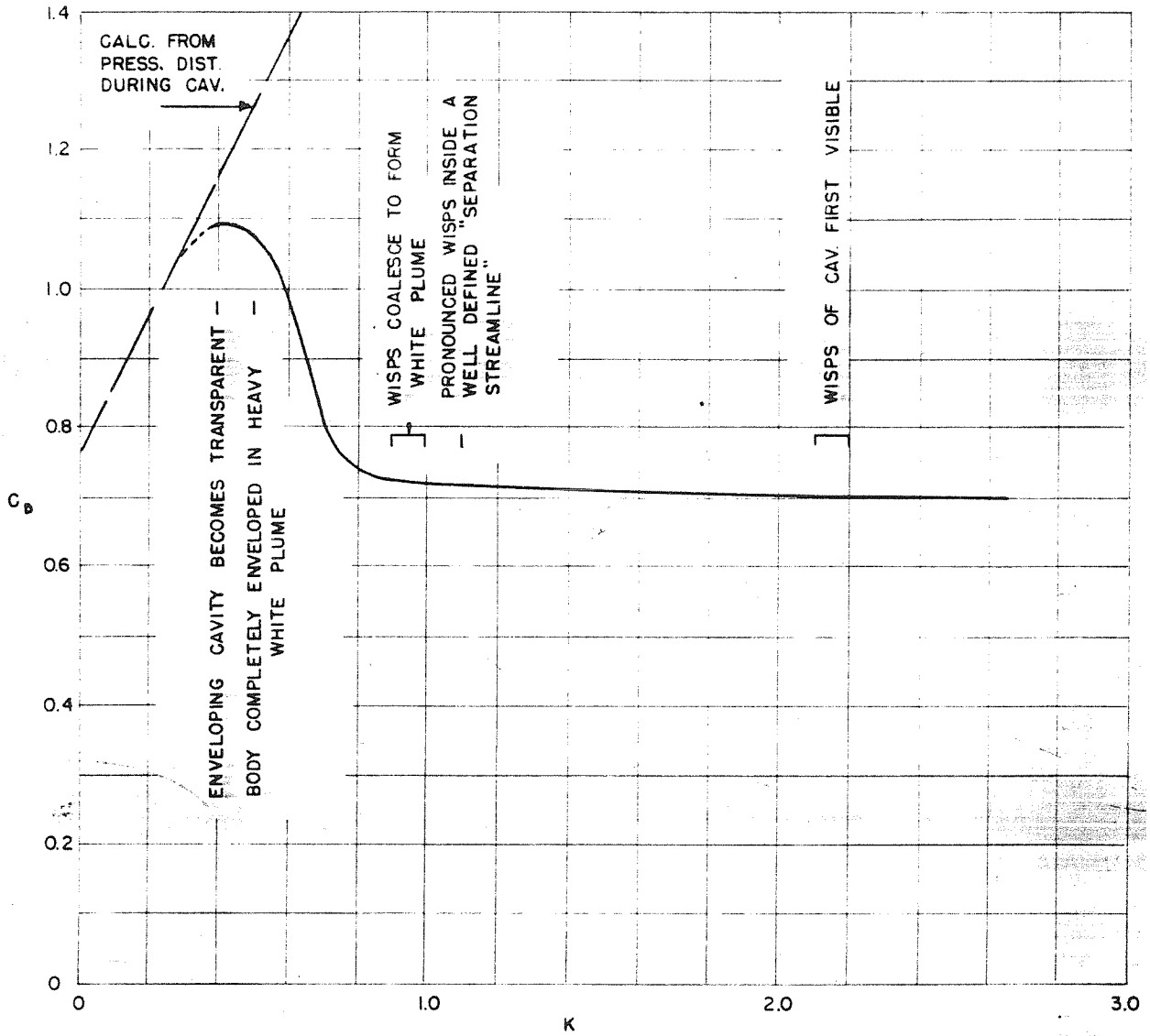

EFFECT OF CAVITATION ON DRAG
OF SQUARE END CYLINDER
WITH TAPERED AFTERBODY
$\psi = 0°$

FIGURE 6

The drag is initially nearly ten times the value for the hemisphere. Again, as cavitation forms and develops, the drag does not change suddenly, but increases very slowly until the wispy formation coalesces to form the white plume. This increase is at about the same rate as observed in the case of the hemisphere, but, of course, is a much smaller percentage of the total drag. Here, in order to increase the drag materially above its already high value, it is necessary that enough cavitation be formed to further displace the flow away from the body and increase the turbulent wake downstream.

Measurements for a ring tailed projectile with exhaust stacks in the ring are shown in Figure 7. No photographs were obtained with the test, but the development of cavitation at various points on the projectile is described by notes on the curves. Two noses were used with this projectile. One, the so-called MK 13 nose, is composed of a 2 1/2° included angle cone, tapering down from full body diameter to 0.92 of the maximum diameter, with a spherical segment tip having an 88 3/4° half angle. The other, a 2.3 caliber by 78° spherogive, is formed by replacing the pointed tip of a 2.3 caliber ogive with a spherical segment which becomes tangent to the ogive surface when its half angle is 78°.

The Mk 13 nose is very little different from a hemisphere and produces the same type of cavitation just aft of the tangent point with the conical surface. Inception is obtained at a K of about 0.66 instead of 0.75 however. The tail structure and the nose begin to cavitate at about the same time. There is no measurable change in drag on this projectile immediately after the onset of cavitation. Only after a moderate band is developed on the nose (less than for the hemisphere on the simple body, however) and pronounced cavitation develops on parts of the tail structure does the C_D increase materially.

The spherogive nose has much better characteristics than either the hemisphere or the MK 13 and, consequently, does not cavitate until K is reduced to approximately 0.42. As a result, tail cavitation is well developed before nose cavitation appears and causes the drag to increase while the nose cavitation is still in its early stages.

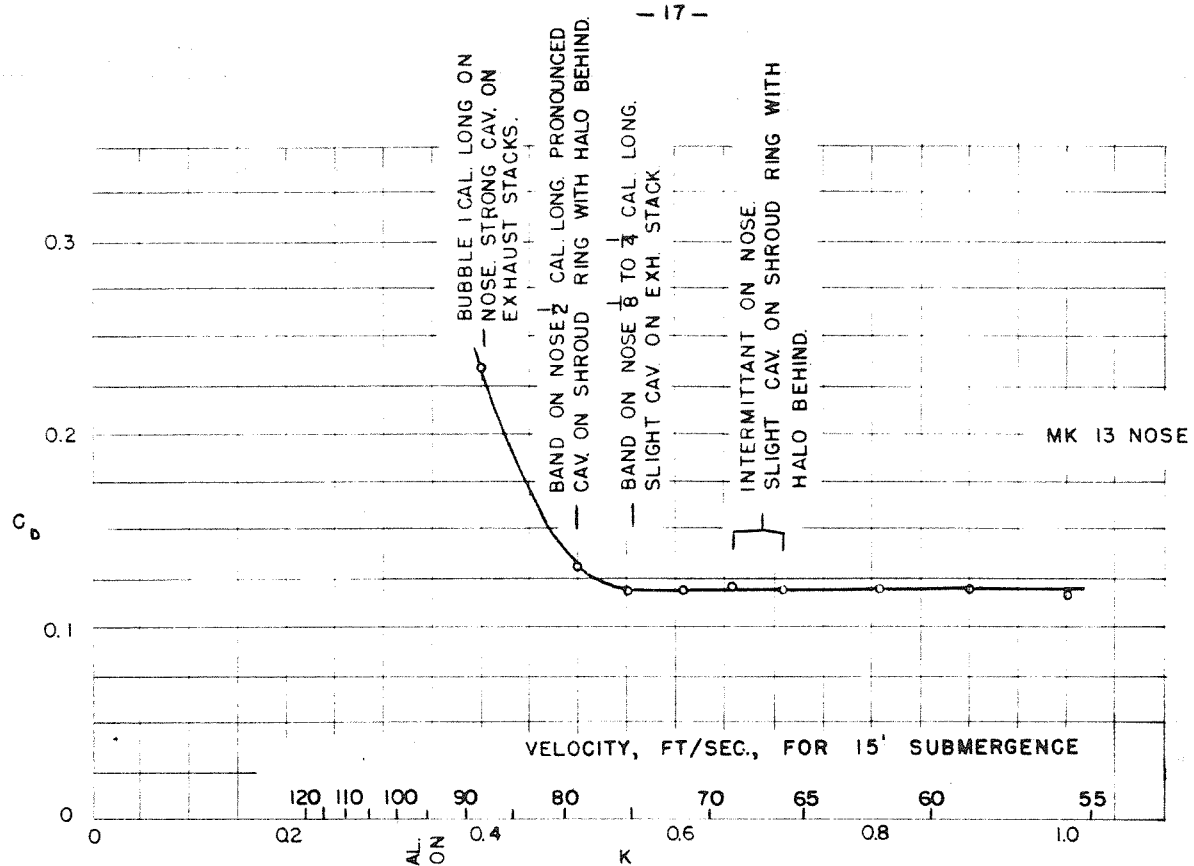

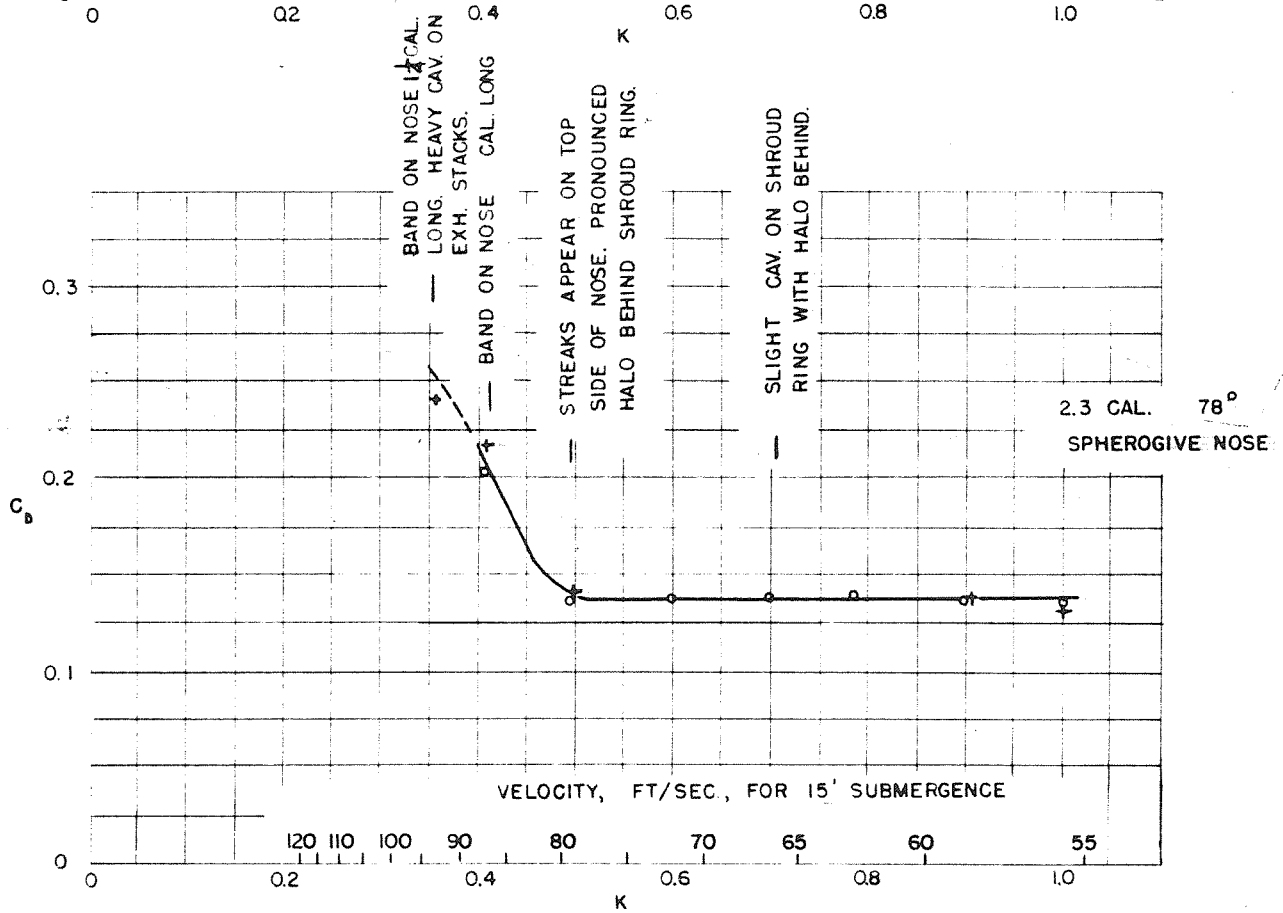

EFFECT OF CAVITATION ON DRAG
OF RING TAIL PROJECTILE
WITH 4 EXHAUST STACKS
$\psi = 0°$

FIGURE 7

Another ring tail projectile with a blunt nose was tested and the results are shown in Figures 8 and 9. The nose is a one caliber ogive truncated at 2/3 caliber. The corner of the flat face is rounded slightly. The initial cavitation on this projectile forms on the ogival surface at the junction with the flat face and is very fine grained in character. The tail surfaces begin to cavitate soon after inception on the nose. The cavitation-free drag of the projectile is about 3 times the value of the drag of the simple body with hemisphere nose shown in Figure 4. With the onset of cavitation, there is, if anything, a slight tendency for the drag to drop off. An increase is obtained, however, with a relatively small amount of cavitation on the nose and the tail. In fact, the rapid increase in drag of this particular projectile occurs with less visible cavitation than on any of the other models discussed thus far.

A set of data showing the effect of cavitation with yaw is shown in Figure 10 for a torpedo with a hemisphere nose, the MK 13 nose, and a 5 caliber by 76° spherogive nose. Photographs of the cavitation are shown for each nose in Figures 11, 12, and 13. These data show results similar to those already observed at zero yaw. With the hemisphere and MK 13 nose very little change in drag occurs until cavitation is fairly well developed on both the nose and the tail surface. Actually cavitation appears first on the tail ring at about $K = 0.9$ and later on the lee side of the hemisphere at $K = 0.83$. The drag is only 10% greater at $K = 0.62$ when the cavitation band on the nose has grown to a length of about 1/2 caliber. With the MK 13 nose, nose cavitation appears at lower K and the sharp increase in drag is delayed correspondingly. Here the influence of the tail cavitation becomes more important. With the 5 caliber by 76° spherogive, nose cavitation does not appear at all until after cavitation on the tail and, in this case, on the afterbody also, has caused the drag to rise.

To summarize, these examples show the common effects that the onset of cavitation as observed visually does not result in an immediate sharp increase in drag. Instead, the drag increases.

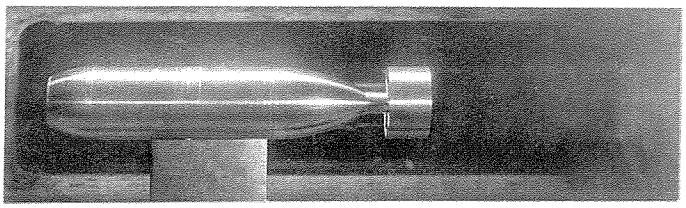

K = 1.63

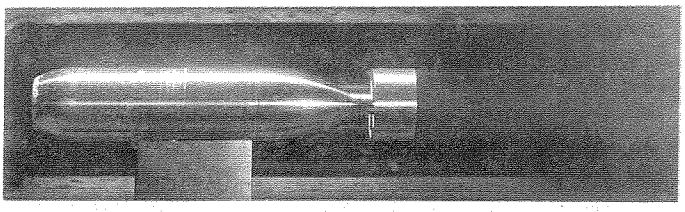

K = 1.30

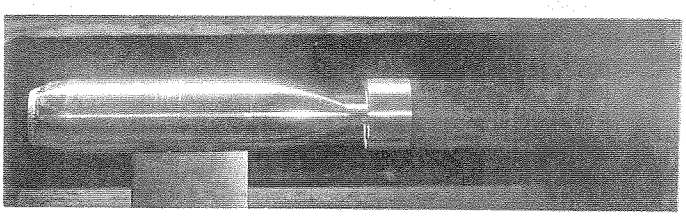

K = 1.03

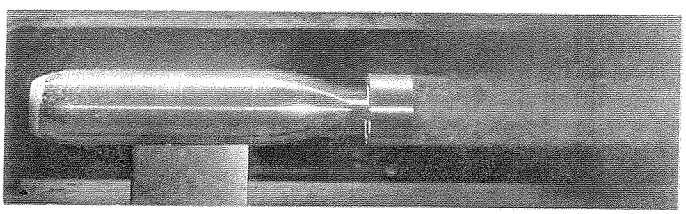

K = 0.81

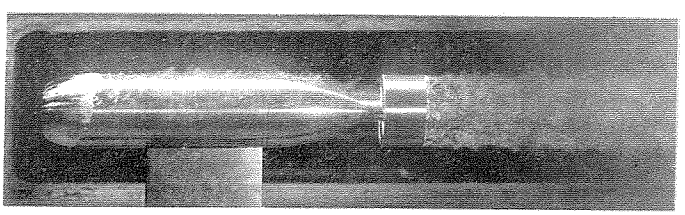

K = 0.68

CAVITATION ON BLUNT NOSED PROJECTILES

(1 CAL. OGIVE TRUNCATED TO 2/3 CAL. FLAT FACE, CORNER ROUNDED)

$\psi = 0°$

Figure 8

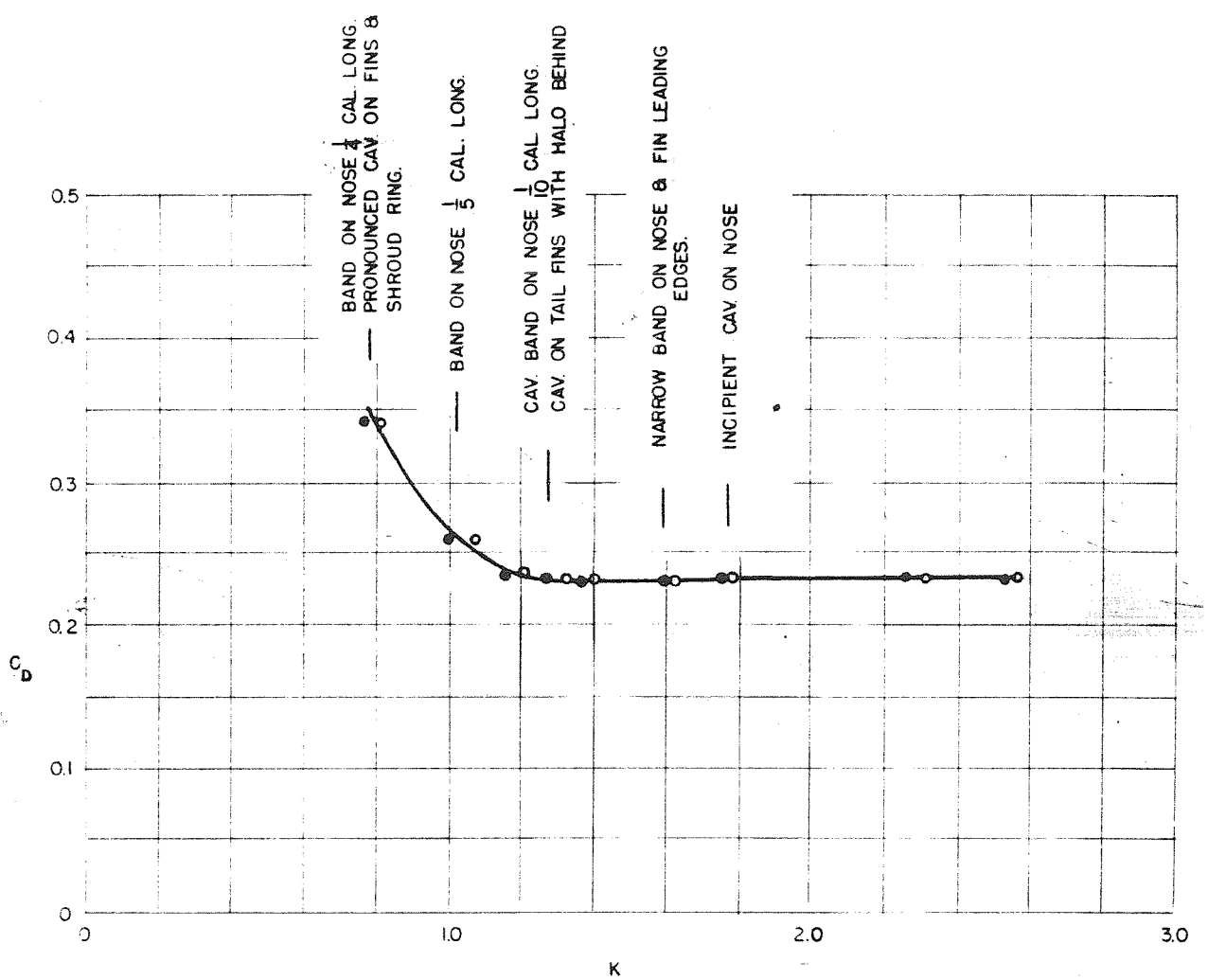

CAVITATION OF BLUNT NOSED PROJECTILE
(1 CAL. OGIVE TRUNCATED TO $\frac{2}{3}$ CAL. FLAT FACE.
CORNER ROUNDED)
$\psi = 0°$

FIGURE 9

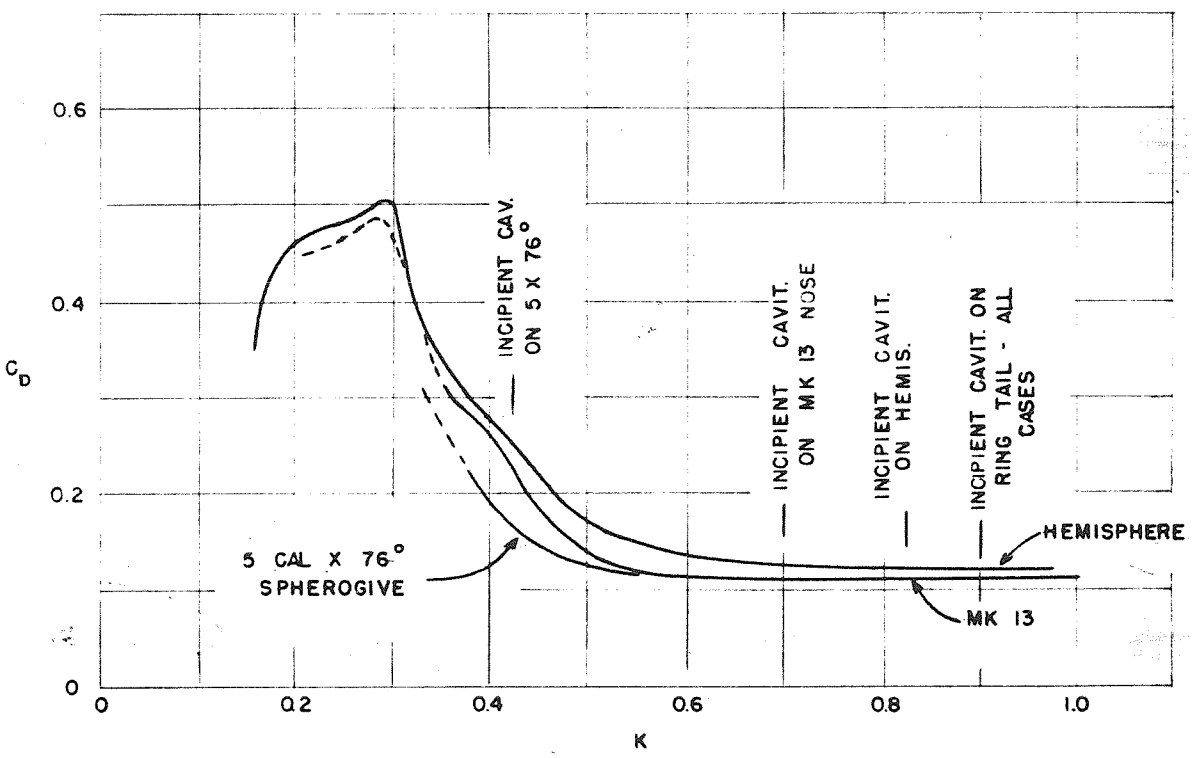

EFFECT OF CAVITATION ON DRAG
OF RING TAIL PROJECTILE
WITH THREE DIFFERENT NOSES

$\psi = 3°$

FIGURE 10

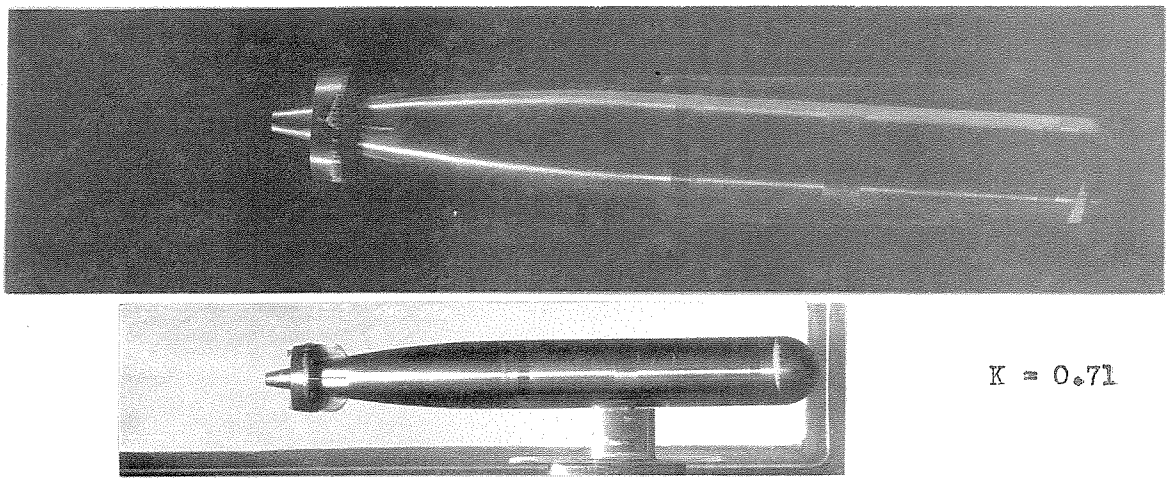

K = 0.71

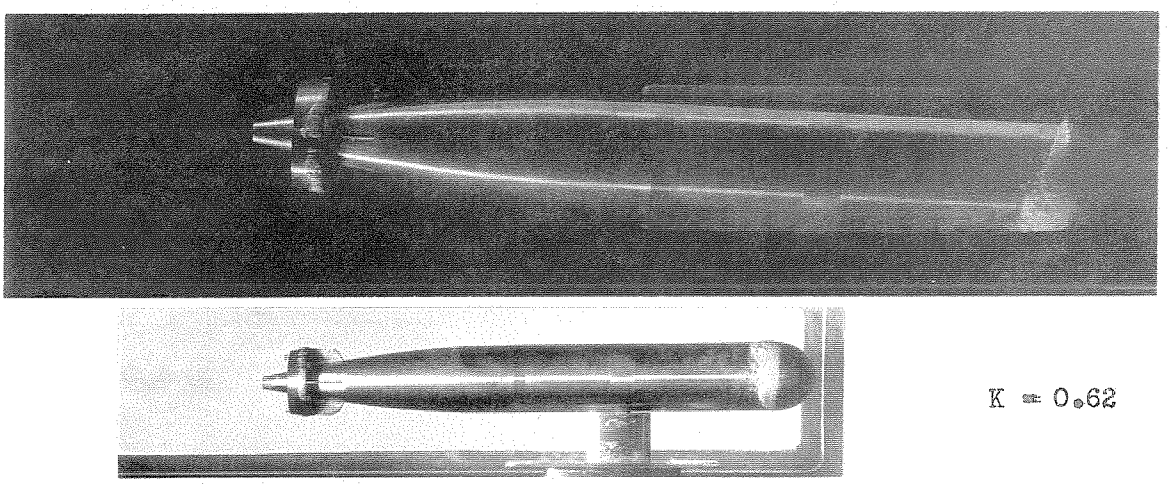

K = 0.62

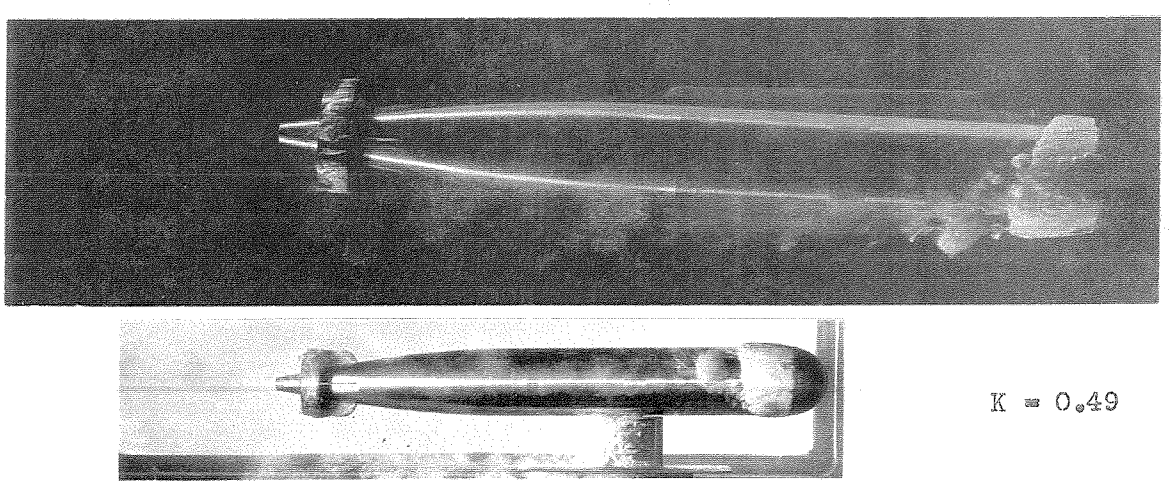

K = 0.49

HEMISPHERE NOSE

ON RING TAIL PROJECTILE

$\psi = 3^\circ$

Top and Side Views

Figure 11

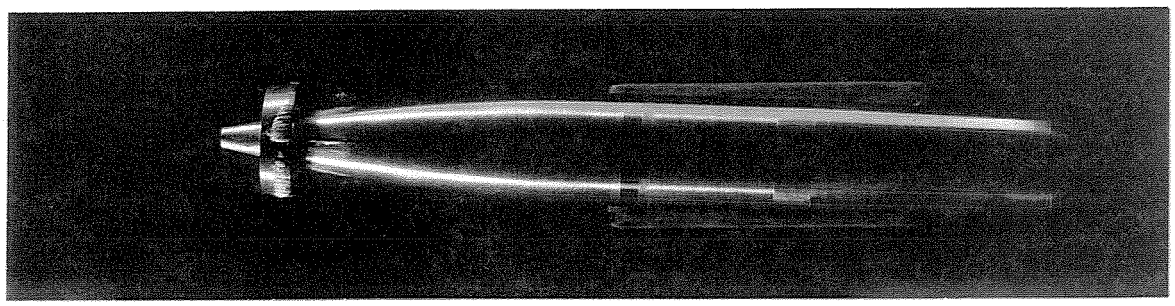

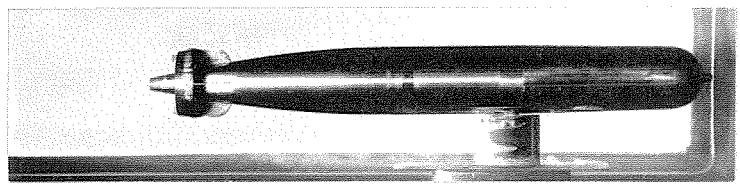

K = 0.60

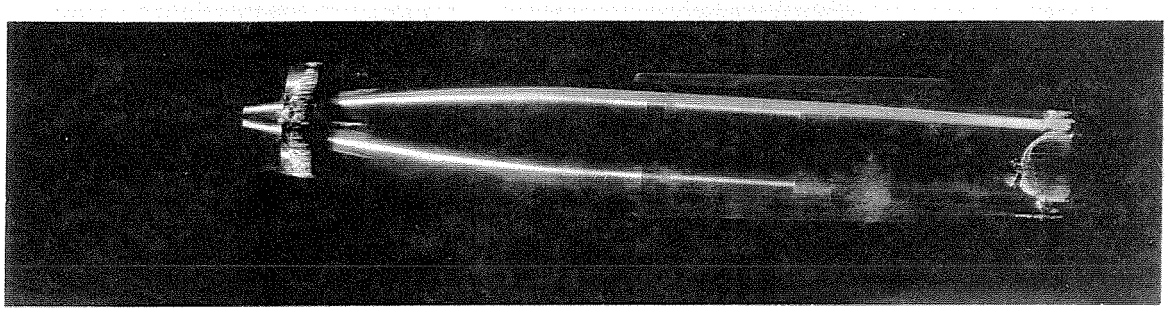

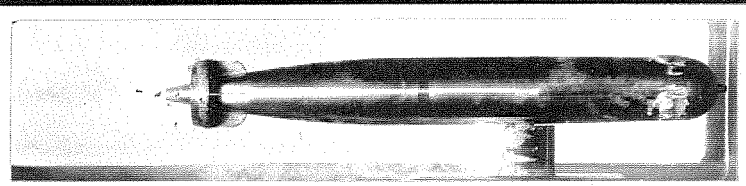

K = 0.50

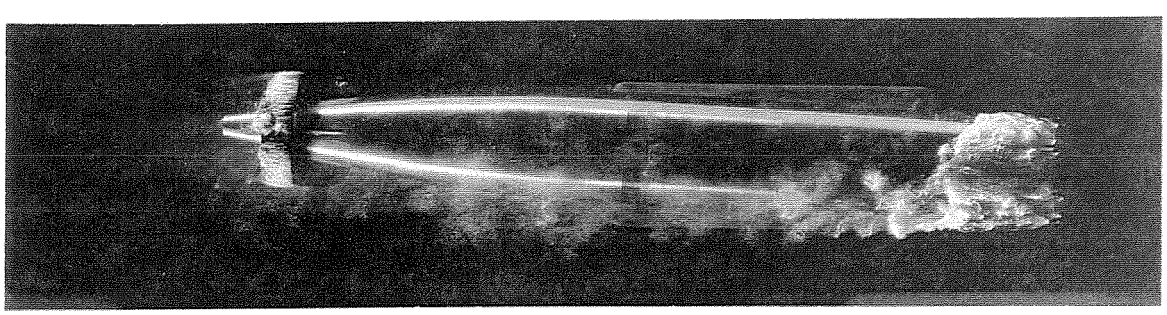

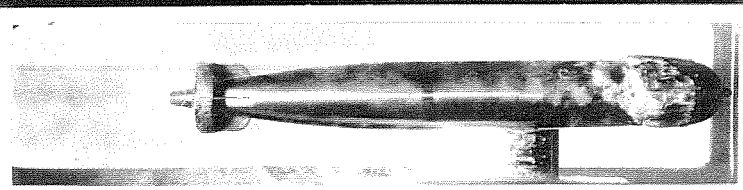

K = 0.40

STD. MK 13 NOSE

ON RING TAIL PROJECTILE

$\psi = 3^\circ$

Top and Side Views

Figure 12

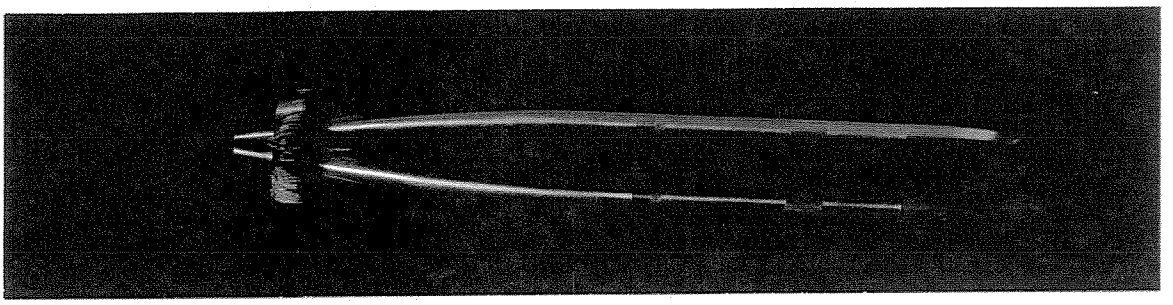

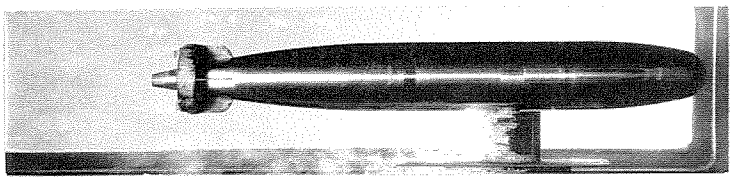

K = 0.50

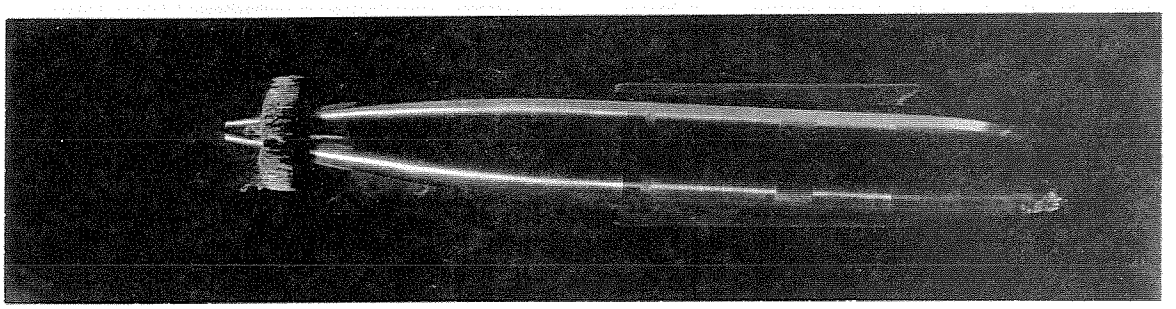

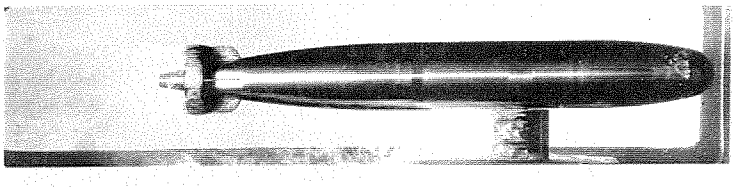

K = 0.39

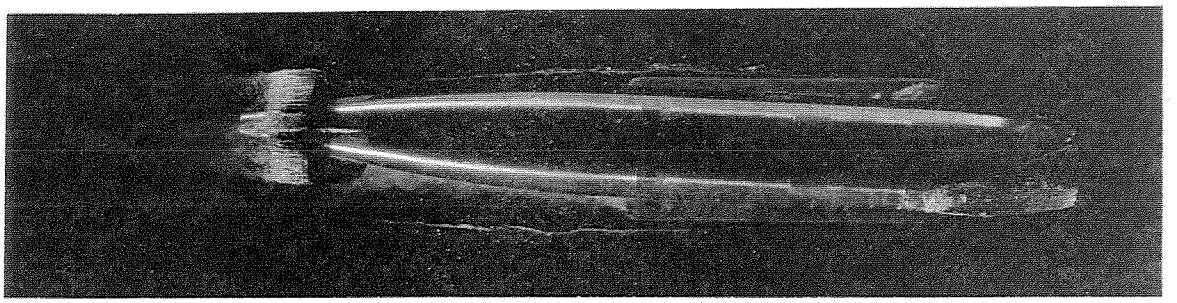

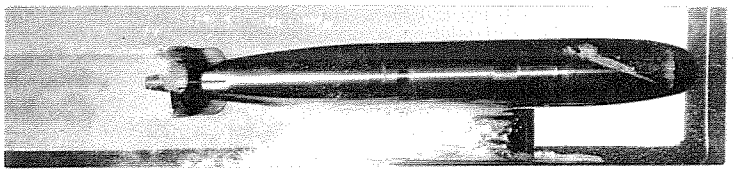

K = 0.31

5 CAL. X 76° SPHEROGIVE NOSE

ON RING TAIL PROJECTILE

$\psi = 3°$

Top and Side Views

Figure 13

slowly, and in one case actually tends to drop off slightly, until sufficient cavitation is formed to change the basic flow pattern around the object. For all cases except one, the amount of cavitation formed at this point occupies an appreciable physical volume.

Effect on Boundary Layer and Skin Friction

In general, the drag of bodies is the sum of skin friction and form drag. As cavitation develops, the relative proportions of the two components are changed until for fully developed cavitation where the projectile is completely enclosed in a cavity, contacting the fluid only over a small area at the nose tip, the drag is almost 100% form drag. It is clear then that the kind of effect cavitation produces will depend on the body shape and hence the ratio of form drag to skin friction for noncavitating conditions. The influence of cavitation in affecting the form drag can be visualized rather clearly, since the effective shape of the body is, of course, changed by the bubble formation. The physical mechanism of its effect on skin friction can be explained qualitatively by comparison with local separation and its effects on the boundary layer development (9)(18)(19)(20).

For cases where the drag is due primarily to skin friction, it will be highest when the boundary layer is turbulent. At a given Reynolds number, if an appreciable portion of the boundary layer is laminar, C_D will be much lower. Consequently, any influence which causes an early transition to a turbulent layer will tend to increase C_D. In noncavitating flow, this can be accomplished by increasing Reynolds number and/or increasing the turbulence in the surrounding fluid. It can also be accomplished artificially by providing roughness or obstructions on the surface of the body, or discontinuities in the curvature at the surface that will cause local separation of the flow, and hence introduce turbulence.

For the two types of cavitation obtained in the cases just discussed, a definite similarity exists between the cavitation

and separation. Reference to Figure 3 shows the fine grained cavitation to form a ring just aft of the junction between the hemisphere tip and the cylinder. Figure 5 shows thin wisps forming in eddies well away from the projectile surface. Figure 8 shows fine grained cavitation appearing at the discontinuity between the flat face and the ogive surface of the nose. Each of these has the common characteristic that cavitation appears first at a discontinuity in surface curvature.

In Figure 14 are flow line diagrams for these same noses on which the zone of separation is shown. These diagrams were drawn from actual observations in the Polarized Light Flume (1)(21) at very low Reynolds numbers so the separation effects are exaggerated. However, it is clear that for these cases, both separation and cavitation occur in the same general vicinity. In the initial stages, therefore, cavitation must be similar to separation in its effect on the drag. This idea is in agreement with the cases discussed thus far.

With the blunt nosed bodies, the form drag is initially high due to severe separation. Incipient cavitation occurs in the same zone as the separation and has practically no effect on the drag. With bodies having surface curvature discontinuities as sharp as on the hemisphere, the boundary layer is probably predominantly turbulent to begin with so that cavitation alters the conditions only slightly. Only with the development of enough cavitation to completely alter the normal boundary layer, and hence both skin friction and form drag, does C_D increase materially.

With more streamlined noses separation does not occur under normal conditions and the boundary layer remains laminar over a longer distance from the tip of the nose. The minimum pressure usually occurs at some point ahead of the maximum diameter, however, so that is is possible that, on small scale objects at least, cavitation occurs in the normal laminar zone. The bottom diagram in Figure 14 for the semi-ellipse illustrates this possibility. This should result in a transition to a turbulent boundary layer with a change in drag. In the case of large scale projectiles, the

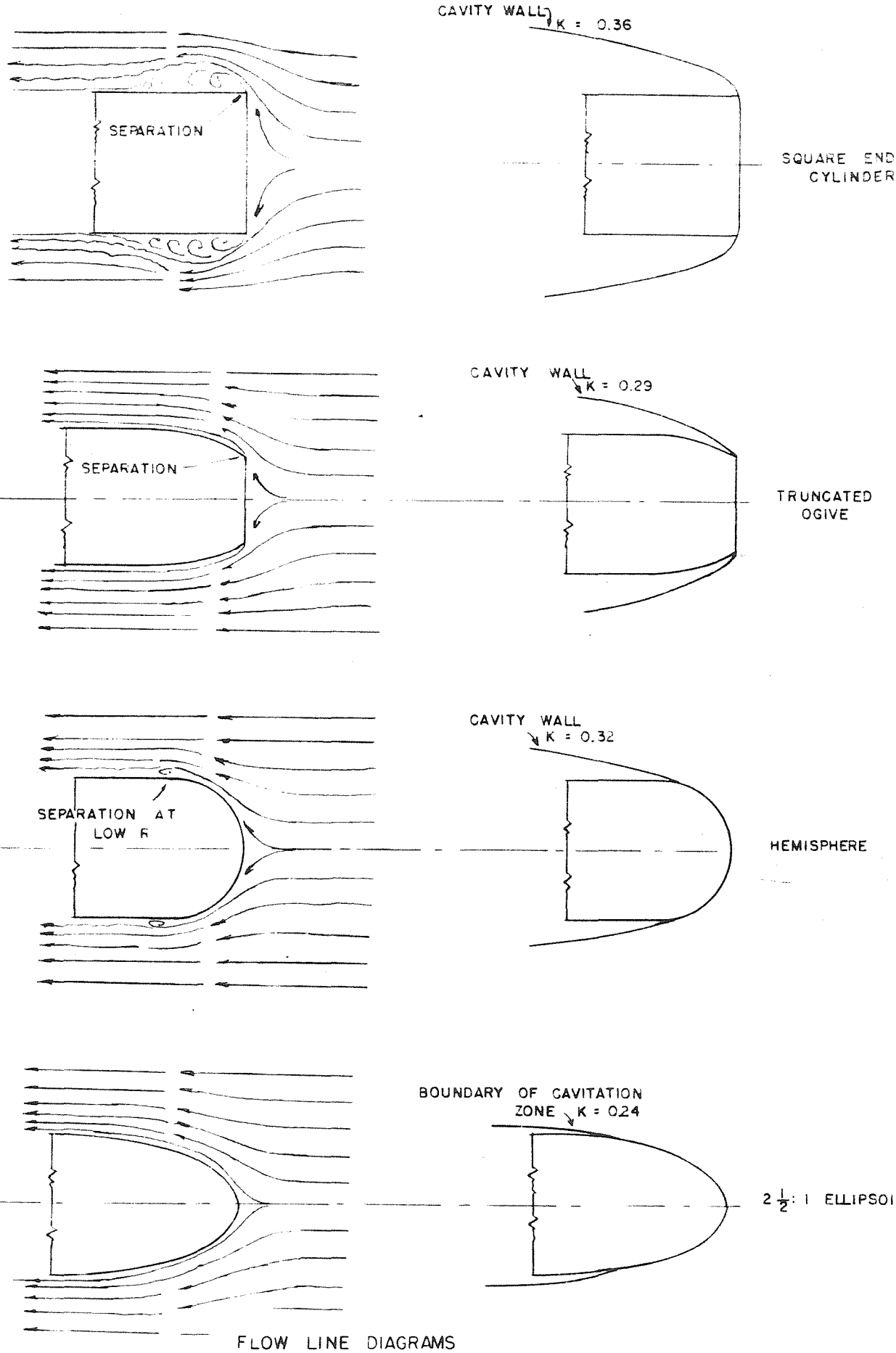

FLOW LINE DIAGRAMS
AND CAVITY SILHOUETTES

FIGURE 14

boundary layers for most velocities are almost always completely turbulent so that this condition is of secondary importance. Also, with increased "fineness", the type of cavitation changes to coarse grained so that, while turbulence is introduced, it is somewhat different from that formed by local separation and the analogy may not hold so closely.

As cavitation grows it effectively changes the shape of the body and thereby alters the form drag. Simultaneously, the skin friction should decrease because there is less high velocity fluid in contact with the surface. Ultimately, if the cavitation envelops the body completely, there remains only form drag due to the difference between the pressure forces on the small wetted area of the nose and the gas pressure in the bubble. The pressure distribution along the surface of the solid body is altered completely, while the effective body is enlarged by the extent of the cavitation bubble. The right hand diagrams in Figure 14 show the full cavity conditions for the noses already discussed.

The drag curve shown in Figure 9 for a projectile with a truncated ogive indicates a slight decrease in C_D with growth of cavitation. Professor Knapp has suggested (14) that with growth of cavitation the interplay between the increase in form drag and possible decrease in skin friction might result initially in such a decrease. A similar phenomenon has been measured in the case of some centrifugal pumps where measurable increases in head and efficiency have been observed when the pump impeller began to cavitate. (22)(23)

Drag in the Cavity

With a completely enveloping bubble such that contact with the water is made only over a small area at the forward portion of the body, skin friction can be neglected and the total drag can be assumed to equal the form drag. This assumption will certainly hold for Reynolds numbers greater than 10^4 on spheres, cylinders and blunter bodies. For more streamlined shapes skin friction will cause a small correction. Assuming the pressure is constant at all points in the cavity, the form drag is obtained by integrating the normal pressures

as follows:

$$D = \int_0^{\theta_s} P \cos\theta \, da - P_B A_w \tag{3}$$

where

P = the total pressure on the surface

= the static pressure in the undisturbed flow plus the pressure resulting from dynamic effects

$= P_o + P_D$

da = an element of area on the body surface

A_w = the wetted area projected onto a plane normal to the direction of motion

θ = angle between a surface element and a plane normal to the direction of motion

θ_s = angle between a surface element and a plane normal to the direction of motion at the point of separation of flow from the body

Noting that $\cos\theta \, da = dA$, and adding and subtracting P_o from the total pressure P, one obtains after simplifying

$$D = \int_{A_w} (P - P_o) dA + (P_o - P_B) A_w \tag{4}$$

Dividing by $\rho \frac{V^2}{2} A$

$$C_D = \frac{D}{\rho \frac{V^2}{2} A} = \frac{1}{A} \int_{A_w} \frac{P - P_o}{\rho \frac{V^2}{2}} dA + K \frac{A_w}{A} \tag{5}$$

where

A = the projected area of the maximum section of the body

The first term in equation (4) is the integral of the pressure intensity caused by dynamic effects. The second is merely the difference between the hydrostatic pressure in the undisturbed fluid and the bubble pressure. When converted into a coefficient as in (5) the first term becomes a function of the dimensionless dynamic

pressure distribution and the second a function of the cavitation parameter K. When K = 0 the limiting C_D equals the former. As the cavity decreases in extent with increasing K, C_D will increase primarily because of the increase in $P_o - P_B$. Usually the variation in wetted area and pressure distribution on the body will have a secondary effect. This trend persists until the cavity no longer envelops the body and hydrodynamic forces begin to act on the after portion as well as the nose or leading edge. Depending on the body shape and attitude with respect to the flow, the drag may increase somewhat farther. Finally, however, as the bubble becomes smaller and smaller, C_D must approach the normal cavitation free value. For streamlined objects, like most projectiles, this will be less than for the cavity stage. For non-streamlined objects, like a cylinder normal to the flow, the cavitation free drag may exceed the cavity drag.

Effect of Body Shape on Cavity Drag

To investigate the effect of body shape on drag in the cavity a series of measurements were made using models short enough to insure that the entire body could be completely enveloped by the cavitation pocket at the lowest value of K obtainable in the Water Tunnel. Six different noses on short cylinders with either a blunt afterbody or with an ogival afterbody were tested. The three basic types of nose shapes that were included were:

1. Noses tipped with spherical segments including the hemisphere, the MK 13, the 2.3 x 78° spherogive, and the 5 x 76° spherogive.
2. Blunt noses including the square end cylinder and the truncated ogive.
3. "Streamlined" noses typified by a 2 1/2:1 semi-ellipsoid.

Typical pictures of the cavities formed by these shapes are shown as viewed from the top and side of the tunnel working section in Figures 15 and 16. These photographs are not all for the same value of K nor for the same degree of bubble development. However, the essential features of the influence of nose shape can be seen,

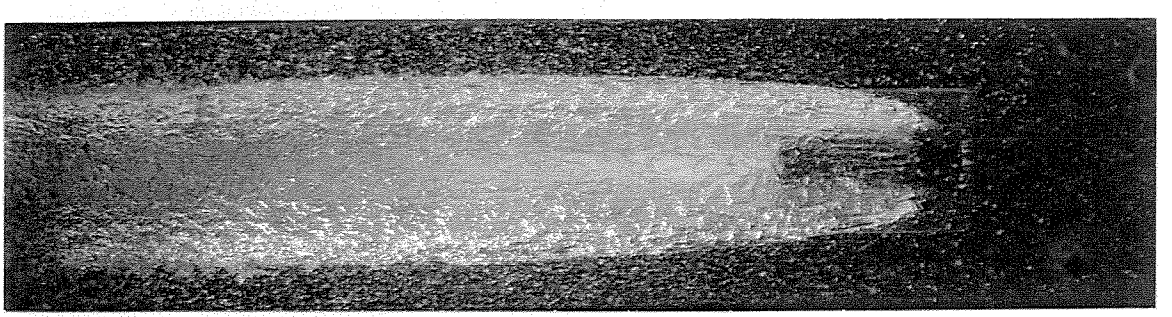

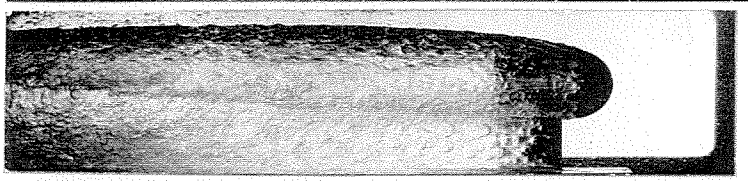

Hemisphere
K = 0.21

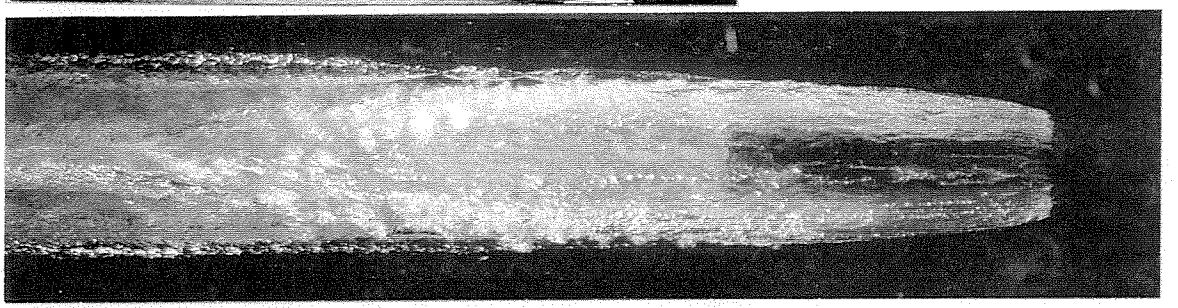

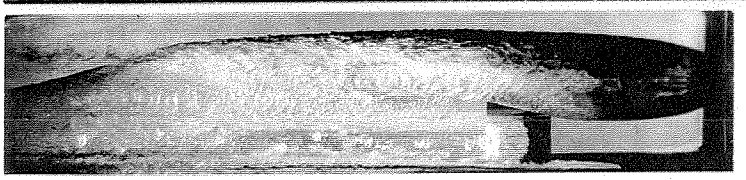

MK 13
K = 0.30

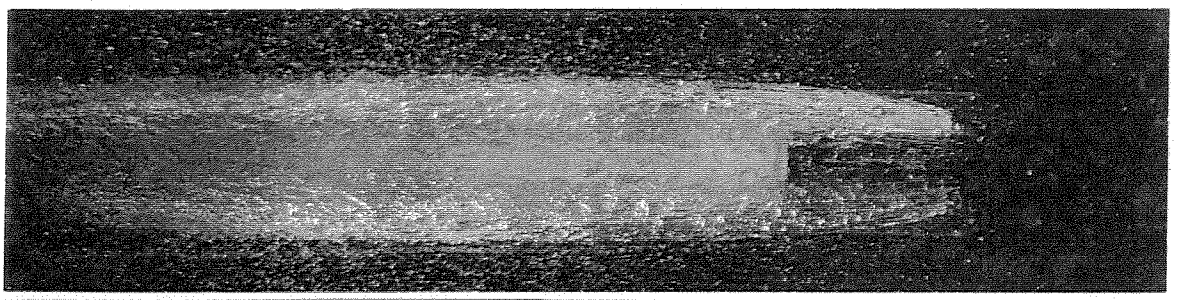

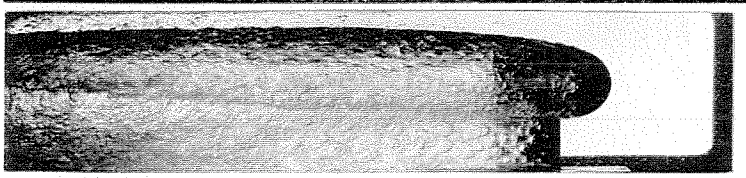

2.3 Cal. x 78° Spherogive
K = 0.27

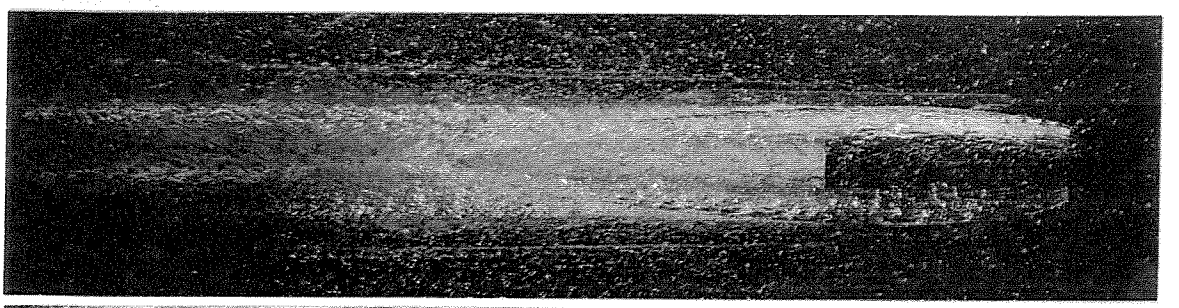

5 Cal x 76° Spherogive
K = 0.21

CAVITATION BUBBLES ON SPHERICAL TIPPED NOSES
$\psi = 0^\circ$
Figure 15

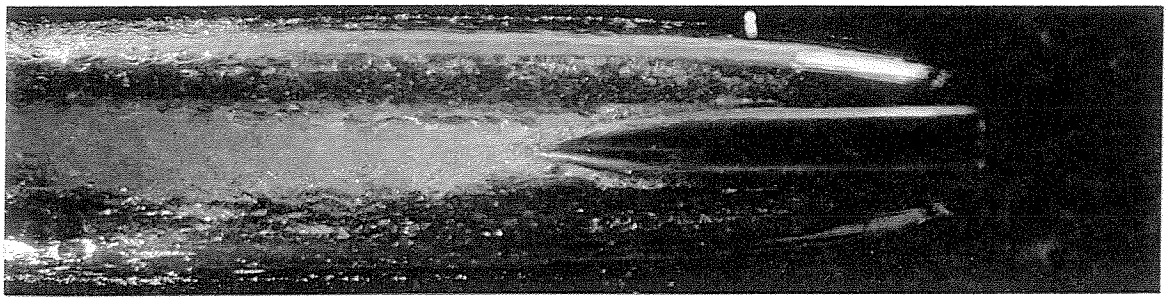

Square End Cylinder

K = 0.39

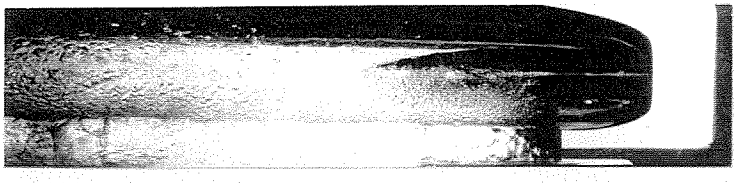

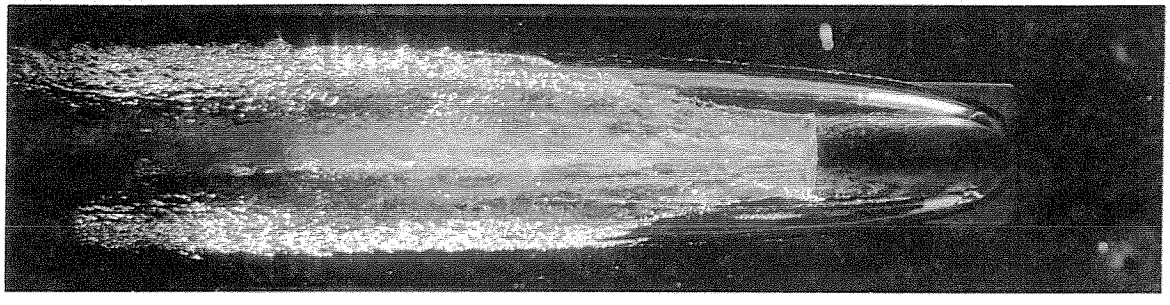

Truncated Ogive

K = 0.29

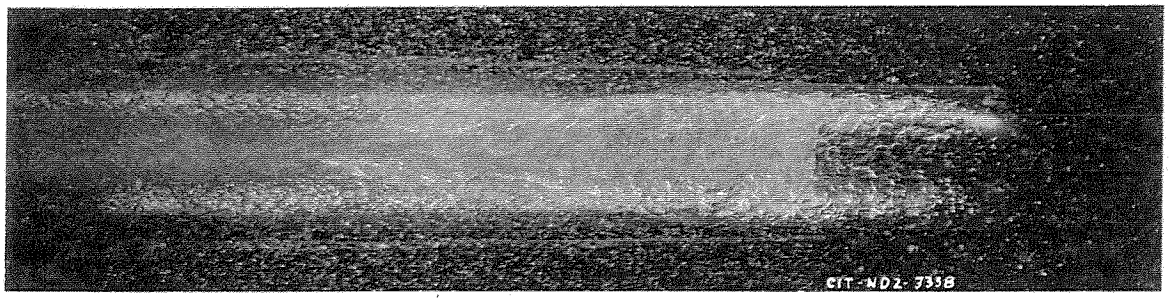

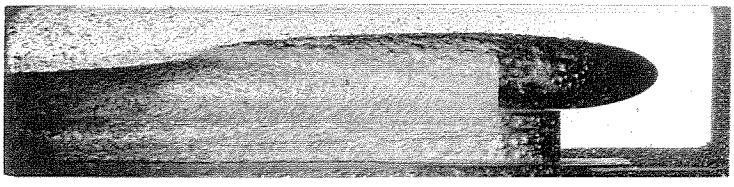

2 1/2:1 Ellipsoid

K = 0.24

CAVITATION BUBBLES ON

FLAT FACED AND ELLIPSOIDAL NOSES

$\psi = 0°$

Figure 16

since further reductions in K do not change the forward position of the cavity appreciably. In Figure 15 it will be noticed that for these models the cavity separates on the spherical tip so that the water is in contact with only a portion of the spherical segment. For the blunt noses shown in Figure 16 the cavity separates from the body at the sharp edge so that water is in contact with only the flat face of the body. For the semi-ellipsoid, also shown in Figure 16, the cavitation is the coarse grained type and clean separation is not obtained even though most of the body is enveloped so that only the nose proper is in contact with the water. The pictures also show the expected result that the cavity diameter increases with bluntness of the nose. Thus the square end cylinder produces the largest cavity, and the 5 x 76° spherogive or the 2 1/2:1 semi-ellipsoid the smallest. It is interesting to note that the truncated ogive produces a bubble about the same diameter as the hemisphere nose in spite of its bluntness. This is no larger because the diameter of the face is only 2/3 of a caliber and because, further, the edge of the flat face is rounded off to a small radius.

The measured values of C_D for these shapes are shown in Figure 17 plotted against the cavitation parameter K. Interest is centered mainly on the low K end of each curve which is shown by a heavier line to indicate that the body is completely enveloped in the cavitation bubble. On this same diagram are plotted calculated values for the square end cylinder and the hemisphere. These were calculated using Equation (5) above, and the measured pressure distributions on the surface of these noses as reported by Rouse (13). The calculated coefficients are extrapolated from the points indicated by crosses down to zero K.

For a given value of K, the measured magnitudes of C_D reflect the difference in bubble size already observed, the square end cylinder showing the largest and the 5 x 76° spherogive and the 2 1/2:1 ellipsoid the smallest. This is a necessary relationship since the cavity diameter is a measure of the momentum change imparted to the water as the nose pushes it aside and hence is proportional to the drag. C_D, then, is proportional to the cavity

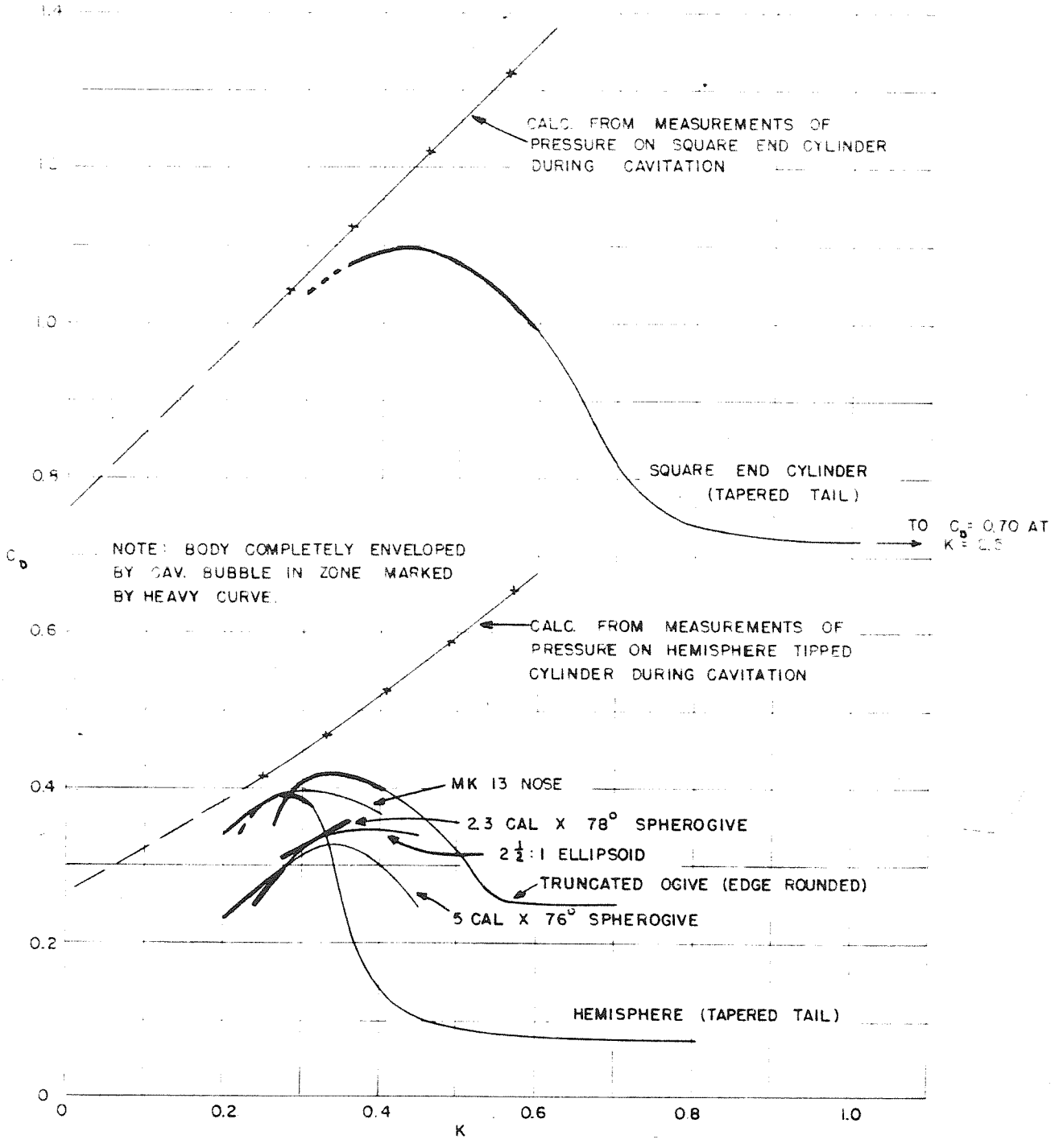

EFFECT OF NOSE SHAPE ON
DRAG IN THE CAVITY
$\psi = 0°$

FIGURE 17

diameter relative to the projectile diameter. This dependence of C_D on the bubble diameter does not hold, however, if one compares cavity sizes produced by the same projectile at different values of K. As K is reduced it is easier for a body to make a cavity because the momentum required is reduced in proportion to the pressure forces, represented by (P_o-P_v) which must be overcome. Consequently, C_D becomes smaller with reductions in K, even though the bubble grows larger.

The truncated ogive has a lower drag than would be calculated normally for the equivalent sized square end cylinder because of the slight rounding of the corner. Its drag coefficient is calculated to be about 50% greater with a sharp edge. In all cases, as the theoretical equation states, a reduction in drag with reduction in K is indicated once the body is completely enveloped. There is some difference at the lowest K shown for the MK 13 and the hemisphere, but the difference is small and within the probable margin of error of the experiments. The measurements for the hemisphere and the square end cylinder are both slightly lower than the calculated values. It is interesting to note that the calculated values extrapolated to K = 0 give C_D = 0.76 for the cylinder and 0.27 for the hemisphere.

The formation of an enveloping cavity has a particularly effective stabilizing influence on blunt nosed bodies. In both the cases of the square end cylinder and the truncated ogive the "bullets" tested were dynamically unstable in the water so long as cavitation was suppressed. The resultant oscillations about the support point loaded the model support system excessively. With the growth of cavitation, however, both bodies quieted down and with the formation of the full clear cavity shown in Figure 16 no oscillations existed and the hydrodynamic forces were uniformly steady.

Drag of a Cylinder in the Cavity

The two-dimensional case of a circular cylinder aligned with its axis normal to the flow was investigated also. A 3/4" diameter rod spanning the 14" diameter working section of the Water Tunnel was tested at 58 feet per second for a range of the cavitation parameter that assured a full cavity. A line made by inlaying a 0.010" wide copper strip extended along the length of the rod so that with the aid of the balance mechanism for "yawing" models, the rod could be turned about its axis and the angular position of the separation point observed. The measured drag coefficients and the observed angles of separation are shown in Figure 18. Photographs showing the end view of the spindle and the cavity outline as seen through the top transparent window of the working section, and simultaneous side views showing the length of the spindle are presented in Figure 19.

Examining the photographs first, it is seen that for the early stages of cavitation the bubble surface is opaque and milky, and is composed of the so-called "fine grained" cavitation. At a critical K of about 0.50, however, the cavity wall suddenly becomes clear and transparent. This is indicated by the glossy texture of the cavity shown in the bottom photograph. At the same time the width of the cavity is reduced somewhat, as can be seen by comparison of the top views for K = 0.51 and 0.50. Note also that the cavity boundary extending back from the point of separation at the cylinder is sharply defined by a clear cut line after the transition occurs. In the side view photographs the separation of the flow at the cylinder surface is indicated by the irregular line in the center of the high light. Ahead of this high light the forward portion of the cylinder is shown in dark relief, while downstream from the high light the cylinder is enveloped by the cavity and cannot be seen until the cavity wall becomes transparent as in the bottom photograph.

Reference to Figure 18 shows that the drag coefficient increases approximately linearly with K. It has a typical value of 0.6 when K = 0.75. As a rough approximation C_D at K = 0 can be obtained by extrapolating linearly. This gives C_D = 0.26. On the same curve

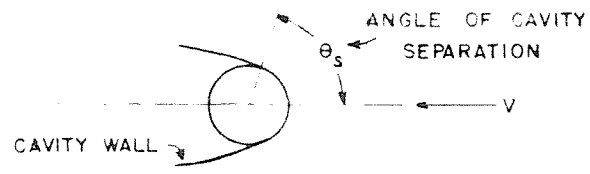

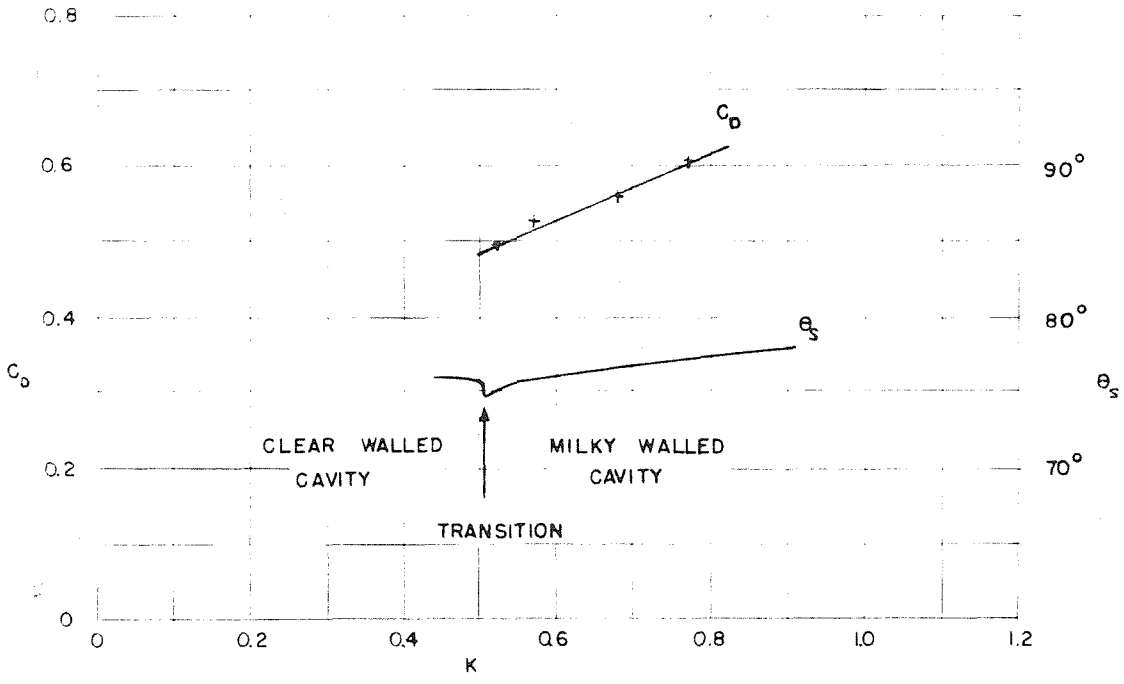

DRAG & ANGLE OF SEPARATION OF CAVITY

FOR

$\frac{3}{4}$" DIA. CIRCULAR CYLINDER

V = 58 FT/SEC

FIGURE 18

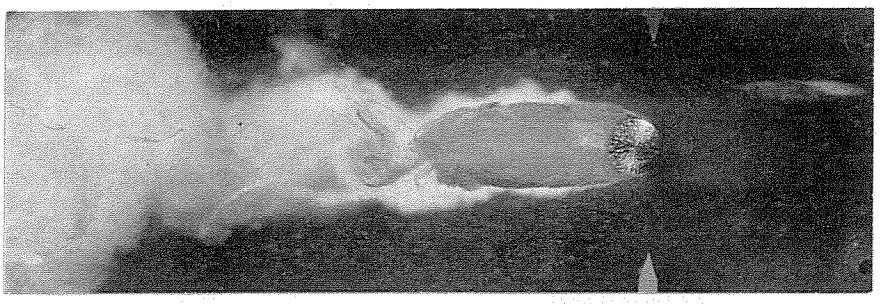

Top

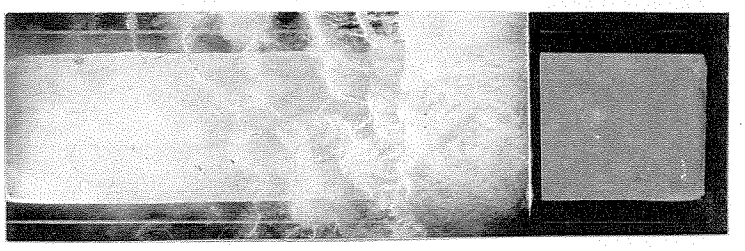

K = 0.77

Side

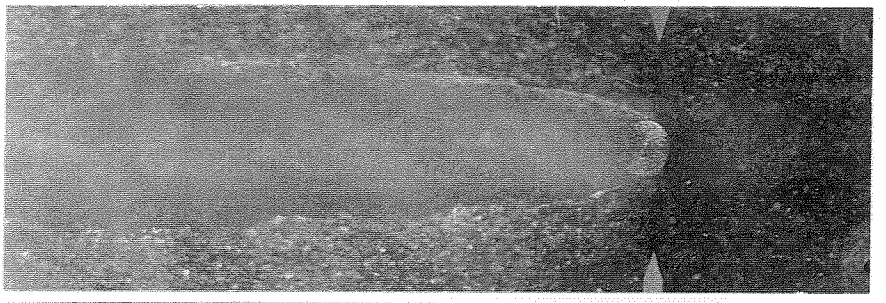

Top

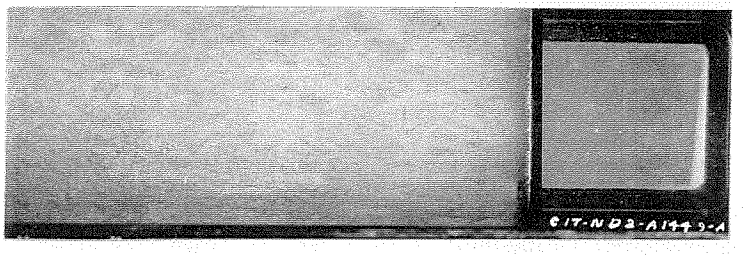

K = 0.51

Side

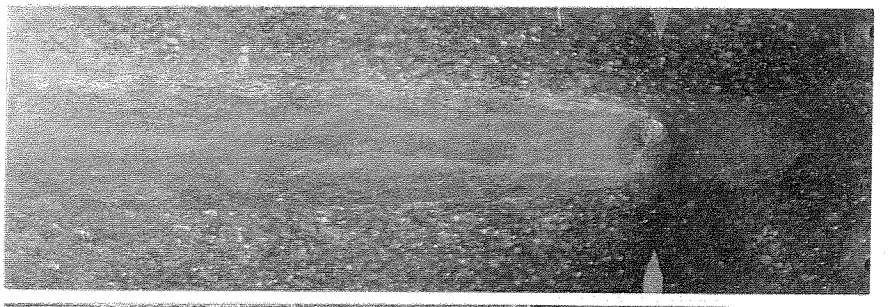

Top

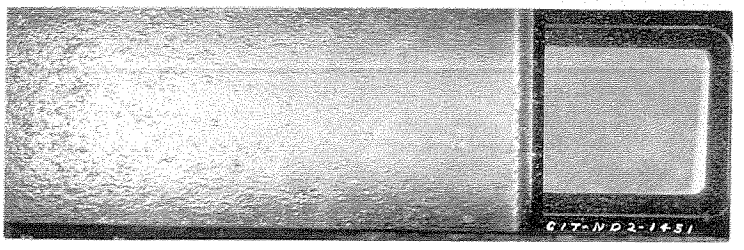

K = 0.50

Note transition to clear walled cavity

Side

3/4" DIA. CIRCULAR CYLINDER IN CAVITY

V = 60 FT/SEC

Figure 19

sheet the angle at which the flow separates from the cylinder surface is seen to shift forward slowly toward the stagnation point as K is reduced. However, at the critical point where the cavity wall was observed to become transparent the angle of separation shifts back again about one degree. The simultaneous decrease in cavity width must correspond to some reduction in drag. However, satisfactory measurements were not obtained for values of K below this because of the difficulty with the accumulation of air in the tunnel working section; so this point is not verified experimentally. It is probable that any change will be small, however, since the change in wetted area represented by the one degree shift in angle is less than one half of one percent, and the change in pressure distribution over the surface is probably not large. If the change is proportional to the decrease in cavity width, it will amount to 10% or 15%.

The numerical values of C_D are some 30% less than values calculated from pressure distributions measured under noncavitating conditions. In these calculations distributions obtained in a wind tunnel (14) at about the same Reynolds number were used and for the full cavity at K = 0 the separation of the flow was assumed to occur where the pressure equalled zero on the surface of the cylinder. For intermediate stages separation was assumed to occur at a pressure corresponding to the assumed difference between P_o and P_v. This method of calculation gives separating points which are much farther forward than those actually obtained. Since the drag coefficient must be proportional to the area under a curve of P versus sin θ, a smaller angle should give a smaller drag. Also, since in the actual case separation alters the pressure distribution and causes higher values just ahead of the separating point, the measured C_D should be more than C_D calculated from noncavitating pressure distributions, if the same separating point is assumed. The same reasoning holds at any other value of K in the range where a cavity can be obtained. Neither leakage past the free tip of the cylinder nor the effect of the boundary layer at the tunnel wall on both ends of the cylinder are considered sufficient to alter the two-dimensional

characteristics seriously. There is a small wall effect because the cylinder occupies 7.3% of the tunnel cross section. Also, the ratio of channel width to the cylinder diameter is 19:1 at the maximum section, but is reduced, of course, towards each end of the cylinder. The change is slow, however, so that all of the cylinder except the extreme end is at a good distance from the wall. Probably the boundary layer, which is of the order of one half inch thick, will have a predominant influence in this zone. Thom (25) reports that the presence of channel walls parallel to the axis of a cylinder causes a correction to the velocity of the order of one percent for a ratio of channel width to cylinder diameter of 20:1, and less than two percent for a ratio of 10:1. It is believed the Water Tunnel measurements are accurate within a margin of $\pm$ 5%, so the reason for this difference from the theoretical drag should be investigated further.

The measurements at 58 feet per second velocity were confined to cavitating conditions because without the cavity excessive lateral vibration of the cylinder prohibited operation at this high velocity. This was due to the alternating cross force resulting from the shedding of vortices of the Karman trail. With the cavity, however, completely stable conditions were obtained, permitting operation at even the maximum velocity of the Water Tunnel. To get to the high velocity without vibrations severe enough to damage the balance equipment, it was necessary to cause the cylinder to cavitate at low velocities and then to raise the speed while maintaining the cavitation bubble. An indication of the alternating force of the vortices generated for noncavitating flow is given by the observed lateral deflections of approximately 3/16" at 25 feet per second velocity. A uniform static load of about 8 pounds per inch, or a total of about 110 pounds, is necessary to cause this. With cavitation at 58 feet per second, as shown in the top picture of Figure 19, a deflection was observed only in the direction of motion. A maximum magnitude of the order of 1/4" (1/3 of the cylinder diameter) for a measured total drag of 150 pounds was obtained. The deflection in the direction of motion can be seen in the top views of the cylinder by comparing the position of its axis with the neutral position indicated

by a line drawn between the two arrow points. Note that the maximum deflection is obtained in the top photograph for the highest K. This deflection also accounts for the inclination of the cylinder observed in the side views.

Measurements were obtained for noncavitating conditions in a velocity range of 10 to 25 feet per second, or a Reynolds number range of 55,000 to 160,000. C_D was constant and equal to 1.13 $\pm$ 0.03. This agrees with published data on the drag of a cylinder of infinite aspect ratio.

B. The Cross Force and Moment in the Cavity

Effect of Body Shape on Cavity Cross Force and Moment

The spherical tipped noses shown in Figure 15 have the common characteristic that the cavitation bubble is formed by separation of the flow well forward on the tip so that water is in contact with only a portion of the spherical segment. As a consequence of this fact, the bubble shape should be independent of yaw as long as the after part of the body does not reach over and touch the cavity walls. Top views of these same noses are shown in Figure 20 yawed at 3°. Note that in each case separation occurs along a clean line normal to the direction of motion, and the resulting cavity, while displaced laterally as viewed from above, is symmetrical about a line parallel to the flow. In the case of the 5 caliber x 76° spherogive the cavity does not completely envelop the body, yet it retains its symmetry back to a point where it intersects the body surface.

In contrast, the shapes shown in Figure 16 all present an asymmetrical obstruction to the flow when yawed. Consequently, separation of the flow cannot occur symmetrically and the resulting cavity must be asymmetric. Yawed views of these noses in Figure 21 show this effect clearly. The cavities for the two blunt noses have trailing bubbles displaced slightly in the direction of yaw, while the ellipsoid has a trail of bubbles displaced slightly opposite the direction of yaw.

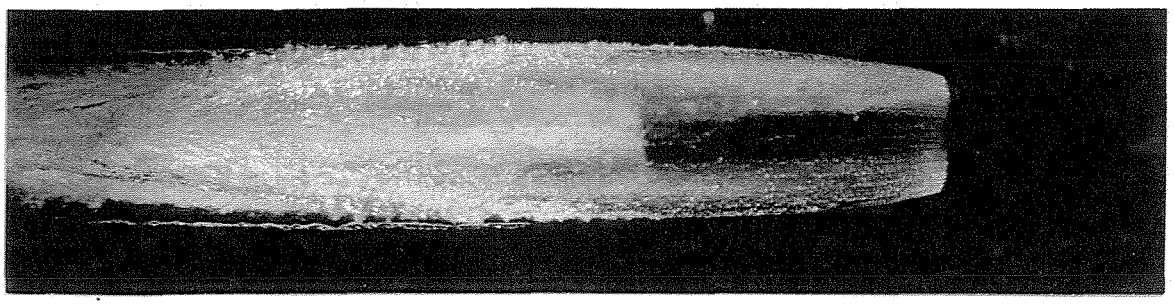

Hemisphere K = 0.30

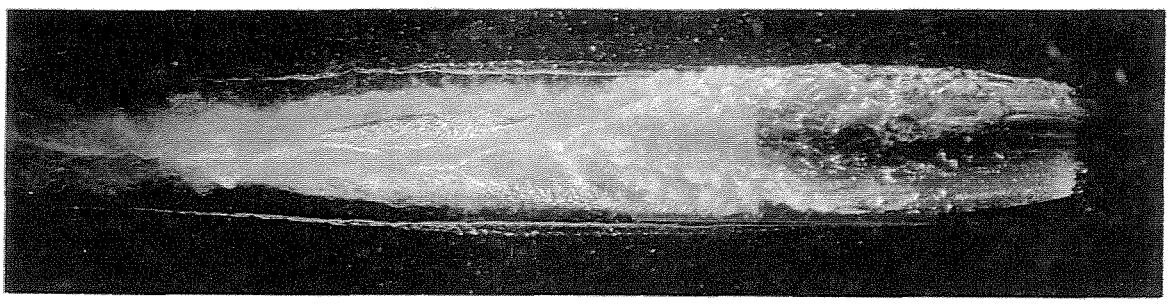

MK 13 K = 0.30

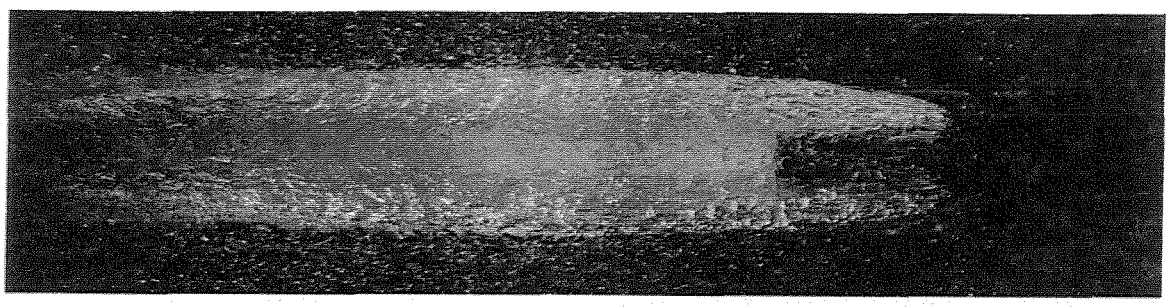

2.3 x 78° Spherogive K = 0.26

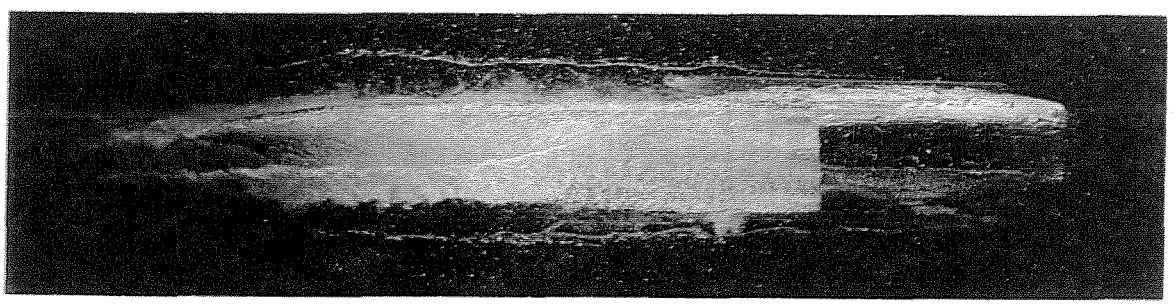

5 x 76° Spherogive K = 0.22

CAVITATION BUBBLES ON SPHERICAL TIPPED NOSES

$\psi = 3°$

Figure 20

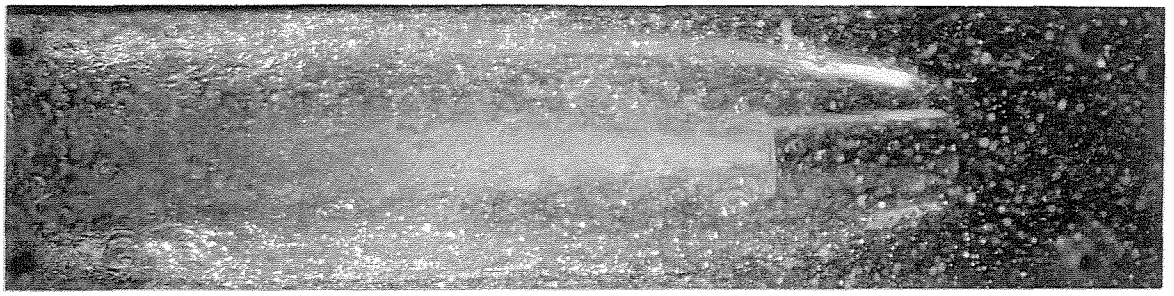

Square End Cylinder

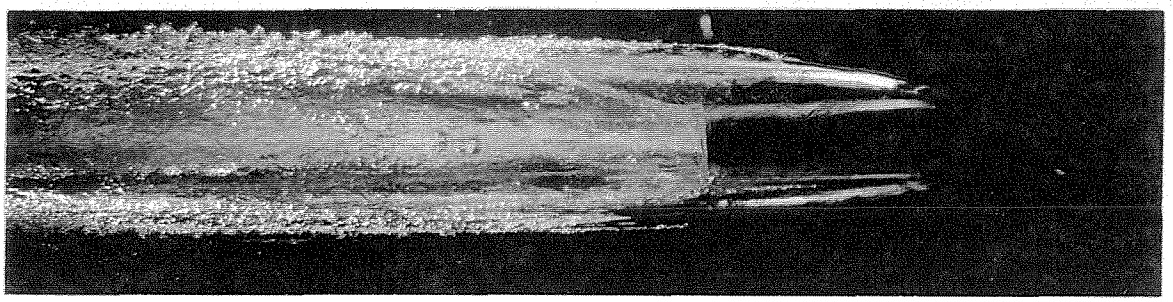

Truncated Ogive

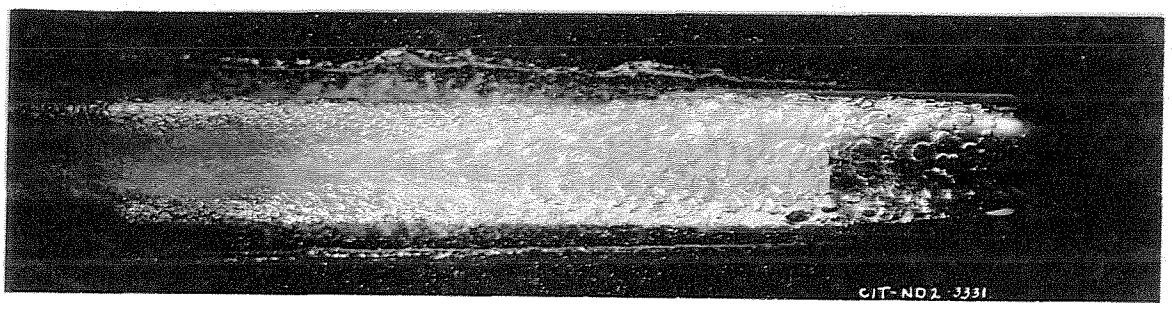

2 1/2:1 Ellipsoid

CAVITATION BUBBLES ON
FLAT FACED AND ELLIPSOIDAL NOSES
$\psi = 3°$

Figure 21

These characteristics are important in determining the hydrodynamic forces that will act on the body under yaw. Since the resultant force must be equal and opposite to the momentum change of the water deflected by the presence of the body, the symmetry or asymmetry of the cavitation cavities determines the existence and sense of moment and cross force. Thus, for the spherical tipped noses used in these experiments, the cross force should ultimately become zero and the moment should be due only to the drag vector acting through the center of curvature of the spherical segment forming the nose tip. On the other hand, a finite cross force should exist on the other noses, causing a definite upsetting or destabilizing moment in the case of the ellipsoid, with a stabilizing moment tending to counteract the destabilizing effect of the drag in the case of the blunt noses.

The cross force and moment coefficients measured for these noses are shown in Figure 22 plotted as functions of the cavitation parameter K. The moment coefficients are calculated for direct comparison with the coefficients for a projectile 7.18 calibers long with the center of gravity at 42% of the distance back from the nose tip. The data is not corrected for support interference effects because it was found that the effect, if any, on C and M was very small once the full cavity was developed. On the other hand, as the curves indicate, both C and M are much larger just before the cavity is formed than after. Since the values for other than the cavity stage are of significance only for indicating trends, no corrections were made.

In general, the trends shown by the curves as K is reduced and the test conditions approach a full cavity, verify the qualitative deductions just stated. The hemisphere nose on which a big cavity was developed at the Ks of the test shows zero cross force and a moment for normal cavitation-free operation of about 1/6 that of the reference projectile without fins, or about 1/3 that of the reference projectile with fins. This measured moment can be approximated with fair accuracy from the drag measurement. For the 2.3 caliber by 78° spherogive, the cross force is finite but very small,

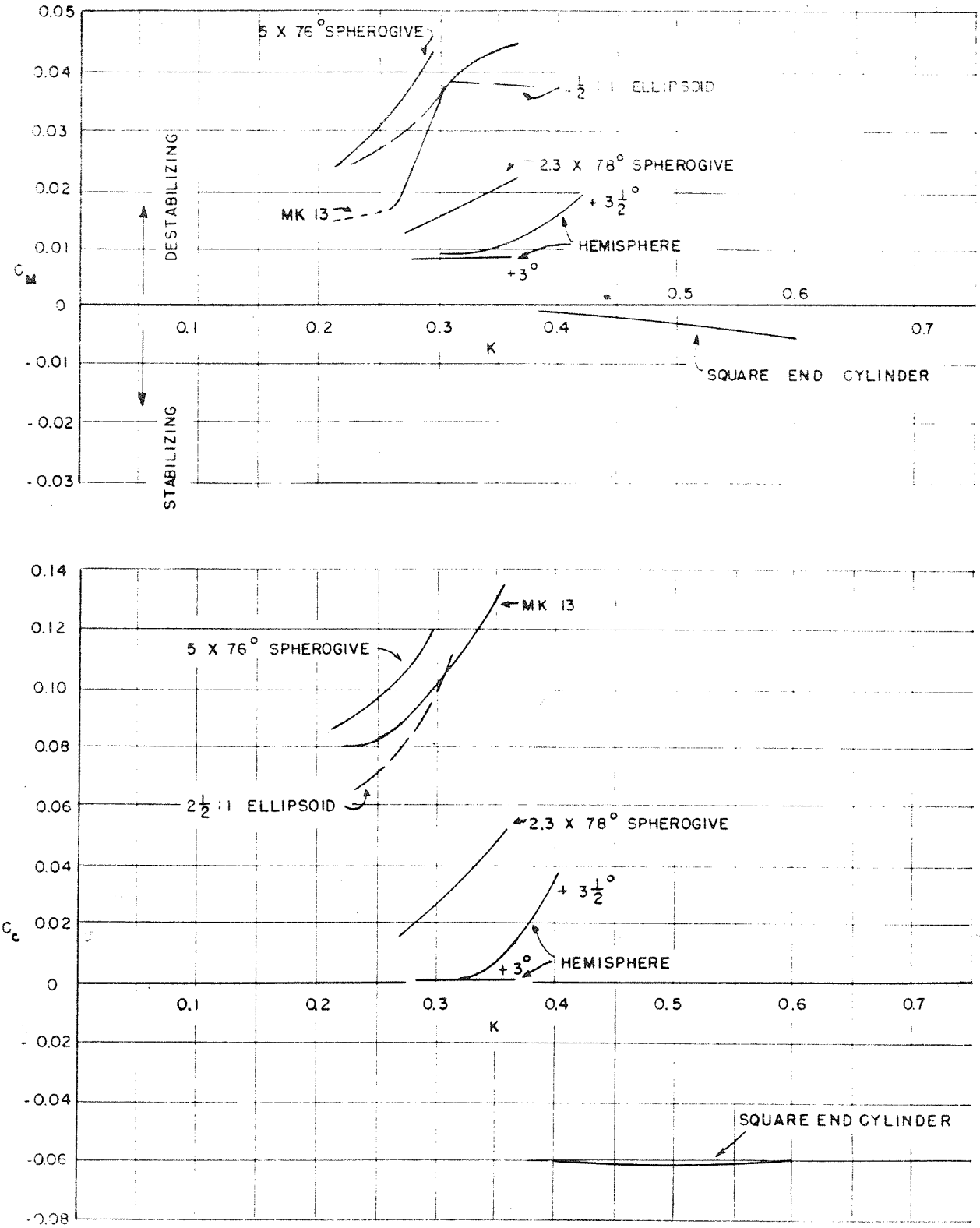

EFFECT OF NOSE SHAPE ON
MOMENT & CROSS FORCE IN THE CAVITY.

$\psi = + 3°$

FIGURE 22

and the moment is also reduced from the cavitation-free value of the reference projectile. Both C_C and C_M are decreasing rapidly with increasing bubble size so that in the light of the observed bubble symmetry in Figure 20, it is probable that C_C will eventually become zero.

For the other two spherical tipped noses, the MK 13 and the 5 caliber x 76° spherogive, both show relatively high cross force and moment. This is attributed to the extra length of these noses and the difficulty of getting a cavity large enough to assure no interference at points aft of the separation zone. This is especially severe in case of the spherogive because of its high resistance to the inception of cavitation. A similar result was obtained with the hemisphere nose when the "bullet" was elongated to the point that there was some question as to whether the cylindrical portion interfered with the cavity wall. By shortening the bullet, however, this was eliminated. It is not possible to assemble these two noses in shorter units so this is included with this reservation. The trend shown is consistent, however, with the symmetry of the cavitation bubble and C_C should eventually fall to zero for both units.

The 2 1/2:1 semi-ellipsoid nose also results in high C_C and C_M but for different reasons. While the cavitation pictured in Figure 21 is well developed, the cavity is not formed by clean cut separation as on the spherical tipped models. Instead, the "coarse grained" cavitation bubbles appear intermittently over a broad zone on the nose surface, and form a close fitting sheet over the surface of the body. In a sense, therefore, a cavity is not really formed on this shape. As a result, the trailing bubble is inclined to the direction of flow, and in light of this assymmetry, it is not expected that C_C will vanish or that C_M will be reduced to the low value shown for the hemisphere.

The square end cylinder produces both a cross force and moment that is stabilizing in effect. This is because the pressure on the flat face acts normal to the face and hence has a lateral component tending to reduce the angle of yaw. But for asymmetry in the pressure distribution across this face, the resultant vector would coincide with the axis of the cylinder and zero moment would result.

The existence of a small moment is an indication of a slight shift in the stagnation point in a direction opposite to the sense of the yawing.

The Cross Force and Moment on a Complete Projectile During Cavitation

It will be recalled that the projectiles pictured in Figures 11, 12, and 13 are equipped with three of the spherical tipped noses just discussed. Figures 23, 24, and 25 show additional pictures of these same projectiles for more advanced stages of cavitation. The same characteristics observed in the photographs of the short bullets are observed when these shapes are used with a full body. Separation occurs on the spherical segment along a clear line which is normal to the flow. Consequently, the bubble is formed with an initial symmetry. This symmetry is maintained back to the point where the body and tail sliced through the bubble interface. For the 5 caliber x 76° spherogive the higher resistance to inception of cavitation results in less bubble growth at the same value of K than for the hemisphere or the standard MK 13, so that at K = 0.25 the nose bubble is scarcely more developed than at K = 0.35 on the hemisphere. Even for the partially developed conditions shown, however, separation occurs along a line normal to the flow on the spherical tip of the nose.

Measurements of the cross force and moment coefficients for these three models are shown in Figure 26. Because these measurements include primarily the intermediate range between no cavitation and complete cavitation, corrections for support interference are necessary, if the results are to be compared with the corresponding values without cavitation. The results show that for the advanced stages obtained on the hemisphere and MK 13 noses, a zero or stabilizing moment is obtained. There is also a tendency for the cross force to be reduced. In these cases the stabilizing effect is caused by the tail and afterbody "biting" into the water and overcoming the very small destabilizing effect of the nose. The latter, according to the measurements on the short bullets, is, of course, reduced once most of the nose is enclosed in cavitation, thus contributing also towards a stabilizing trend. The curves also show

K = 0.35

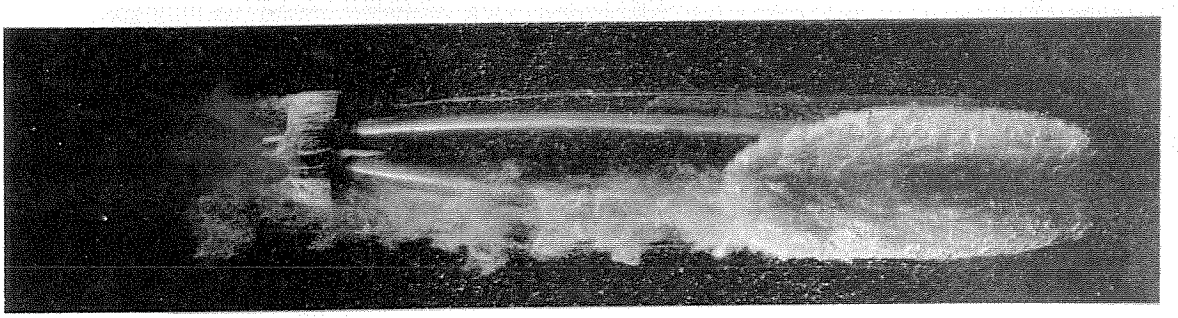

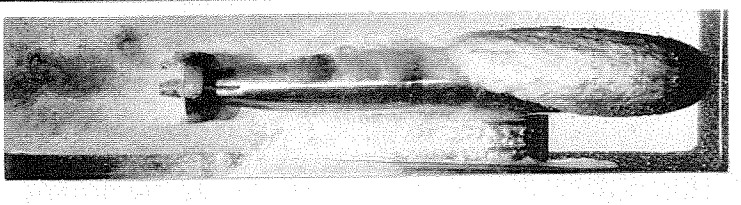

K = 0.30

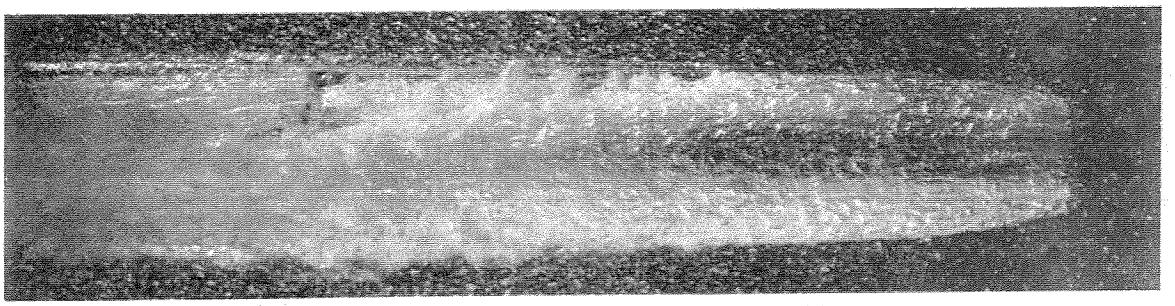

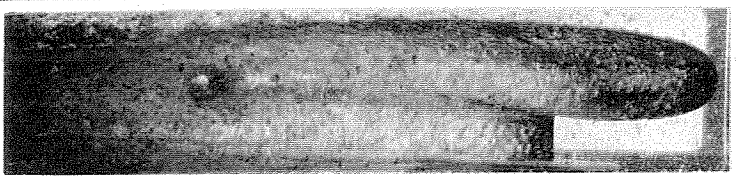

K = 0.26

HEMISPHERE NOSE

ON RING TAIL PROJECTILE

$\psi = 3°$

Top and side views

Figure 23

K = 0.35

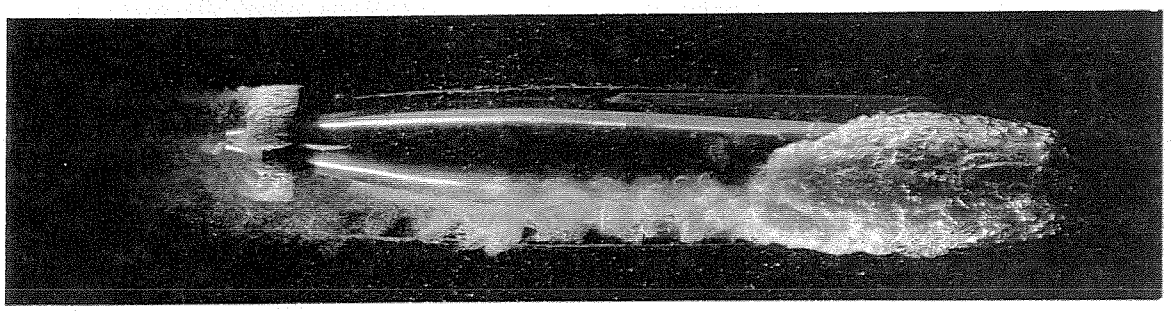

K = 0.31

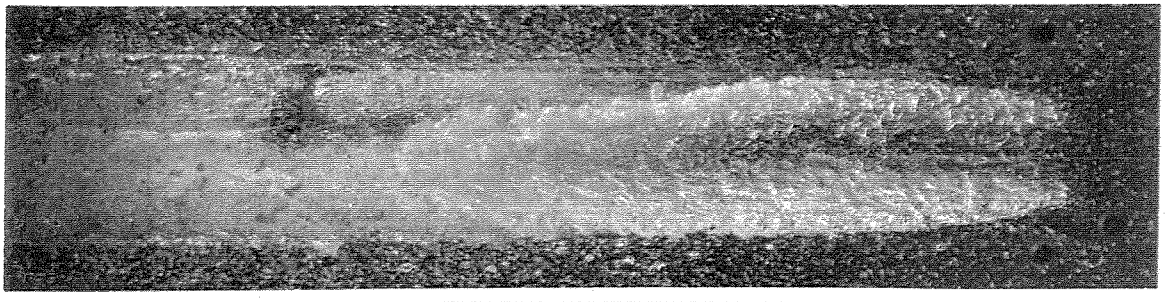

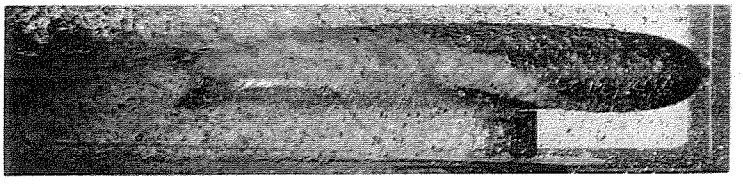

K = 0.22

STD. MK 13 NOSE

ON RING TAIL PROJECTILE

$\psi = 3^\circ$

Top and Side Views

Figure 24

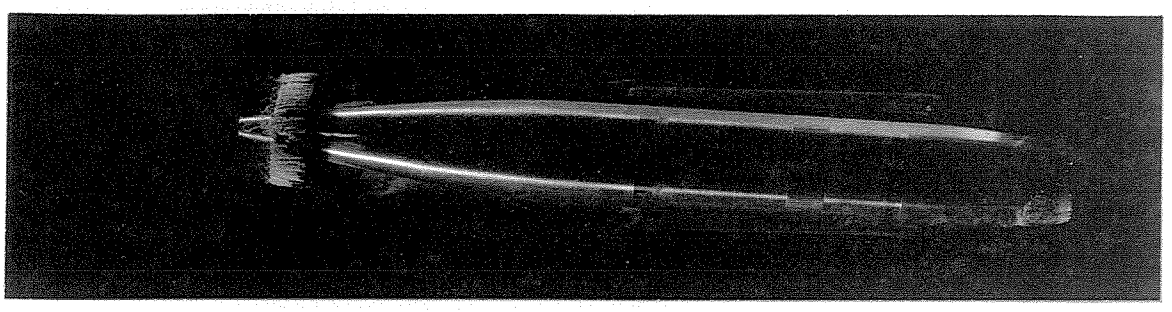

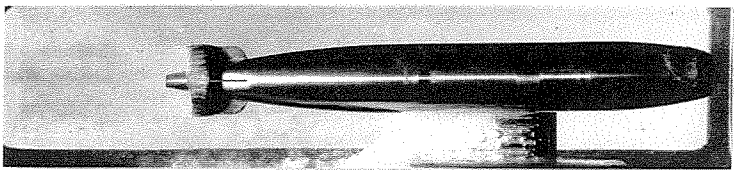

K = 0.35

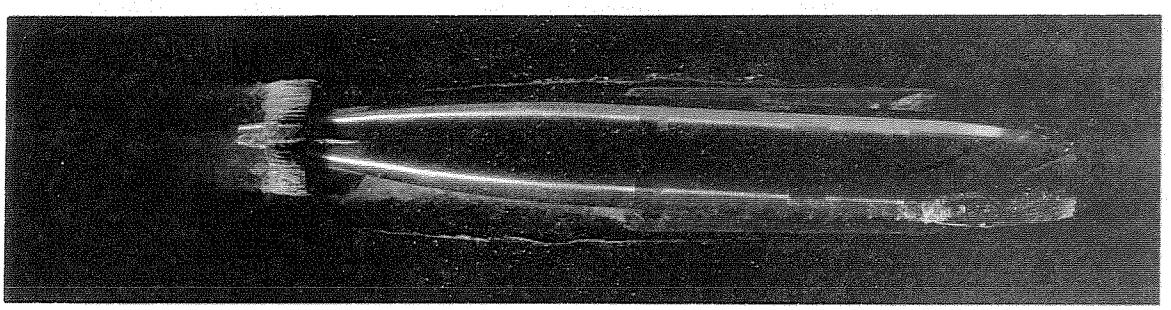

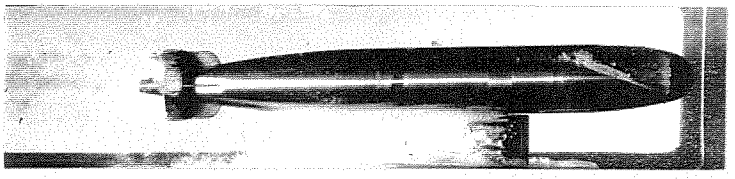

K = 0.31

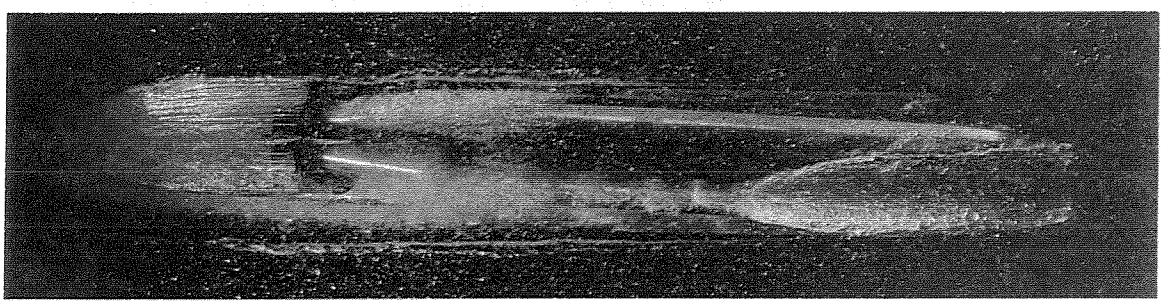

K = 0.25

5 CAL. X 76° SPHEROGIVE NOSE
ON RING TAIL PROJECTILE
$\psi = 3°$
Top and Side Views

Figure 25

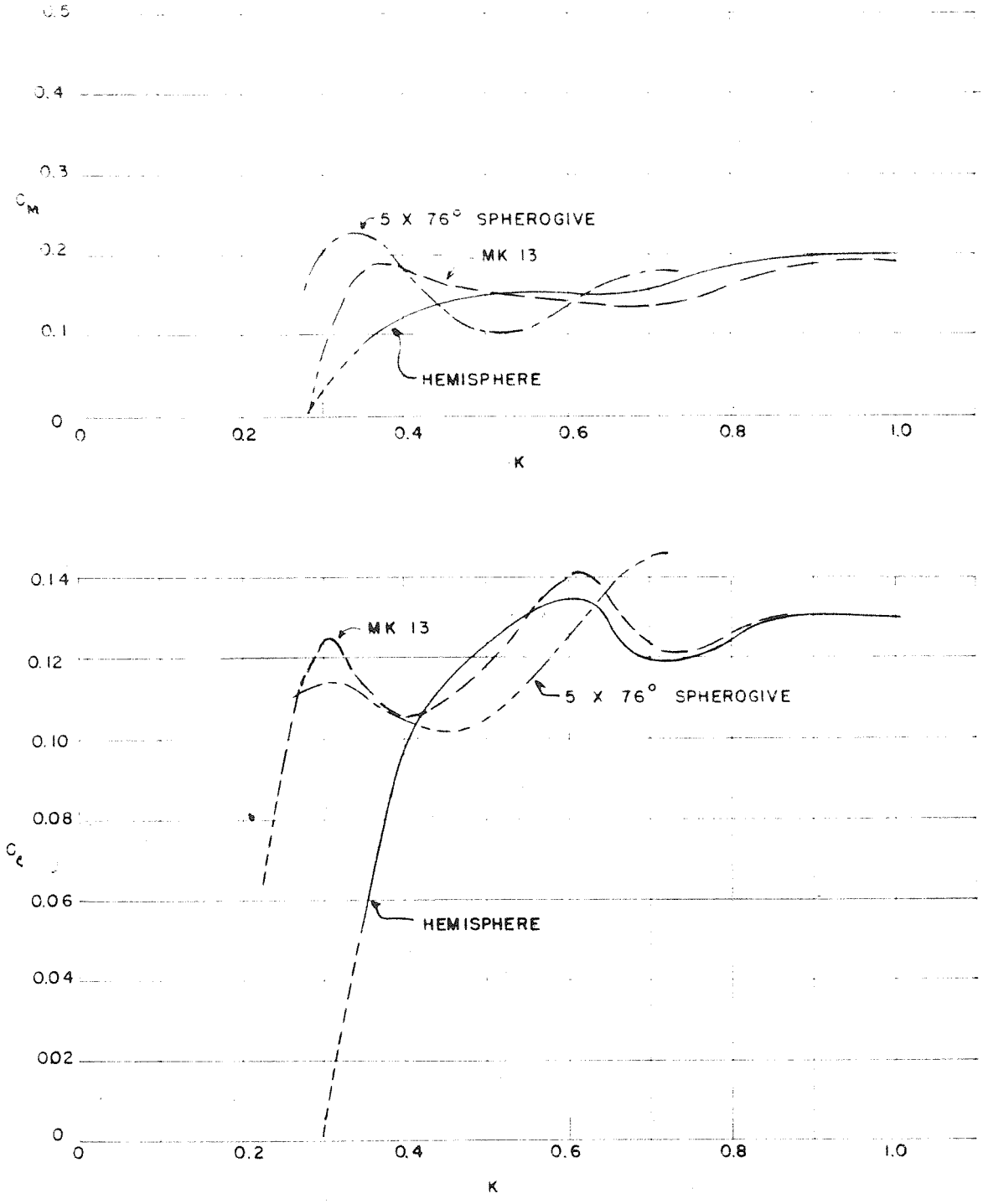

EFFECT OF CAVITATION ON CROSS FORCE & MOMENT
OF RING TAIL PROJECTILE WITH THREE DIFFERENT NOSES
$\psi = 3°$

FIGURE 26

a tendency towards a reduced cross force when the bubble is well developed. It will be noted by comparing the photographs in Figures 23 and 24 that a larger cavity is obtained on the hemisphere than on the MK 13 at the same values of K. Thus the hemisphere results in a more pronounced effect on the cross force and moment as shown. These curves extend to a high enough K to include also the noncavitating performance and the effect of the initial stages of cavitation on the performance. In the case of the hemisphere and the MK 13, both the cross force and the moment drop off with the onset of cavitation on the nose and/or the tail structure. As cavitation develops the cross force increases again to slightly above its noncavitating value. Apparently, there is a differential effect so that the increase is greater at the nose because the moment begins to increase slightly at the same time. With continued growth the distorted flow pattern causes a complicated additional fluctuation of both C and M until the cavitation envelops most of the body. At this stage the reduced moments and cross forces already mentioned are obtained. The curves for the 5 x 76° spherogive nose begin at K = 0.72 when cavitation is already formed on the tail structure. The nose does not begin to cavitate until K is approximately 0.42. At the lowest K of the tests and the maximum bubble development, Figure 25 shows that nose cavitation is still confined to the lee side of the body although there is strong cavitation on the afterbody and the tail. For these conditions both moment and cross force show a tendency to drop off. This is more pronounced in the case of the moment which is caused primarily by the high drag of the tail. Both the nose and tail cavitation, however, contribute to the reduction in cross force and, depending on the relative magnitude of their changes, may also cause less moment. This case is more difficult than the other two to analyze because there is so little cavitation on the body that the interference effects of the cavitating shield beneath assume more importance.

C. Summary of Observations and Conclusions

The main findings of the investigation of the forces and moments acting during cavitation are summarized as follows:

1. There is no sudden rise in the drag coefficient with the inception of cavitation.

2. Enough cavitation must develop to alter completely the normal flow pattern before the drag is affected materially. When this occurs the amount of cavitation as observed visually occupies an appreciable physical volume.

3. Between inception and the marked increase in drag the coefficient may increase slowly, may remain unchanged, and in some cases has been observed to decrease slightly.

4. A qualitative comparison between cavitation and separation indicates
   (a) For blunt bodies with severe separation under noncavitating conditions the appearance of cavitation does not immediately alter the flow pattern around the body, and hence introduces no immediate effect on C_D.
   (b) For other bodies with a normal boundary layer, cavitation and local separation both have the same basic effect on the flow in the boundary layer, and hence on the skin friction components of C_D.

5. As cavitation develops beyond the inception point the skin friction component is probably reduced because there is less high velocity fluid in contact with the surface. The slight decrease in C_D observed in one instance as cavitation develops beyond the inception point is probably caused by the skin friction decreasing at a faster rate than the form drag increases.

6. Drag is proportional to the change in momentum imparted to the water so that at a given value of K, drag in the cavity is proportional to the bubble size relative to the diameter of the body. For a given body, as K is reduced the cavity drag decreases, although the cavity size grows, because the momentum required to form the cavity is reduced in proportion to the pressure forces, represented by $(P_o - P_v)$, which must be overcome.

7. For the square end cylinder and hemisphere, C_D in the cavity agrees within a few percent with values calculated from the measured pressure distributions.

8. The effect of rounding the corner of the flat face of the truncated ogive is to reduce C_D in the cavity to about 2/3 the value calculated for a sharp edge.

9. Cross force and moment depend upon the cavity shape and hence upon the shape of the body at the point where cavity separation occurs.

10. With spherical tipped noses proportioned so that the cavity always separates on the spherical segment, not only at zero but at the maximum yaw, the cross force is zero independent of yaw, and the moment is caused by the drag only.

11. With other shaped bodies the cavity produced is asymmetric and a definite cross force exists. The sense of this cross force depends on the sign of the lateral momentum imparted to the water, and hence on the direction of the cavity asymmetry.

12. With a complete projectile a reduced cross force and a zero or stabilizing moment are obtained when most of the body is enveloped in a cavity but the tail projects through the cavity wall into the passing stream of water.

13. For intermediate stages between the above condition and no cavitation, the growth of cavitation alters both the cross force and the drag contributions from various parts of the projectile body.

The shift in magnitude, direction, and point of application of the resultant hydrodynamic force causes simultaneous variations in C_m.

D. Remarks on Application of Observation and Conclusions

The basic problems around which this research has centered have been connected with underwater projectiles and consequently applications of the results to this field are most direct. Consider first the normal underwater operation of high speed torpedoes. Cavitation is known to be detrimental and in the absence of definite information regarding the limits of its effect, every effort is normally made to keep the operating velocities below the cavitating value. It was shown that appreciable cavitation can be tolerated on typical torpedo shapes before the drag increases as much as 10%. In the examples shown in Figures 7 and 10 an increase of about 10 feet per second or 10% to 15% above the cavitating velocity was allowed. Thus it may easily be worth some sacrifice in power to boost the speed by such an amount. Of course, the simultaneous effect of cavitation on the cross force and moment can not be ignored. For example, normal operation with a negative buoyancy calls for an angle of attack to support the load. Since the torpedo shape with the hemisphere nose in Figure 10 showed about a 10% loss in cross force at 3° yaw for the same K at which the drag increased 10%, cavitation could cause difficulty in maintaining the proper depth. With the decrease in cross force (lift in the vertical plane), the depth mechanism would operate the rudders to give the body the increased angle of attack necessary to carry the load. This trend would persist until a new set of equilibrium conditions was obtained. Of course, more drag would result. Variations in the moment and cross force will result in other variations in maneuverability. For example, the

turning radius will be rather unpredictable if excessive cavitation exists, so that behavior on "angle shots" will not be consistent. The selection of shapes for the projectile components such that cavitation occurs as uniformly as possible on the lee and windward sides will tend to reduce the unbalanced effect on the hydrodynamic forces.

All these effects are particularly serious when the projectile operates without much submergence and K is correspondingly reduced. In fact, for very low submergence, cavitation will occur first on the top side of the projectile even with no angle of attack. A torpedo seeking depth can easily be subjected to intermittent cavitation as it rises and falls along its course and the resultant unbalance in hydrodynamic effect should certainly contribute to delay in reaching equilibrium conditions. It is possible also that cavitation of this type could aggravate the dynamic behavior of the projectile and make it break surface. Asymmetry of the projectile head in the vertical plane is a possible method of correcting this tendency to cavitate when running shallow.

Reference has already been made to the similarity of cavitation bubbles to the cavities obtained at air water entry. A basic difficulty in translating these results to entry problems is the unsteady character of the latter. However, qualitative conclusions can still be used to obtain some useful conceptions regarding the effect of shape and consequent cavitation development on the behavior at entry. The most obvious application is to the effect of nose shape in the cavity on cross force and moment, and hence on the tendency of the projectile to yaw and drift. The spherical tipped noses, of which the spherogive series is typical, have the special properties of resulting in zero cross force if proportioned to assure separation of the cavity on the spherical segment. In this case the only moment is that due to drag. Blunter noses, it was observed, actually produce a large stabilizing cross force and a resulting moment that overcomes the effect of the drag to give a net stabilizing moment. It should be possible to design a nose shape slightly blunter than a hemi-

sphere which would produce a similar effect and make C_M stabilizing or equal to zero with a desired yaw range. Cavitation characteristics at inception and the early stages of development which are better than those of the hemisphere have been obtained for a shape differing only slightly in size or volume from a hemisphere by making the slope and curvature of the surface profile continuous. With judicious treatment of the profile up to the zone of separation at least good results should also be obtainable for the cavity stage. The insensitivity of moment and cross force to yaw will contribute toward less sensitivity to yaw or pitch at entry, and tend to reduce deflections from the set trajectory during the cavity stage.

Of course, any nose shape should be investigated for its behavior on impact at entry, since the projectile breaks the surface with one side of its nose, resulting in a nonsymmetrical cavity and nonsymmetrical forces in this stage. However, qualitative conclusions for this condition can be obtained also from steady state cavitation data since, neglecting the additional apparent mass effects, the sense and point of application of the resultant forces on impact must be the same as the corresponding forces measured with a large cavitating bubble. If the launching conditions are such that the whip induced on impact is serious, the shape of the initial cavity formation, and hence the forces acting on the projectile, can be modified by changing the nose shape. This procedure has been tried on a preliminary scale on full size torpedoes.

The existence of moment and cross force in the cavity results in two well known effects. First, the moment causes the projectile tail to go to one side of the cavity where it sticks through the bubble until enough stabilizing moment is built up to offset the destabilizing moment from the nose. Second, the cross force produces a lateral motion of the center of gravity and causes a curved trajectory. Bowen (26) has reported that for even long projectiles the resultant curve is dependent primarily on the nose shape. Hemispherical noses cause little cross force and the

curvature is practically infinite. Noses with sharper ogives than 2.0 calibers result in large cross forces and short radii of trajectory curvature. The beneficial effect on drag in the cavity of reducing the area contacted by the water is well known. This idea has been applied to blunt nosed projectiles particularly where the reduction in drag is appreciable. Spherogives and other combination forms can be used to produce the same effect with basically low drag shapes.

The loss of lift and increase in drag associated with the onset of cavitation is a serious problem in applications to lifting surfaces of various types. The fixed and adjustable guide surfaces on projectiles, submarines, and surface ships are vulnerable to cavitation, particularly for conditions of yaw such as obtained during a maneuver. The shroud ring tail on the typical torpedo already discussed is one example. Movable rudders of course are the most likely to cavitate, and in some cases can be rendered quite ineffective by large cavitation zones. In general, it is probable that there will be less loss in lift if the cavitation is of the "coarse grained" type and the development of a full cavity on the low pressure side of the surface can be avoided.

Pumps, turbines, and propellers are basically "lifting surfaces" that are also subjected to cavitating conditions. In general, cavitation causes a loss of head or thrust and torque. However, as already mentioned, an actual increase in head, torque, and efficiency has been observed with the onset of cavitation in some radial flow type pumps. As was noted, it has been suggested that this effect is caused by a slight reduction in skin friction as cavitation grows. The effect of vane shape, of course, controls this behavior, just as in the case of the three-dimensional bodies investigated. Shaping the vanes to give coarse grained cavitation should prove beneficial on two counts. First, inception should be delayed, since it was the higher resistant forms that gave this type of bubble formation. Second, with the more advanced cavitation there probably will be less loss in "lift" on the blades.

In the case of pumps and turbines, the "lattice" effect of the vanes will modify the cavitation behavior over that obtained

with a single blade. The modifications are similar to "wall effects" obtained in the Water Tunnel tests, but of greater magnitude. The main deviations will be in the advanced stages of cavitation where the vapor occupies an appreciable volume of the total between blades, and hence seriously restricts the water passage. For the initial stages the conceptions presented here of incipient cavitation's effect on the boundary layer and/or the general flow around the blade should apply with good accuracy.

III CAVITATION FROM UNDERWATER BODIES

In the acknowledgements it was noted that the following section of this thesis is taken from a confidential report of research sponsored by the National Defense Research Committee. The report (3) includes a description of the acoustic equipment used for the experiment, and a discussion of the results of measurements of noise from underwater bodies. The latter material represents the writer's primary responsibility and is included in full here. The measuring equipment for which Mr. H. Shapiro, Dr. W. H. Pickering, and Mr. H. S. Baller are responsible, is described in detail in reference (3).

A. Purpose of Investigation

The central purpose of this study was to determine the variation of supersonic noise emitted with the formation of cavitation on underwater bodies of different shapes. The following section describes a series of measurements using sound focusing reflectors in conjunction with the hydrophone, and includes discussions of:

1. Measurements of the variation in noise emitted with the beginning and growth of different types of cavitation.
2. Location of the source of noise during cavitation.

B. Apparatus

The basic sound measuring equipment, as described in reference (27), is designed to amplify the output of a detecting hydrophone in selected frequency ranges and to indicate the amplified voltage on a meter. With the use of high and low pass filters, various bands in the 5 to 100 KC range can be chosen. The measurements described here were all made in the 20 to 100 KC range.

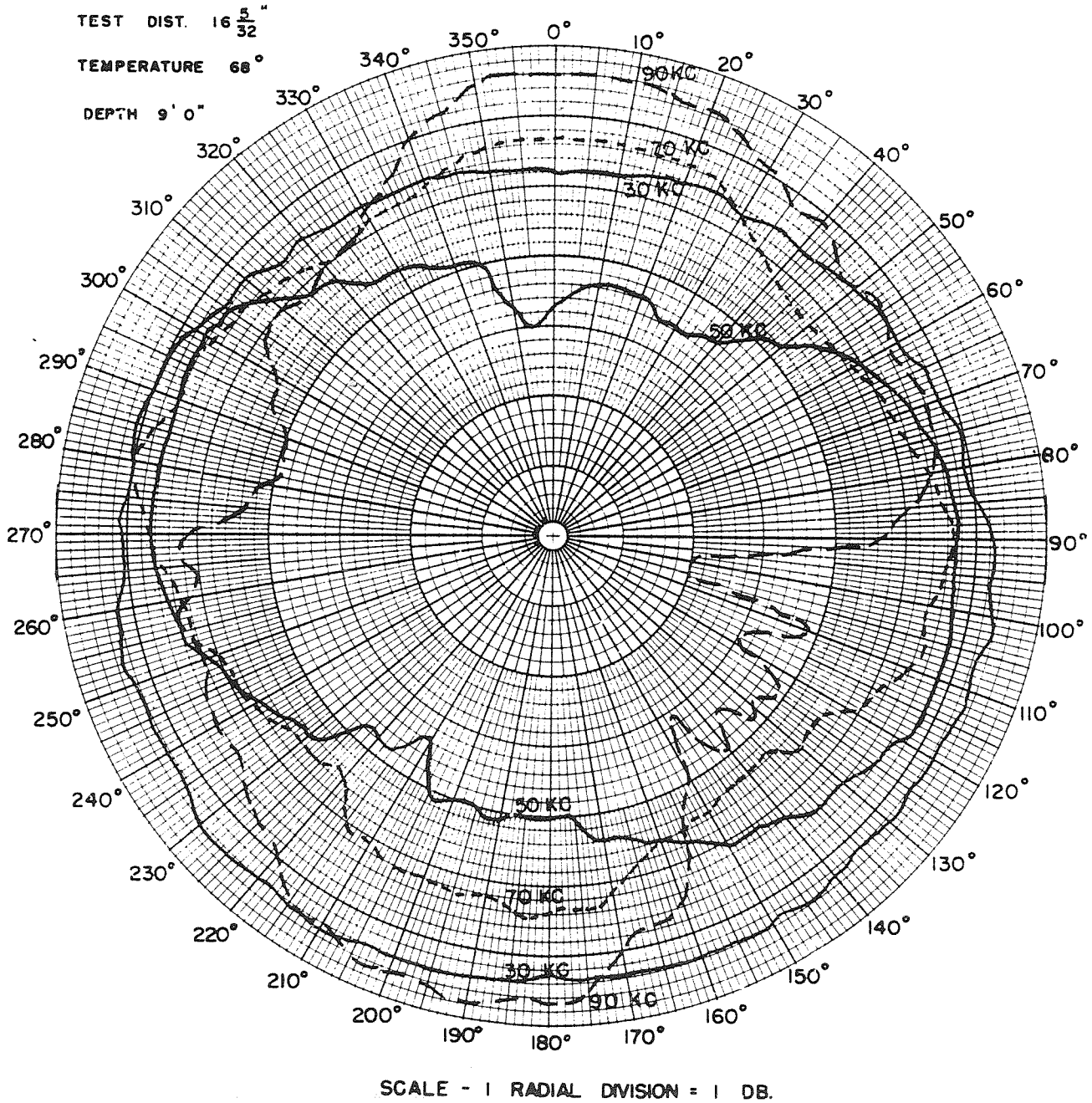

FIG. 27 C-11A HYDROPHONE

DIRECTIVITY PATTERNS IN PLANE NORMAL TO HYDROPHONE SPINDLE

Data from Tests by University of California Division of War Research. See Reference (28)

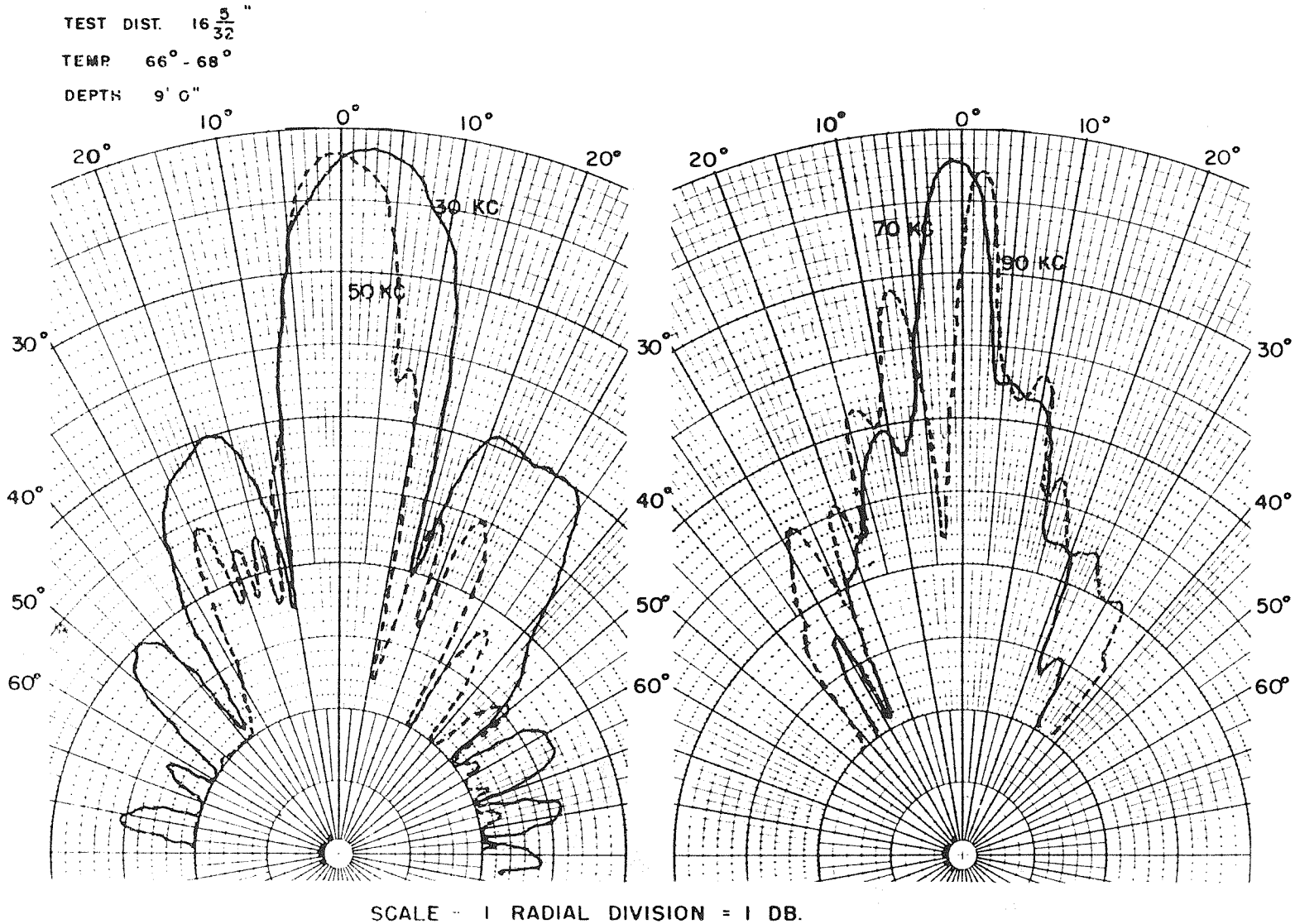

SCALE - 1 RADIAL DIVISION = 1 DB.

FIG. #28 C-LIAL HYDROPHONE WITH ELLIPSOIDAL REFLECTOR
DIRECTIVITY PATTERNS IN PLANE NORMAL
TO HYDROPHONE SPINDLE

Data from Tests by University of Calif ...
... Research. See Reference (28)

The hydrophone was used with focusing reflectors or "mirrors", and the hydrophone and mirror assembly was submerged in a water-filled tank which was attached to the side of the working section. Noise originating at the cavitating body in the tunnel was transmitted through a water medium, continuous except for a lucite window, to the reflecting mirror and back to the hydrophone. Provisions were made for moving the hydrophone and mirror so that the focus could be adjusted to pick up noise from any point in the tunnel working section. Spherical and ellipsoidal reflectors were used. The reflecting surface was formed for the former by a coating of sponge rubber with non-intercommunicating air pockets, for the latter by an air pocket between two concentric copper shells. The focusing effect obtained is shown by the typical directivity characteristics in Figures 27 and 28 of the hydrophone alone, and the hydrophone with the ellipsoidal reflector. A detailed description of the reflectors and a complete discussion of their characteristics will be found in references (3) and (28).

C. BACKGROUND NOISE

The measurements of sound from cavitating projectiles in the tunnel working section include, of course, a certain amount of "background" noise generated by the tunnel flow circuit and its mechanical drive. To be sure that over the frequency range of interest the magnitude of this noise was small relative to the cavitation noise, a series of measurements was made without the model or its supporting strut in the working section. With the hydrophone-mirror assembly focused on a fixed point on the tunnel axis, noise was measured over a wide pressure range for different constant velocities.

EFFECT OF VELOCITY AND PRESSURE

The typical curves shown in Figure ~~15~~ 29 illustrate the magnitude of the background noise and the effect of velocity and pressure on the noise. In this figure measurements for velocities of 40 to 70 feet per second are plotted as a family of curves of sound pressure in dynes per square centimeter (with linear decibel scale) vs. the cavitation parameter, "K". The data were obtained from two sets of tests, both with spherical mirror and with the sound filters set to include the entire 20 to 100 kc band. These curves show the same characteristic trends as were obtained by the

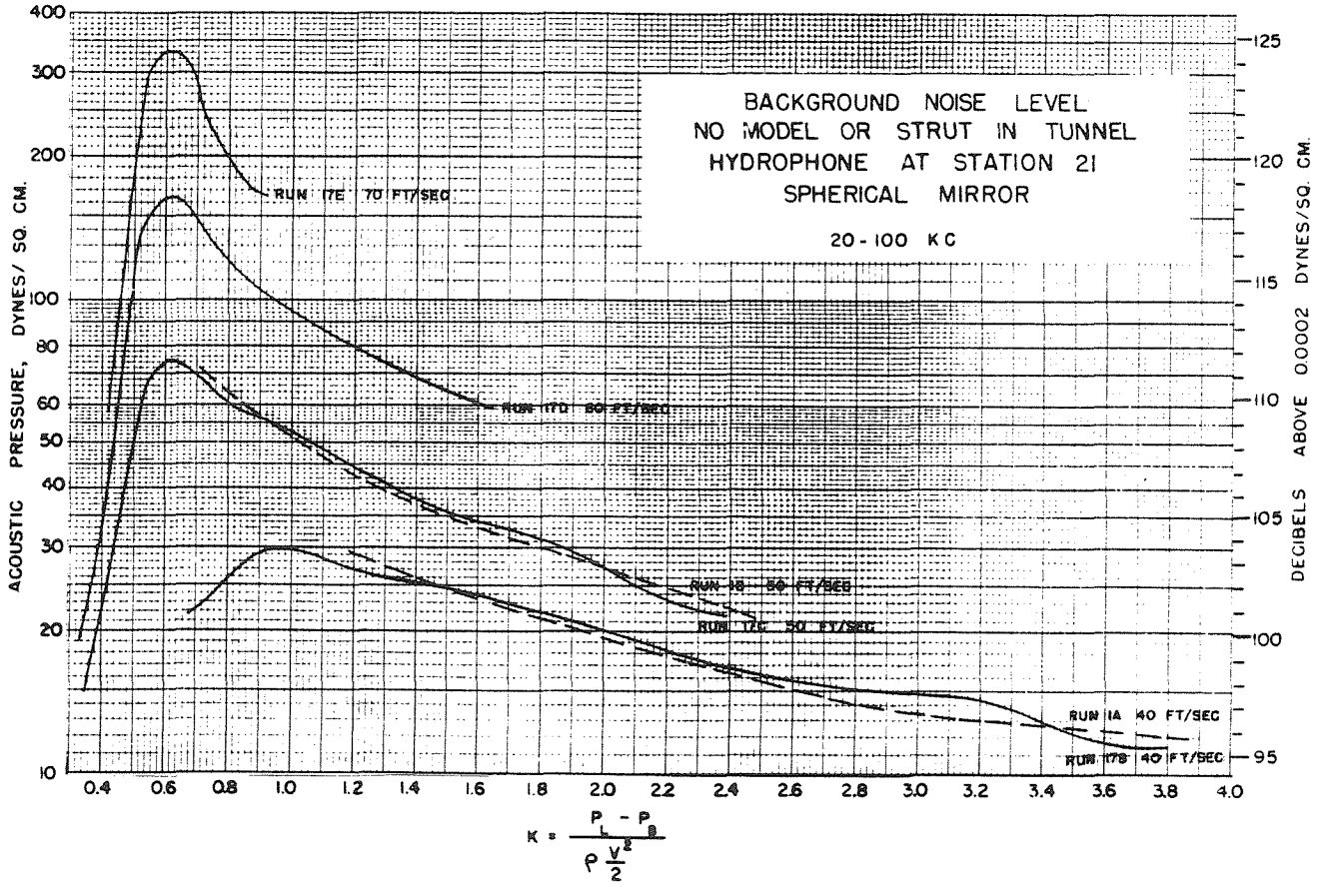

Figure 29

earlier measurements without a reflector described in Reference (28). For each velocity, as the pressure is reduced from an initially high value, the increased tendency for flow separation and cavitation in various parts of the flow circuit caused an increase in noise until at a low K a peak is reached and the level drops off. The sudden reduction in this figure coincides with cavitation in the contracting nozzle at the entrance to the working section, and an accumulation of vapor and air bubbles which clouded the working section.

EFFECT OF TUNNEL CIRCUIT VARIABLES

The data plotted in Figure 29 could be duplicated as long as tunnel conditions remained the same. However, changes in the condition of the circulating pump, changes in relative settings of the valves in the pressure control circuits auxiliary to the tunnel, and, of course, any change in the flow circuit itself, caused some variation in the magnitude of the background noise. Differences of as much as 10 db have been observed for the same combination of these variables. Figure 30 shows the results obtained with the spherical mirror assembly but at a later date than

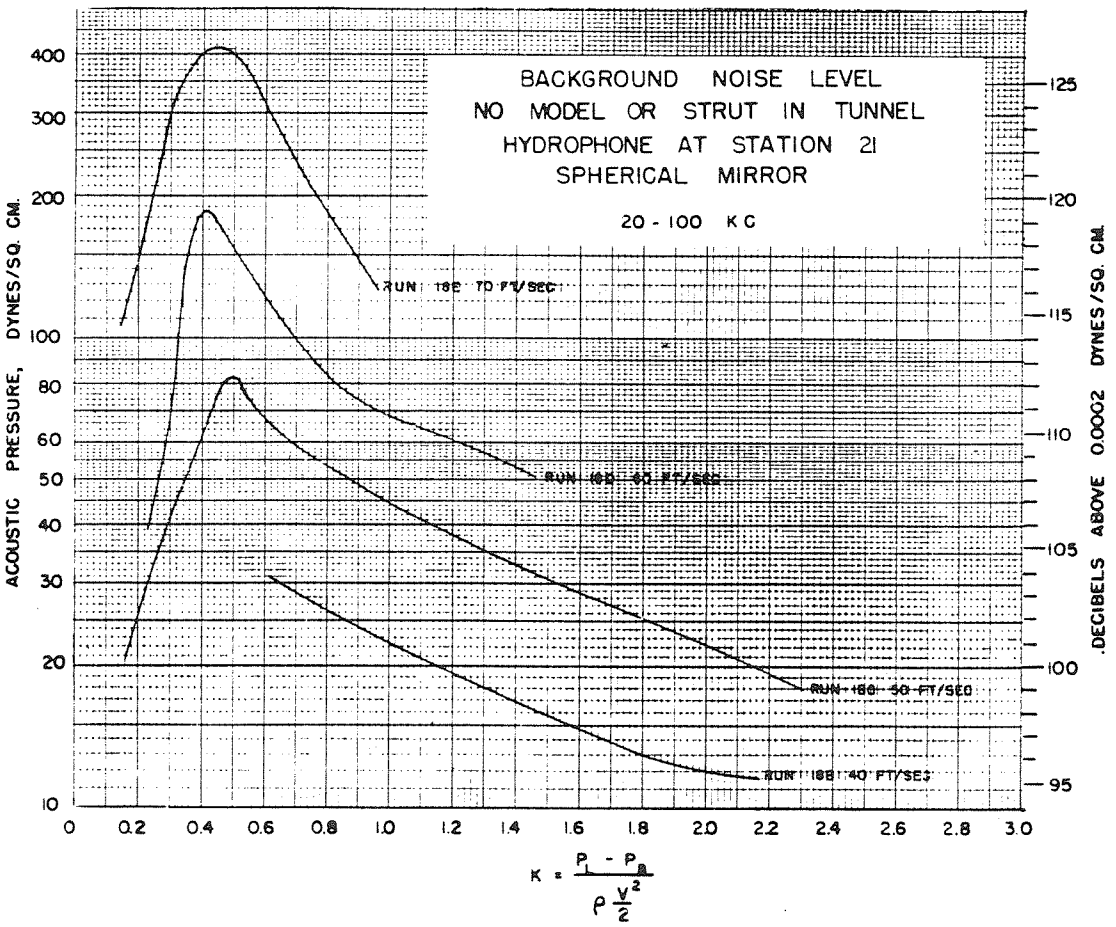

FIG. 30

for Figure 29 and with an improved contracting nozzle at the inlet to the working section. These curves are similar to those in Figure 29 but show from 2 to 5 decibels lower noise levels at the same K. Also, a lower K is reached before the noise drops. In this case no nozzle cavitation was obtained, but with sustained operation at the low absolute pressures corresponding to the lowest K values, an accumulation of air was obtained in the tunnel and the noise level dropped.

BACKGROUND NOISE VS. CAVITATION NOISE

The highest sound pressure measured in the clear tunnel at 70 ft/sec, the maximum velocity at which noise from projectiles was recorded, was about 420 dynes per square centimeter. As will be discussed later, pressures of 1000 to 2000 dynes per square centimeter were measured with the spherical mirror as cavitation developed on the projectile shapes. Since the recorded level is approximately the root-mean-square value of all the sound contributions, the background noise has no significant effect on these pressures. It is possible also, for the same reason, to ignore the relatively small effect of background noise variations caused by different tunnel setups as illustrated by the two figures, 29 and 30.

Similar background noise measurements made using the ellipsoidal mirror showed 5 to 8 decibels higher levels than with the spherical mirror. However, peak noise pressures of 5000 dynes per square centimeter or greater were measured from cavitating projectiles with this reflector making the background noise even less significant. It is interesting to note that for the particular test conditions of Figures 29 and 30, and for K greater than 0.6, the background sound pressure is approximately proportional to the fourth power of the water velocity and inversely proportional to the water pressure. For low K values nozzle cavitation or air accumulation changes this relationship.

UNIFORMITY OF BACKGROUND NOISE

A comparison of the background noise obtained at different positions along the center line of the tunnel is shown in Figure 31. These measurements were made with the velocity and pressure fixed (K = constant) by moving the hydrophone and mirror parallel to the tunnel axis. They show the same noise level throughout the length of the working section normally occupied by the model.

BACKGROUND NOISE WITH PROJECTILE IN TUNNEL

In order to verify that these "clear tunnel" measurements gave the same background noise that would be obtained with actual test installations, a projectile was installed in the working section and a survey made for noncavitating conditions. With V = 40 ft/sec and K = 3.74, the conditions of test used to obtain the data in Figure 29 were duplicated as nearly as possible and measurements made of noise vs distance along the tunnel axis.

With such a high value of K no cavitation existed at any place on the model. These measurements shown in Figure 32 gave an average noise level within 2 db of the clear tunnel noise shown for the same K in Figure 29.

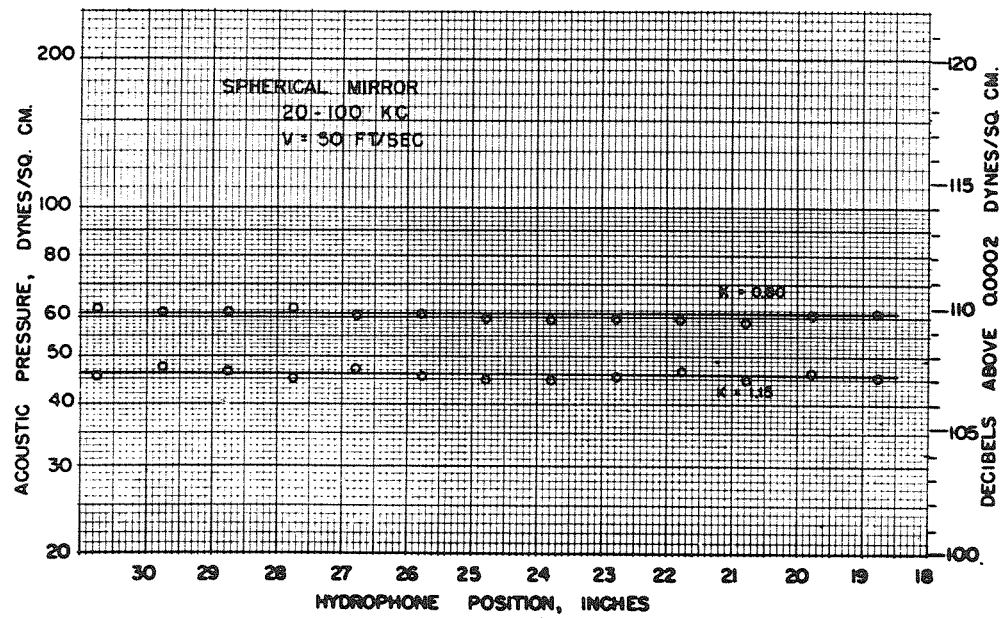

FIG. 31 BACKGROUND NOISE LEVEL AT DIFFERENT POSITIONS ALONG CENTERLINE OF TUNNEL
No model or strut in tunnel

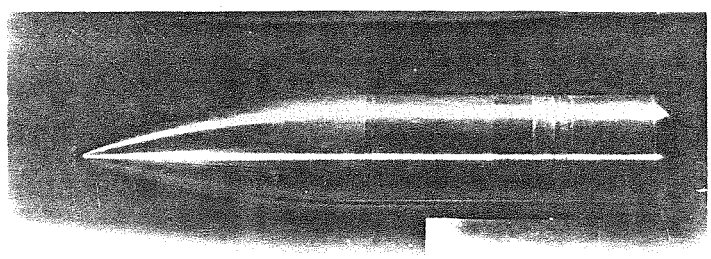

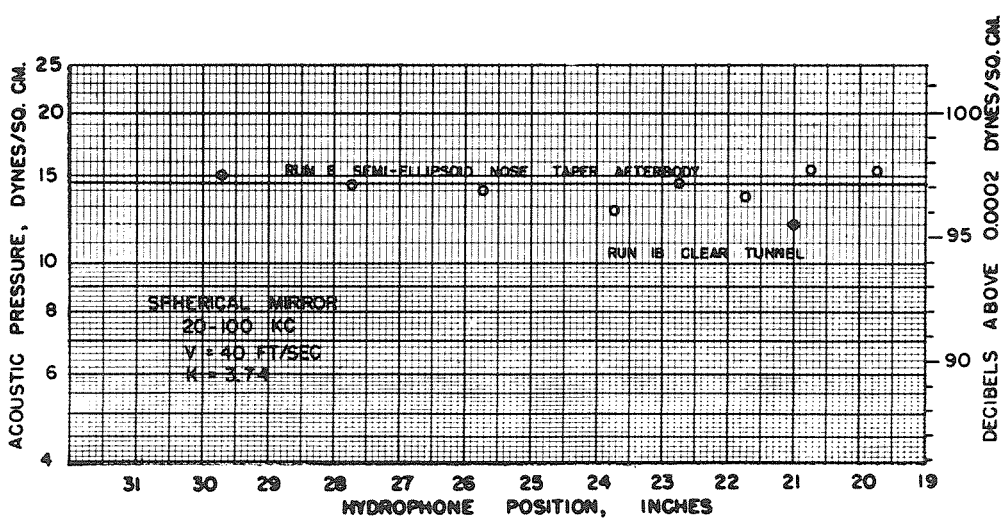

FIG. 32 BACKGROUND NOISE WITH MODEL IN TUNNEL
SEMIELLIPSOID NOSE
(Model 26.1-1)

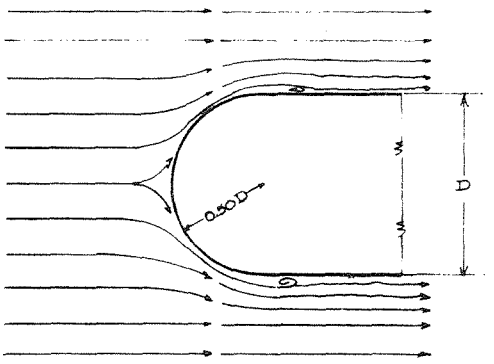

HEMISPHERE NOSE

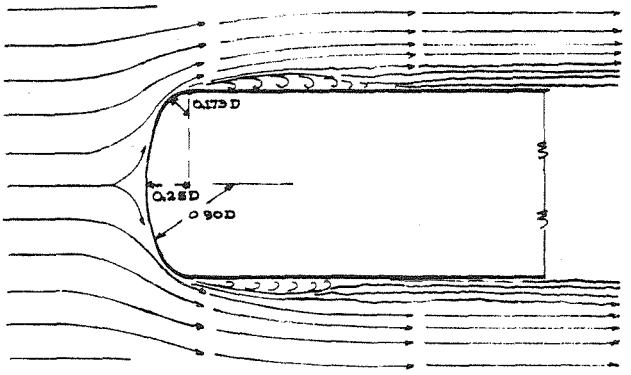

SEMIELLIPSOID NOSE

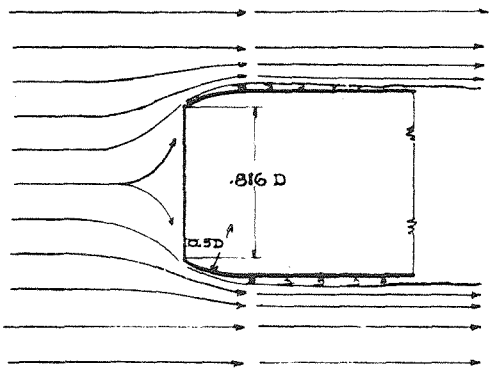

TRUNCATED HEMISPHERE NOSE

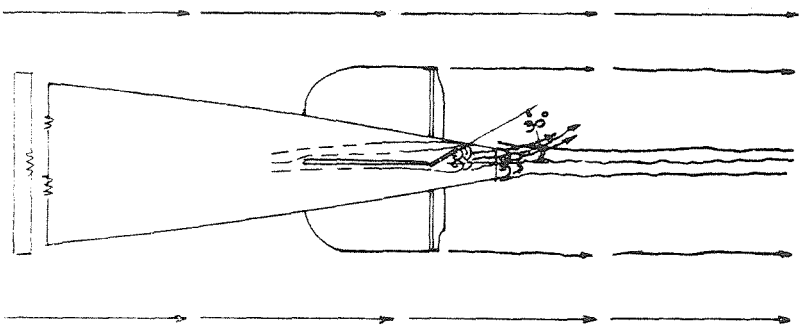

UPTURNED TAIL RUDDER ON PROJECTILE AFTERBODY

FIG. 2033, PROJECTILE PROFILES WITH FLOW DIAGRAMS

D. MEASUREMENTS OF NOISE PRODUCED BY CAVITATING PROJECTILES

1. CORRELATION WITH THE BEGINNING AND GROWTH OF CAVITATION

CAVITATION TYPES AND INFLUENCE OF PROFILE SHAPE

During observations of various projectiles in the Water Tunnel, it was noticed that as cavitation first appeared, the formation and collapse of the cavitation bubbles were different for varying degrees of abruptness of the body at the cavitation zone. Where the profile was not too abrupt, the zone of cavitation bubbles appeared to form, grow, and collapse right on the surface of the body. For more abrupt bodies the bubbles seemed to form at the surface of the body, but to spring clear of the body before collapsing and disappearing. For some very abrupt shapes the cavitation vapor pocket originated and collapsed in the stream away from the disturbing surface and with no visible connection to the body itself. Consequently, in studying the correlation of sound generated with the beginning and growth of cavitation, the several different forms of cavitation were investigated by using several body shapes. The four bodies for which measurements are reported here and the type of *incipient cavitation* obtained are listed below:

1.	Hemisphere Nose	Cavitation forms and collapses on the surface of the projectile
2.	Semiellipsoid Nose	Similar to above
3.	Truncated Hemisphere Nose	Cavitation vapor bubbles originate at the sharp edge but collapse in the stream away from the projectile surface
4.	Tail Rudder Tilted into Stream	No visible connection between cavitation bubbles, which form and collapse in water, and the rudder surface

A comparison of the shapes of the four bodies and the types of flow about each for noncavitating conditions are shown by the scale drawings in figure 33 The three noses and the upturned rudder present to the flow successive changes from smooth to blunt and abrupt profiles. The flow line diagrams, which were drawn from detailed observations of the actual flow in the Polarized Light Flume [1] are useful for qualitatively determining the pressure field around the projectile and, hence, locating the zones of low pressure where cavitation is most likely to occur Wherever the

flow, which has been pushed aside by the projectile surface, begins to curve back around the body (concave towards the body), local reductions in pressure are affected. The greater this curvature, the lower the pressure and the greater the possibility of developing cavitation. The flow lines show the maximum curvature near the junction between nose and cylinder for the hemisphere and semiellipsoid noses at the sharp edge on the truncated hemisphere, and at the tip of the rudder on the finned afterbody. In addition, the diagrams show varying sharpness in maximum curvature, indicating earliest cavitation for the truncated hemisphere nose or upturned rudder, and later cavitation for the semiellipsoid and hemisphere noses.

SOUND PRESSURE VS. CAVITATION GROWTH

With the hydrophone and spherical mirror focused on the zone of incipient cavitation and using the test procedure outlined in Appendix I, curves showing the variation in sound pressure with the amount of cavitation were obtained for each projectile. A corresponding series of photographs showing the successive stages of cavitation development were also made. All tests were made with zero yaw and zero pitch. The results are shown in Figures 34, 35, 36, and 37 where the sound pressure is plotted against the cavitation parameter. A scale for the sound level in decibels is also shown. The photographs included in the same figures are arranged in the order of decreasing values of K and each is marked with the corresponding measured sound level. Note that in all cases the total sound in the 20 to 100 kc band is shown, but that the data for each nose were obtained at a different constant velocity.

Each set of curves and photographs in Figures 34 to 37 show the following common characteristics:

1. With reduction in the cavitation parameter, K, the sound pressure rises sharply to several times the magnitude of the background noise in the tunnel as soon as the slightest trace of visible cavitation is observed.

2. The rise in sound begins with the appearance of minute cavitation bubbles and reaches a peak value while the ring of bubbles is still very narrow.

3. The sound pressure decreases with continued development of cavitation until, for fully developed conditions, the noise is but a fraction of the peak magnitude. For some cases it drops to approximately the same level as the tunnel background noise.

These characteristics are shown clearly by examining Figure 34 for the hemisphere nose. For high values of K at which no cavitation occurs on the projectile, the measured noise is only that due to background disturbances. However, as K is reduced by reducing the hydraulic pressure or increasing the velocity, and

cavitation begins the noise rises sharply to a high value In this instance the increase is from 95 to 1700 dynes per square centimeter a gain of about 25 db With continued growth of cavitation the noise peaks and then falls off until with very large bubbles enveloping the body the measured level equals the background noise level During tests at the K corresponding to Figure 34 (a) only small intermittant bubbles of cavitation could be discerned by careful visual examination They were too small to be detected photographically Figure 34 (b) shows a small amount of cavitation along the top half of the body at the junction between the hemisphere and the cylinder Note that it is a very narrow band yet as the noise curve shows it is between this condition and the slightly more developed one shown in the next photograph that the maximum noise is measured

Examination of Figure 35 shows the semiellipsoid nose to cavitate at a higher K but otherwise to exhibit the same characteristics Because the background noise was very low for this 40 ft/sec test the noise gain at the inception of cavitation is nearly 37 db Again as indicated in Figures 35 (b) and 35 (c), the maximum noise is measured with only a thin ring of cavitation near the junction between the cylindrical body and the nose contour A second small noise peak of undetermined cause is evident at K = 1.0 when a relatively wide zone of cavitation exists

Figures 34 and 35 both showed similar types of incipient cavitation where the bubbles lay close to the body surface Figure 36 for the truncated hemisphere nose shows the second type of cavitation where the bubbles collapse in the water away from the body Figures 36 (a) and 36 (b) illustrate this clearly The trailing ends of the small cavitation wisps which originate at the sharp edge on the nose are separated from the body by a definate space With continued growth of cavitation the bubble zone becomes more dense and this characteristic is less discernible The same trends in measured sound were obtained as for the other two noses with about a 23 db increase in level as cavitation began

Figure 37 shows sound measurements and photographs for a tail rudder tilted up into the stream As the first photographs of the series show the initial cavitation occurs at the rudder post as well as at the tip and finally at very low K values the entire wake behind the tilted rudder becomes filled with vapor The noise curve shows the characteristic increase to a peak value and then reduction with cavitation growth Note that as Figure 37 (d) shows the peak noise a 40 db gain over the background is obtained with very little visible cavitation

These measurements confirm the results obtained without the focusing device and which have already been reported [27] With the focusing system however the sensitivity of the noise measurements was increased so much that the detection of the onset of cavitation was more definitely marked leading to a much sharper rise in the measured sound pressure curve

It might be noted that surface condition is very critical in making the cavitation measurements. The noise measurements and cavitation photographs of the four noses were made after carefully polishing the assembled models and wiping the surface and joints between body sections with a waxed cloth. These precautions caused the onset of cavitation to be more uniform by eliminating early cavitation at isolated points around the periphery of the projectile.

SOUND PRESSURE AND BUBBLE COLLAPSE

The fact that for all three types of cavitation the maximum sound was measured when the visible cavitation was small and that the magnitude was reduced with the growth of the bubbles might be tied in with the concept that the noise originates primarily at the bubble collapse. With small cavitation bubbles which form and collapse cleanly and sharply within a small physical zone the energy release and, hence, the noise is of high intensity. As the zone of cavitation grows, the bubbles collapse throughout a larger space and mutual interference and absorption due to the damping properties of the bubbles themselves reduces the intensity of the noise radiated.

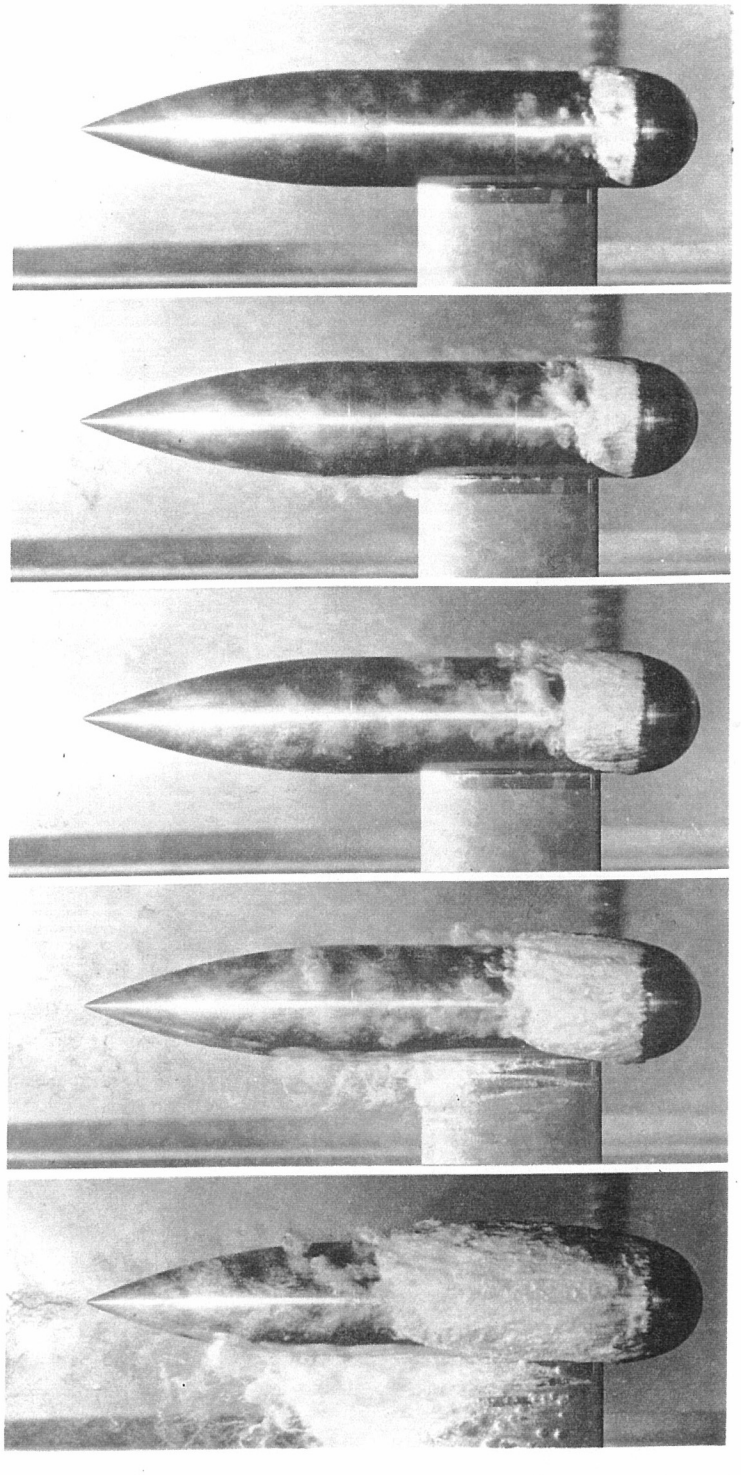

(g)

K = 0.56

SOUND = 129 db

(h)

K = 0.50

SOUND = 128 db

(i)

K = 0.45

SOUND = 125 db

(j)

K = 0.41

SOUND = 123 db

(k)

K = 0.31

SOUND = 115 db

29 28 27 26 25 24 23 22 21 20 19 18

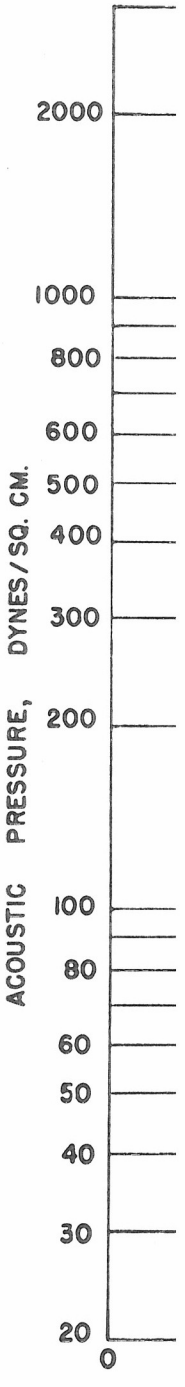

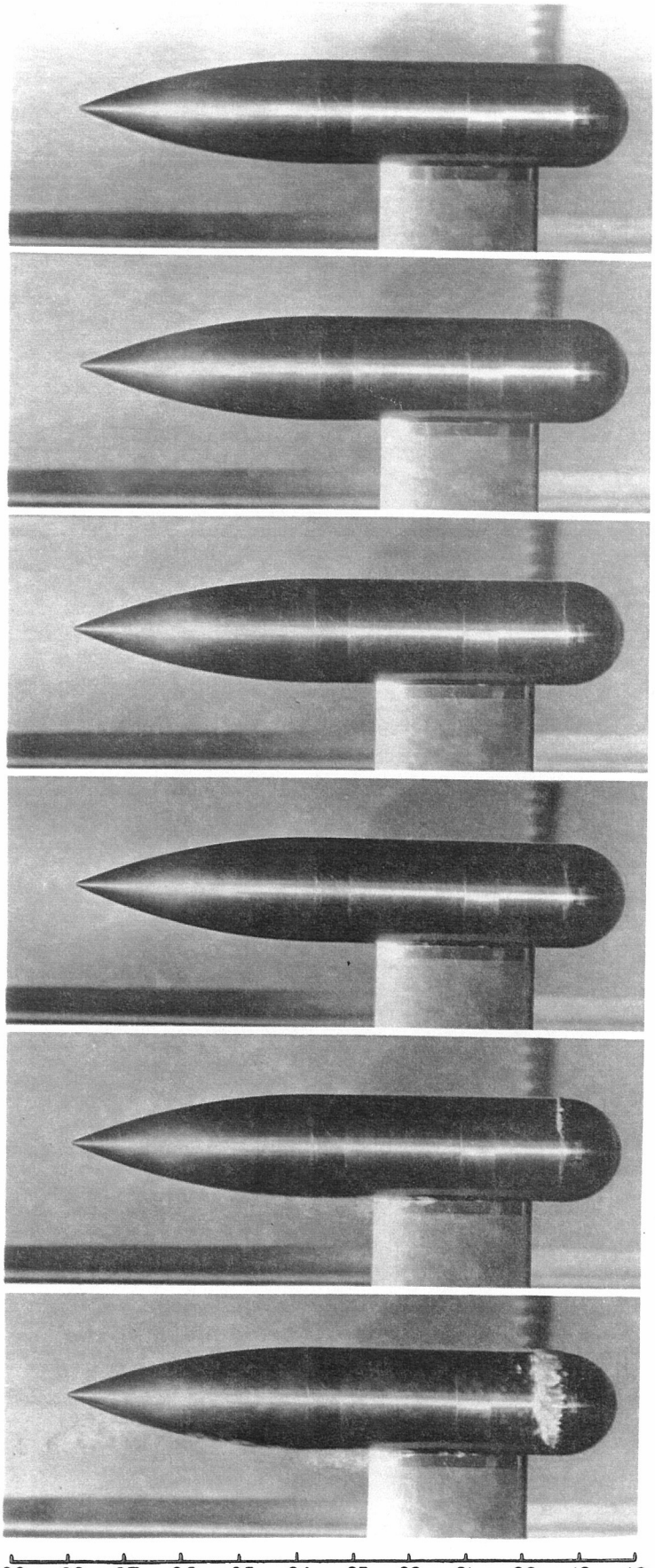

(a)

K = 0.79

SOUND = UNSTEADY NOISE LEVEL DUE TO INTERMITTANT CAVITATION.

(b)

K = 0.77

SOUND = 137 db

(c)

K = 0.73

SOUND = 139 db

(d)

K = 0.68

SOUND = 138 db

(e)

K = 0.65

SOUND = 135 db

(f)

K = 0.60

SOUND = 130 db

CAVITATION
ON HEMISPHERE NOSE

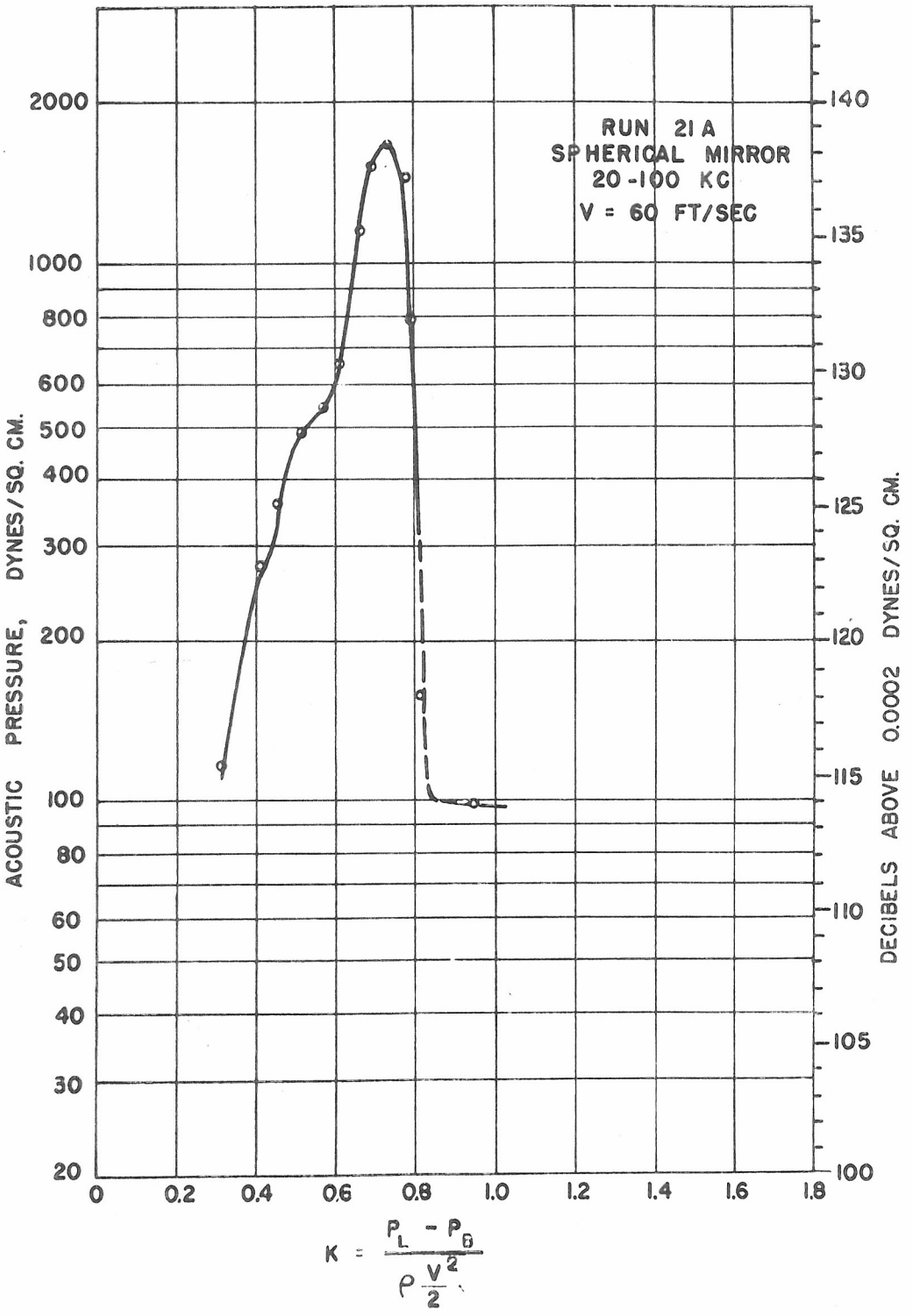

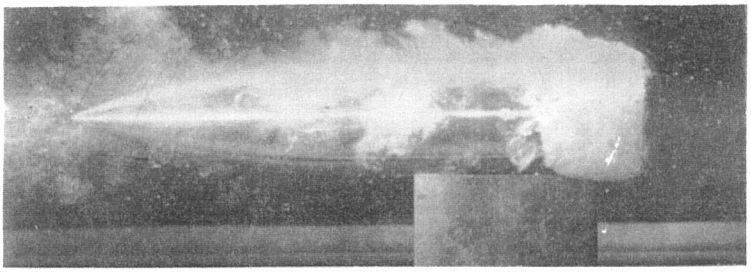

(g)

K = 0.71

SOUND = 120 db

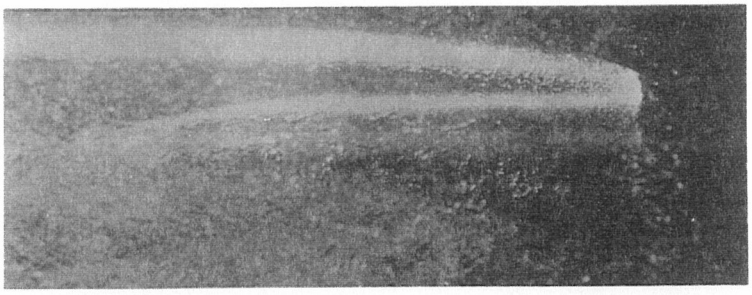

(h)

K = 0.40

SOUND = NO DATA.

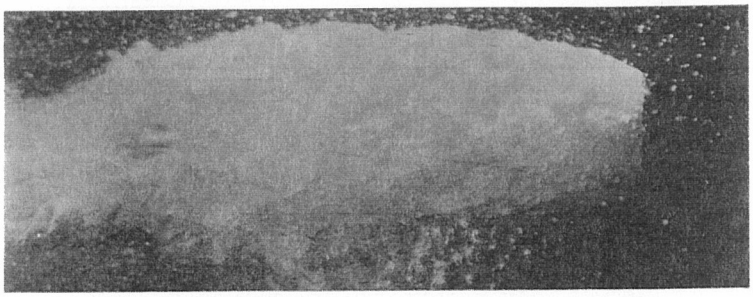

(i)

K = 0.53

SOUND = NO DATA

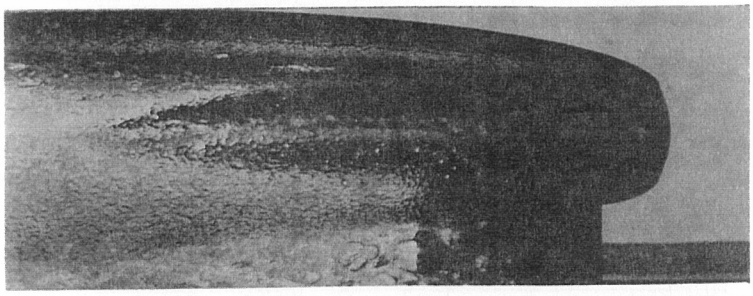

(j)

K = 0.46

SOUND = NO DATA

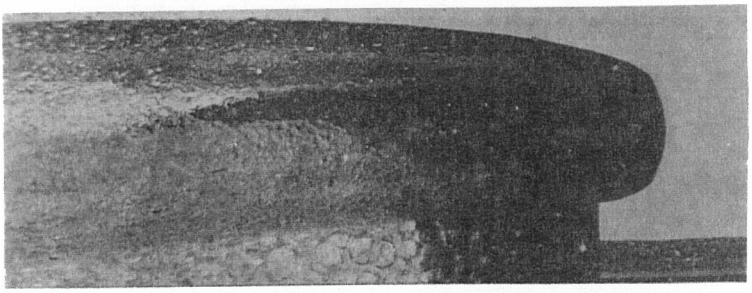

(k)

K = 0.47

SOUND = NO DATA

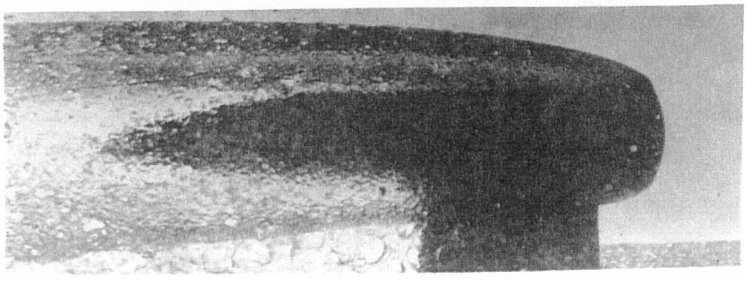

(l)

K = 0.44

SOUND = NO DATA

29 28 27 26 25 24 23 22 21 20 19 18

DISTANCE ALONG AXIS, INCHES

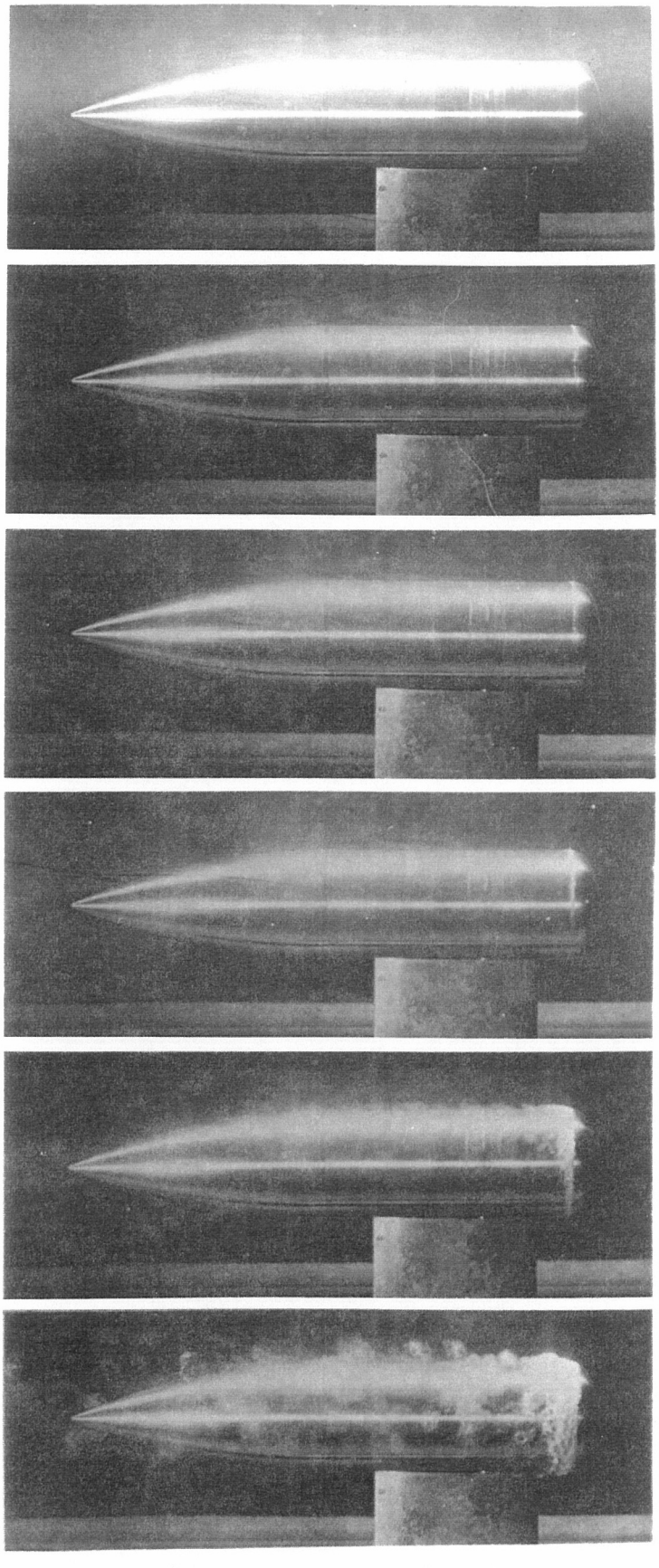
(a)
K = 2.55
SOUND = 96 db
(b)
K = 1.82
SOUND = 138 db
(c)
K = 1.74
SOUND = 138 db
(d)
K = 1.52
SOUND = 131 db
(e)
K = 1.29
SOUND = 129 db
(f)
K = 1.03
SOUND = 127 db
29 28 27 26 25 24 23 22 21 20 19 18
DISTANCE ALONG AXIS, INCHES

CAVITATION
ON SEMI-ELLIPSOID NOSE

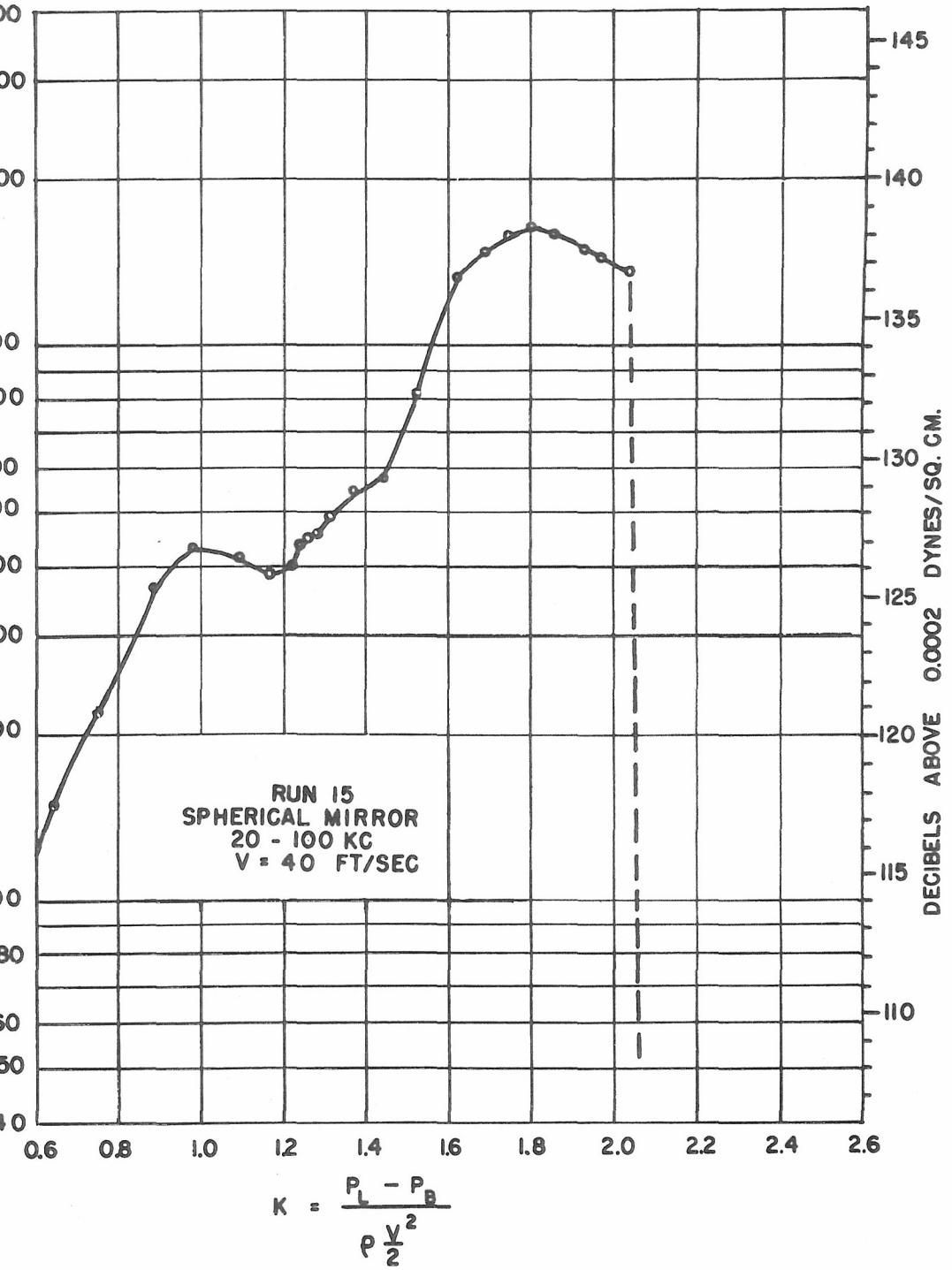

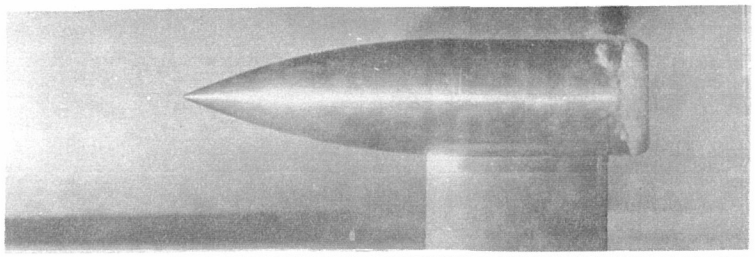

(g)

K = 1.32

SOUND = 123 db

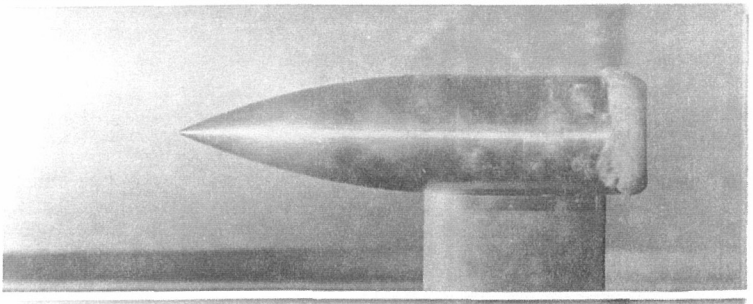

(h)

K = 1.19

SOUND = 122 db

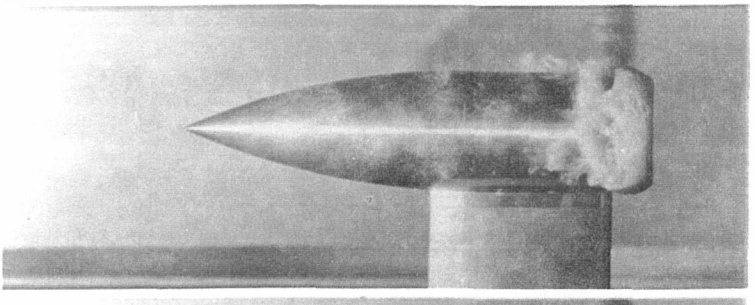

(i)

K = 1.01

SOUND = 123 db

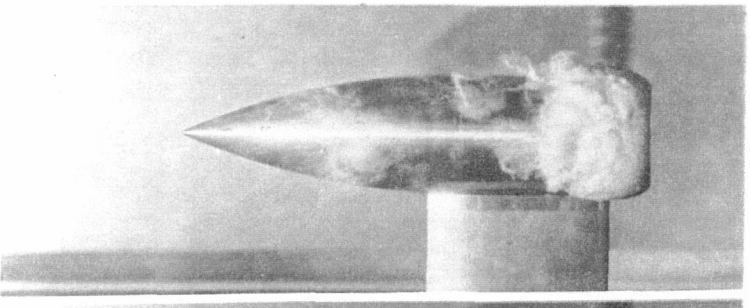

(j)

K = 0.82

SOUND = 119 db

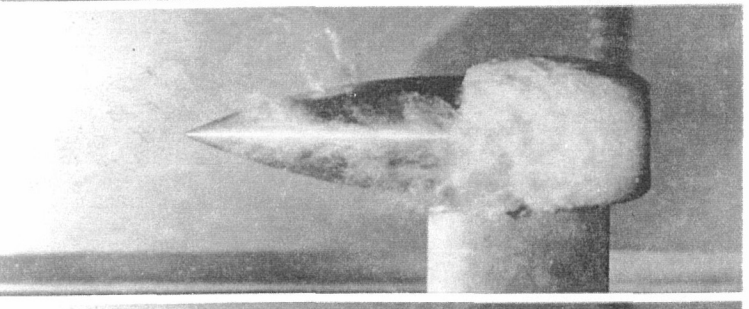

(k)

K = 0.56

SOUND = 117 db

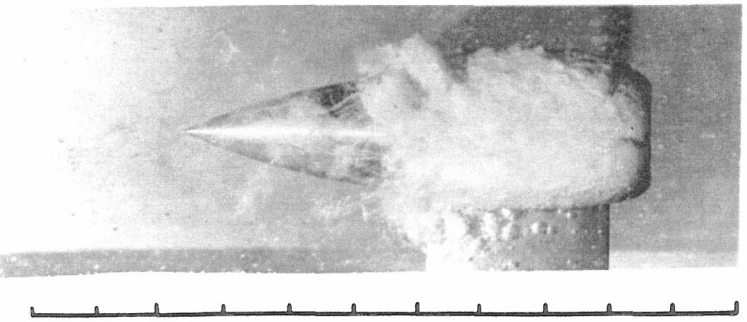

(l)

K = 0.53

SOUND = 117 db

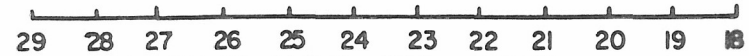

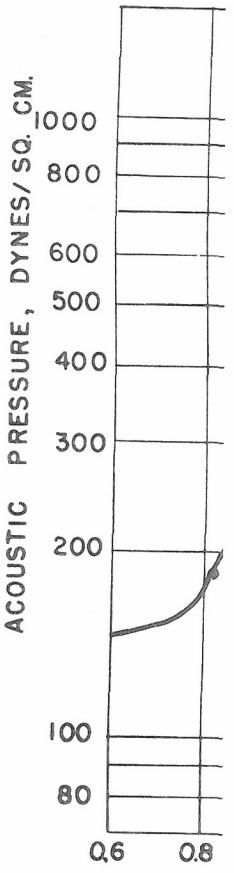

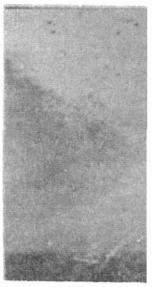

.32
123 db

19
22 db

01
123 db

.82
119 db

.56
117 db

53
117 db

CAVITATION
ON TRUNCATED HEMISPHERE NOSE

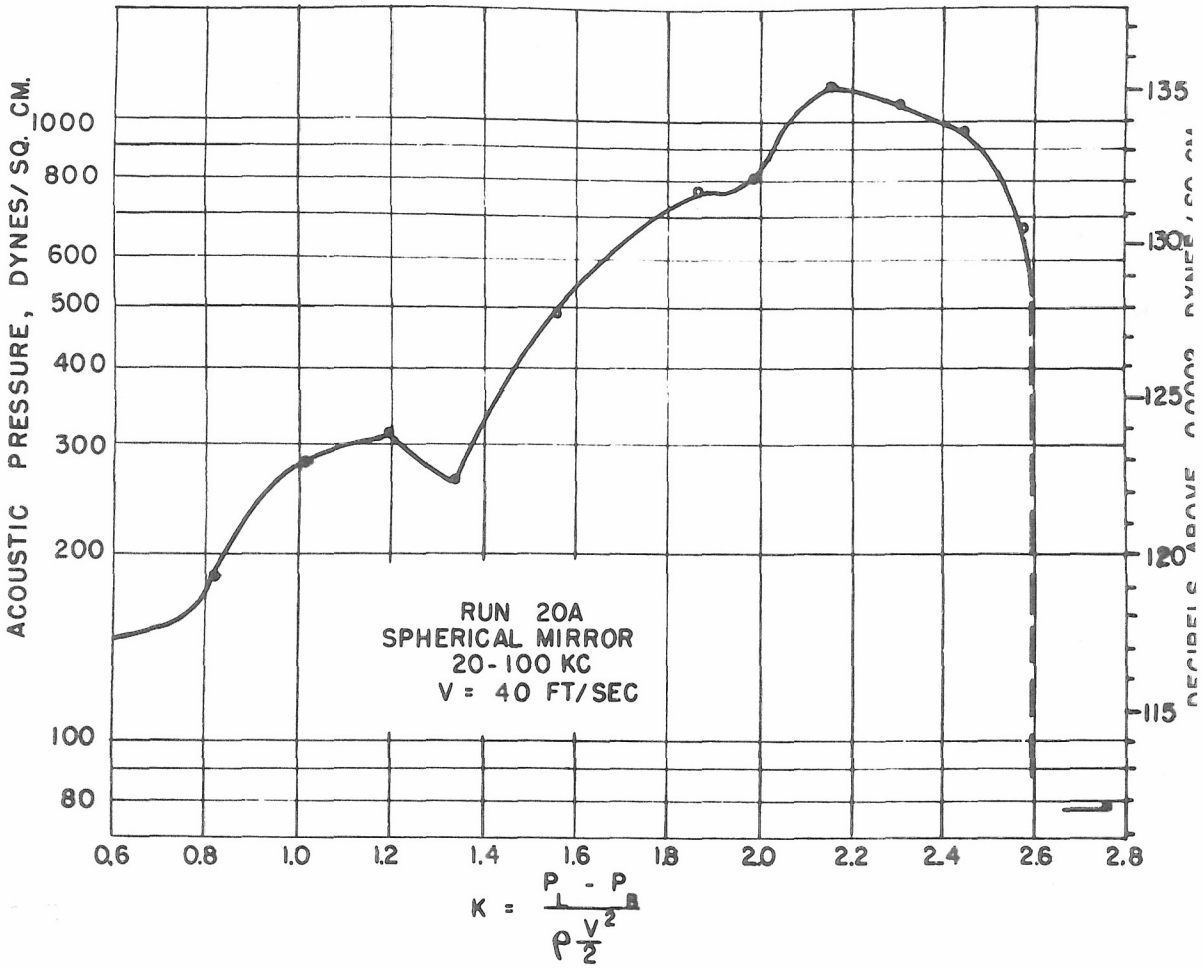

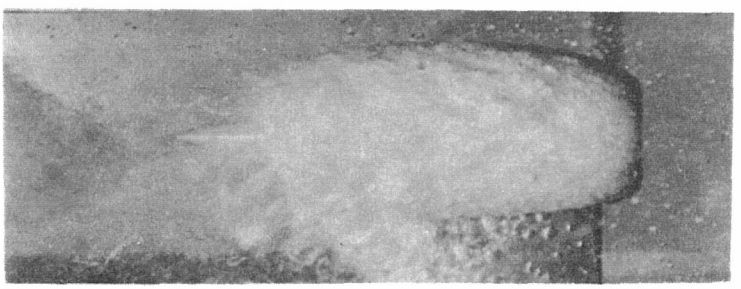

(m)

K = 0.43

SOUND = 113 db

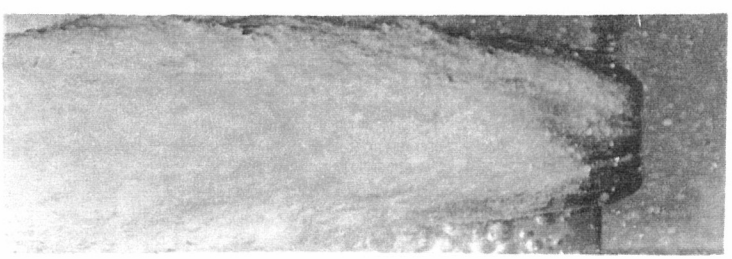

(n)

K = 0.33

SOUND = 108 db

29 28 27 26 25 24 23 22 21 20 19 18

DISTANCE ALONG AXIS, INCHES

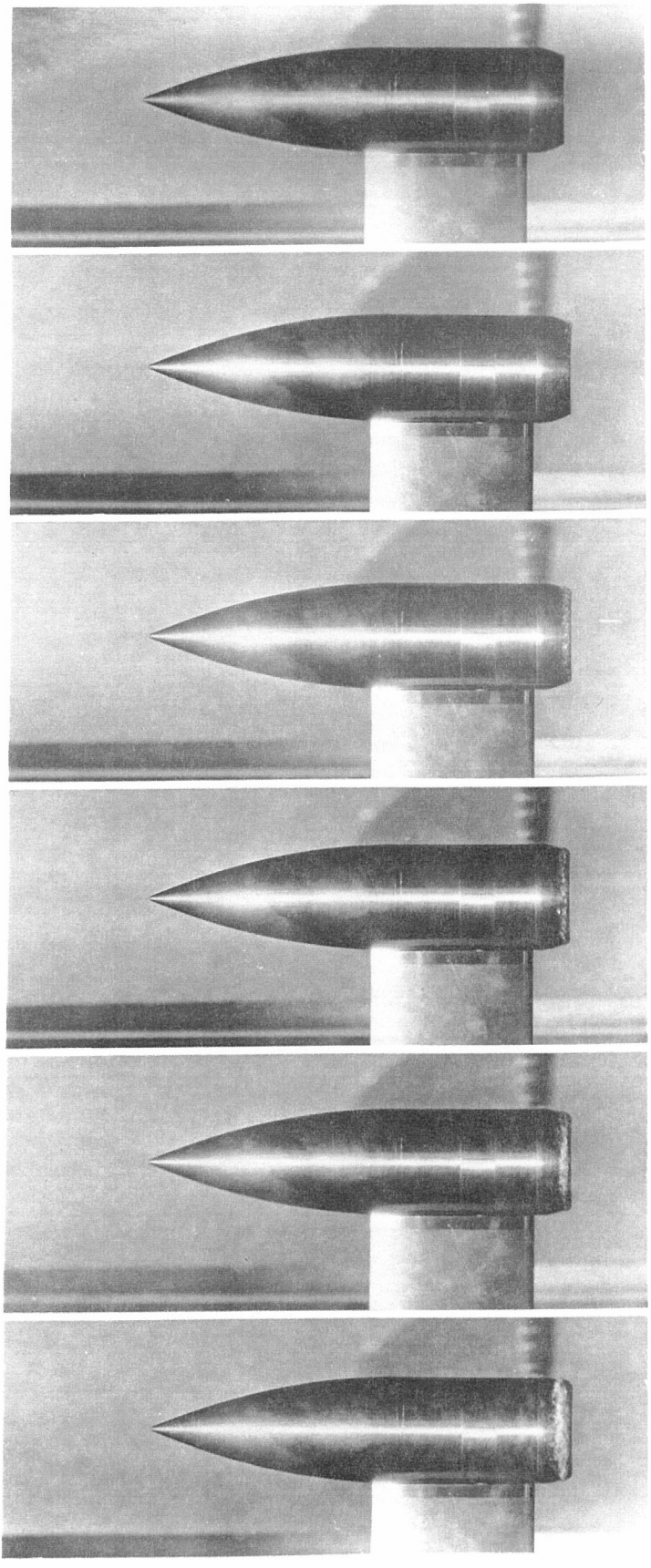

(a)

K = 2.44

SOUND = 134 db

(SEE ENLARGEMENT ON PANEL AT LEFT

(b)

K = 2.30

SOUND = 134 db

(c)

K = 2.14

SOUND = 135 db

(d)

K = 1.99

SOUND = 132 db

(e)

K = 1.83

SOUND = 132 db

(f)

K = 1.55

SOUND = 128 db

29 28 27 26 25 24 23 22 21 20 19 18

DISTANCE ALONG AXIS, INCHES

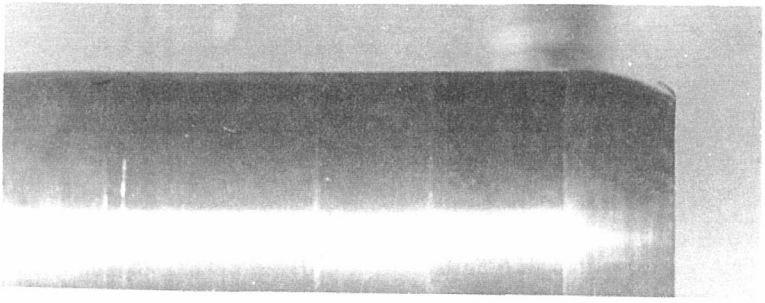

ENLARGEMENT OF FIG. 23a
WITH SMALL WISPS OF CAVITATION
ACCENTUATED

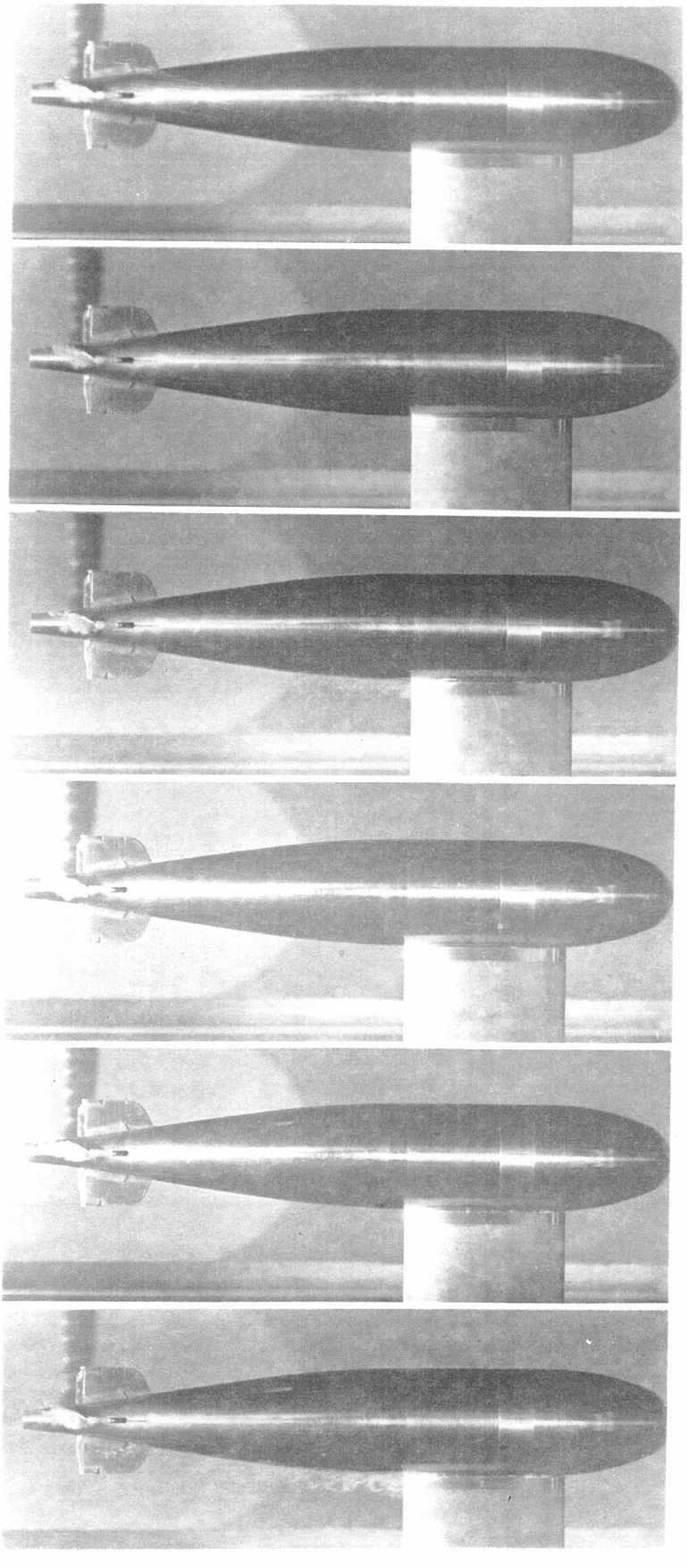

(g)

K = 0.87

SOUND = 133 db

(h)

K = 0.75

SOUND = 130 db

(i)

K = 0.71

SOUND = 130 db

(j)

K = 0.67

SOUND = 129 db

(k)

K = 0.65

SOUND = 129 db

(l)

K = 0.59

SOUND = 126 db

29 28 27 26 25 24 23 22 21 20 19 18

DISTANCE ALONG AXIS, INCHES

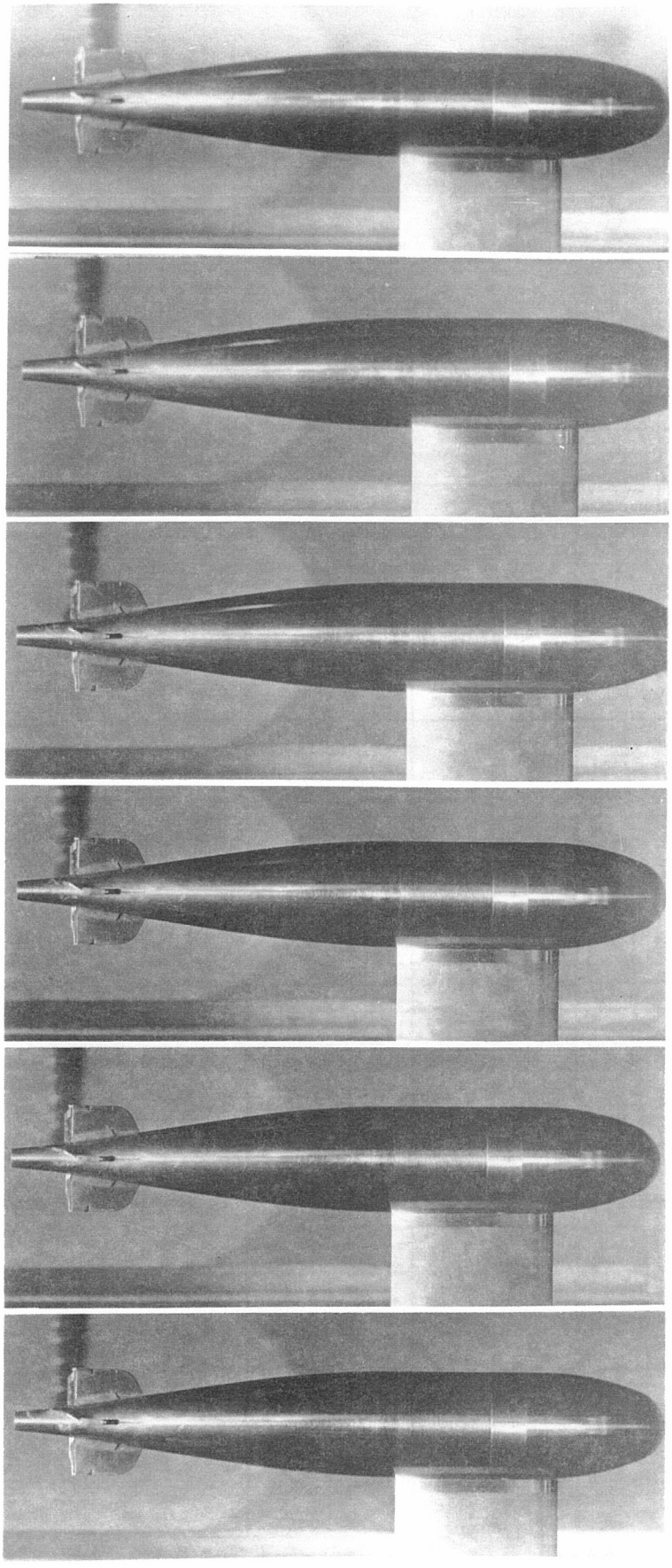

(a)

K = 1.48

SOUND = 130 d

(b)

K = 1.38

SOUND = 132 d

(c)

K = 1.25

SOUND = 134 d

(d)

K = 1.15

SOUND = 134 d

(e)

K = 1.03

SOUND = 134

(f)

K = 0.95

SOUND = 133 d

29 28 27 26 25 24 23 22 21 20 19 18

DISTANCE ALONG AXIS, INCHES

CAVITATION

ON UP TURNED RUDDER OF FIN TAIL

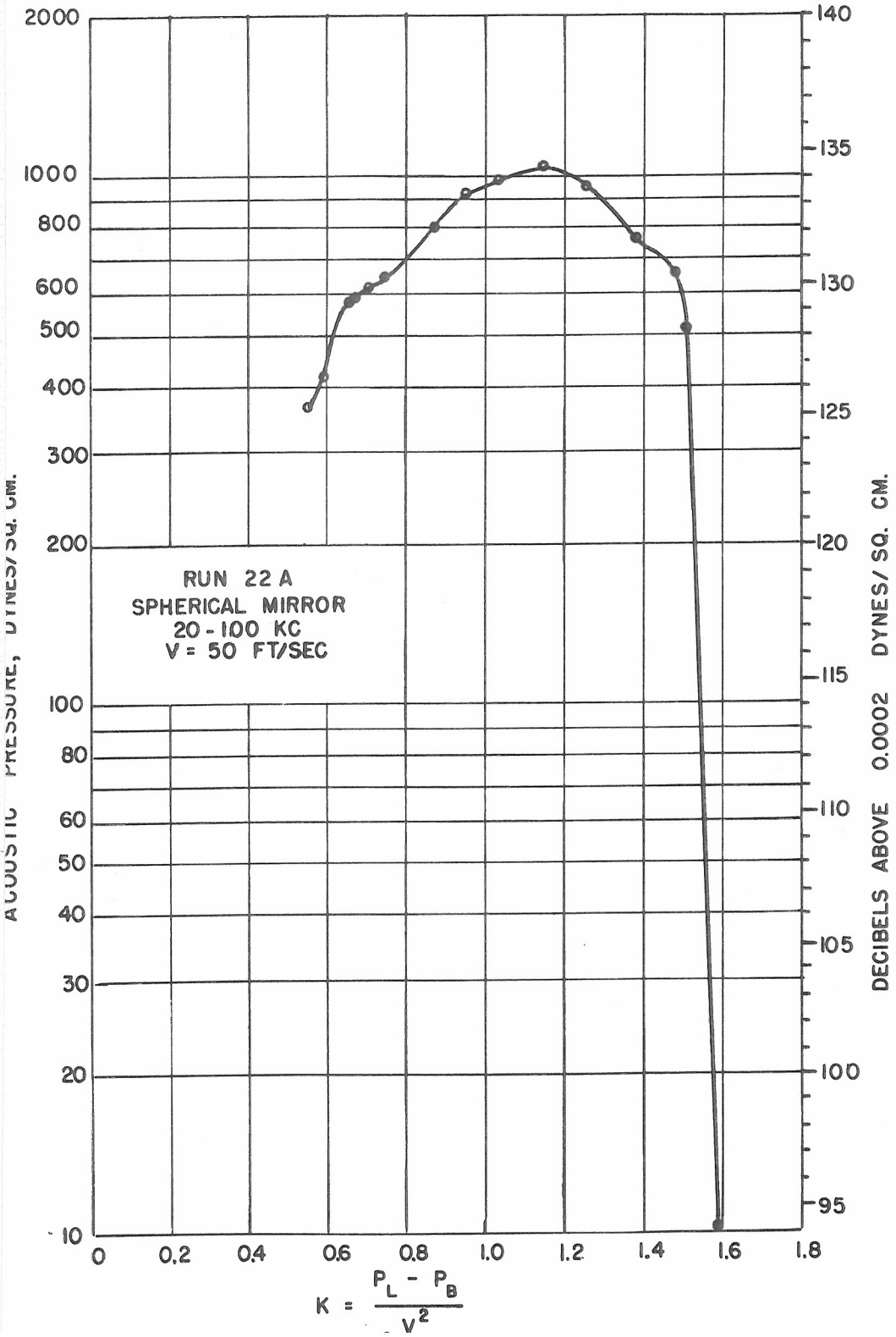

COMPARISON OF FOUR TYPES AT SAME VELOCITY

It should be noted again that each set of data in Figures 34 to 37 is for a different velocity and, furthermore, the inception of cavitation occurs at a different pressure for each body. Consequently, there is no satisfactory basis for comparison of the magnitudes of the sound levels measured. Measurements of the noise produced by each of the projectiles at the same velocity of 47 ft/sec were obtained using the ellipsoidal reflector instead of the spherical mirror. These results are shown in Figure 38. The

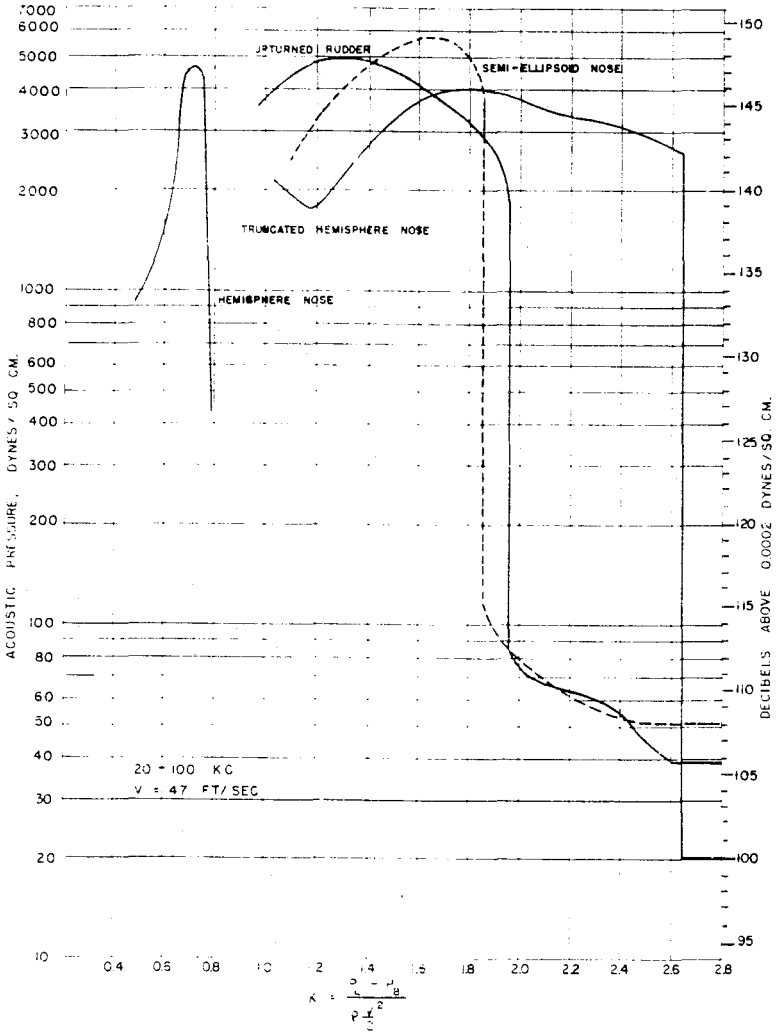

FIG. 38 NOISE CAUSED BY CAVITATION ON FOUR PROJECTILES

increased effectiveness of this reflector over the spherical mirror is apparent. For example, the hemisphere nose curve shows a maximum sound pressure of 4800 dynes per square centimeter for this 47 ft/sec test, as against about 1100 shown in Figure 34 for a 60 ft/sec test with the spherical mirror. Similarly higher peaks are obtained for the others. These curves show some difference in the magnitudes of the noise peaks for the different bodies. There is also some difference in the shapes of the curves, the peak occurring at a K somewhat lower than the inception value for the two most abrupt shapes, the truncated hemisphere and the upturned rudder. For the hemisphere and the semiellipsoid the peak occurs soon after the inception point. The sharp discontinuities also show the most sensitivity to change in K near the inception point. For both the truncated hemisphere and the upturned rudder, the determination of the beginning of cavitation was very critical so that sound measurements in that region were difficult to obtain. With the other two noses, however, the increase, while sudden, could be traced and with extreme care measurements made at levels intermediate between the background and highest pressures.

NOISE VS. VELOCITY

In Figure 38 are curves for the hemisphere nose showing the change in noise with velocity. For the velocity range of 40 to 70 ft/sec the increase in maximum noise for each speed is approximately linear. This holds for both the 20 to 100 kc and 80 to 100 kc frequency bands. This maximum noise is not obtained at the same pressure (submergence) for all speeds, but rather at nearly a fixed value of the cavitation parameter, K. If a projectile travels under water at a fixed depth, the maximum noise represented by the straight lines in Figure 26 will be generated only at one velocity where K assumes the above fixed value. For all other velocities the noise will be less than the maximum. The other curves in Figure 39 snow the variation in noise in 20 to 100 kc band for this nose submerged to 10 feet and 15 feet. It will be noted that the noise level is low up to the criticdl velocity for inception of cavitation where it increases several fold to the maximum level curve shown. Beyond this peak a reduction occurs. Of course, cavitation is postponed to higher

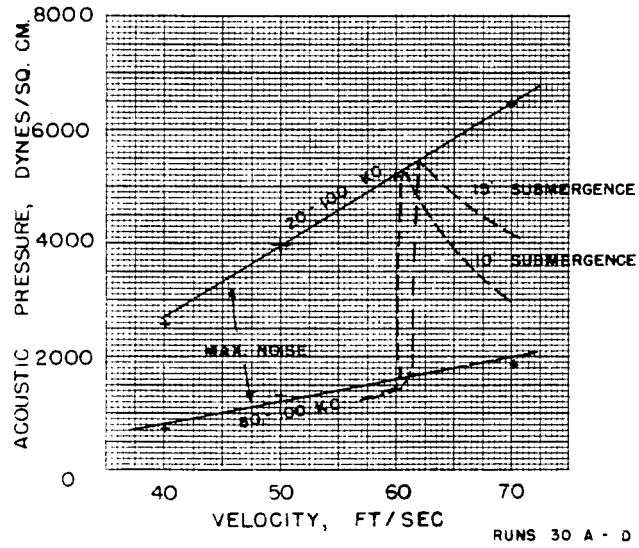

FIG. 39 NOISE VS. VELOCITY
Hemisphere Nose

velocities as submergence increases, but when cavitation does occur, the peak noise is higher also. It might be noted that the data from which these curves were drawn were obtained with a different arrangement in the Water Tunnel setup, so the magnitudes of the maximum noise are not directly comparable to those illustrated in Figure 38.

NOTE ON MAGNITUDE OF MEASURED NOISE

It should be emphasized that the absolute magnitudes of the sound levels measured in the Water Tunnel bear no particular relation to what might be obtained in the field. In any event, in either laboratory or field measurements the hydrophone receives only such a portion of the total sound emitted as the geometry of the setup permits. The magnitudes reported here are good for comparative purposes only.

2. LOCATION OF NOISE SOURCE DURING CAVITATION

VISIBLE CAVITATION AND THE NOISE SOURCE

It is generally agreed that on the collapse of cavitation bubbles a large store of energy is released, and that at the point of energy concentration very high local pressure intensities are obtained. The resulting high frequency pressure waves are the cause of the mechanical damage commonly known as "cavitation corrosion" and of noise, both acoustic and supersonic.[7] That the source of noise measured is concentrated at the zone where cavitation is visible is clearly shown by traverses giving the sound pressure as the hydrophone is moved parallel to the Water Tunnel axis. As the examples for the hemisphere nose in Figure 40 show, when the hydrophone is positioned to focus on the cavitation zone in the photographs, the maximum noise level is obtained. At 1" on either side of this position the sound is reduced 3 to 5 db. The ring source shown in the photographs appears as a line to the hydrophone receiver so that, as might be expected, focusing of the hydrophone in a position 1" above or below the center line of the working section gives less than a 1 db reduction in the level. The measurements in Figure 40 are for the 80 to 100 kc band because, ~~as the curves already presented in Figure 14 show,~~ the most pronounced focusing was obtained at the higher frequencies. ~~Figure 44 also shows that~~ The maximum sound pressure is obtained at the same position regardless of frequency.

MOVEMENT OF SOURCE WITH SHIFTING ZONE OF COLLAPSE

If it is assumed that the bulk of the total noise measured from a cavitating object is obtained from the collapse of the bubbles, the physical observation that the collapsing zone moves downstream with the growth of cavitation should indicate the movement of the noise zones. The curves in Figure 40 also indicate this trend. The peak obtained for a cavitation parameter K of

0.56 is approximately 1/2" farther back than the peak for K = 0.73, whereas photographs of Figures 34 (c) and 34 (g) indicate about 0.6" downstream elongation of the cavitating zone.

It has been suggested that growth of the sound source could indicate an apparent shift in its location, or that some combination of the effects of the screening and reflections peculiar to the projectile and tunnel configuration could explain the measured shift. It is felt, however, the agreement between length of cavitation bubble and movement of the sound peak measured in this and other cases is good evidence that the noise source is moving with the collapsing trail of bubbles.

Measurements for the cut hemisphere nose in Figure 41 show the same typical trends observed with the hemisphere nose. In Figure 42 are shown the results obtained with cavitation on the upturned rudder. These curves do not indicate a consistent shift in peak, even though cavitation at the lowest K is much more severe than at the highest. Reference to Photographs 37 (h), 37 (i), and 37 (j) show, however, that the visible zone of vapor

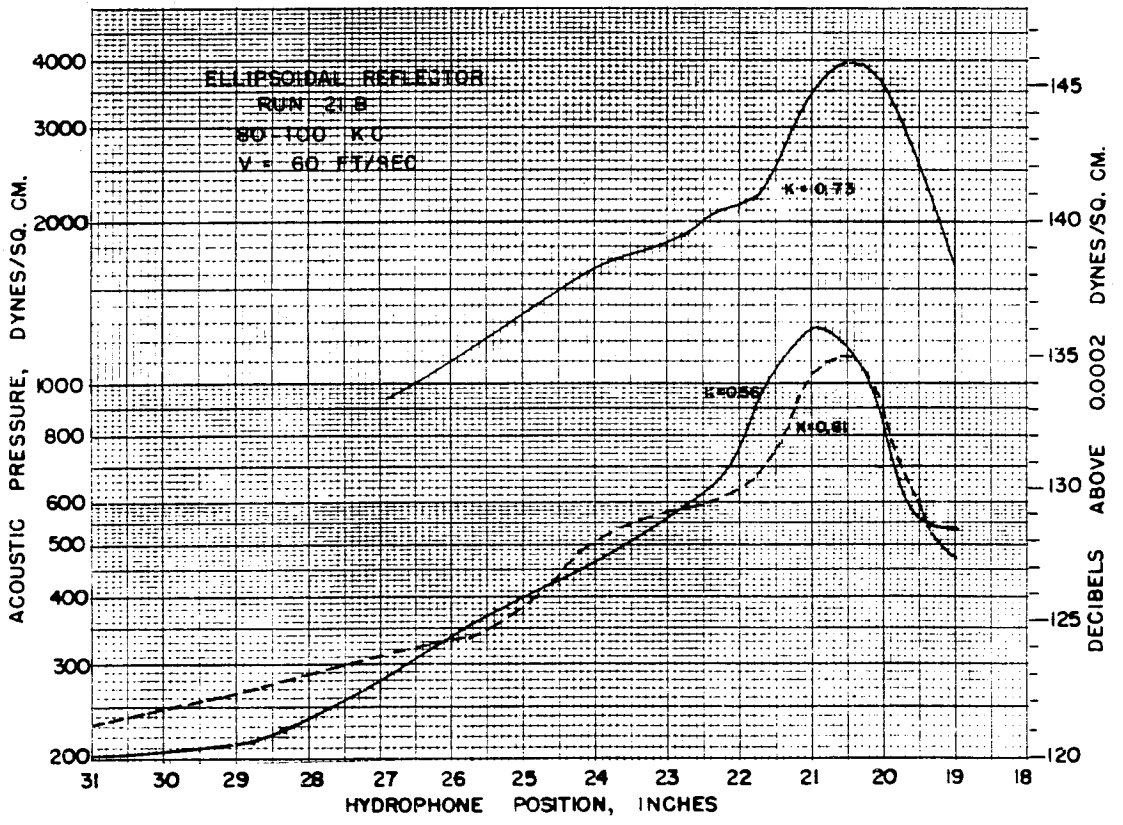

FIG. 40 MOVEMENT OF NOISE SOURCE WITH GROWTH OF CAVITATION ON THE HEMISPHERE NOSE
Compare with Fig. 34 (c), (f), (g)

on the lee of the rudder was changed very little as K was reduced. With more severe conditions, more and more vapor was entrainedby the water and swept downstream to collapse outside the range of the hydrophone system, but the main cavity shown was almost uninfluenced.

In Figures 40 to 42 only the relative position of the noise peaks is indicated. Definite determination of the exact position of the zones was not possible since, in mounting the hydrophone reflector assembly, the possible errors in angular adjustment in the horizontal plane could contribute as much as the indicated difference between the hydrophone position and the cavitation zone when the peak noise was measured. Measurements made with a given installation, however, gave good comparative results since the whole assembly was attached to a carriage which could be moved parallel to the tunnel on machined rails.

The effect of the movement of the sound peak with the growth of cavitation has a secondary effect on the accuracy of the sound vs. K curves shown in Figures 34 to 38, which were obtained with

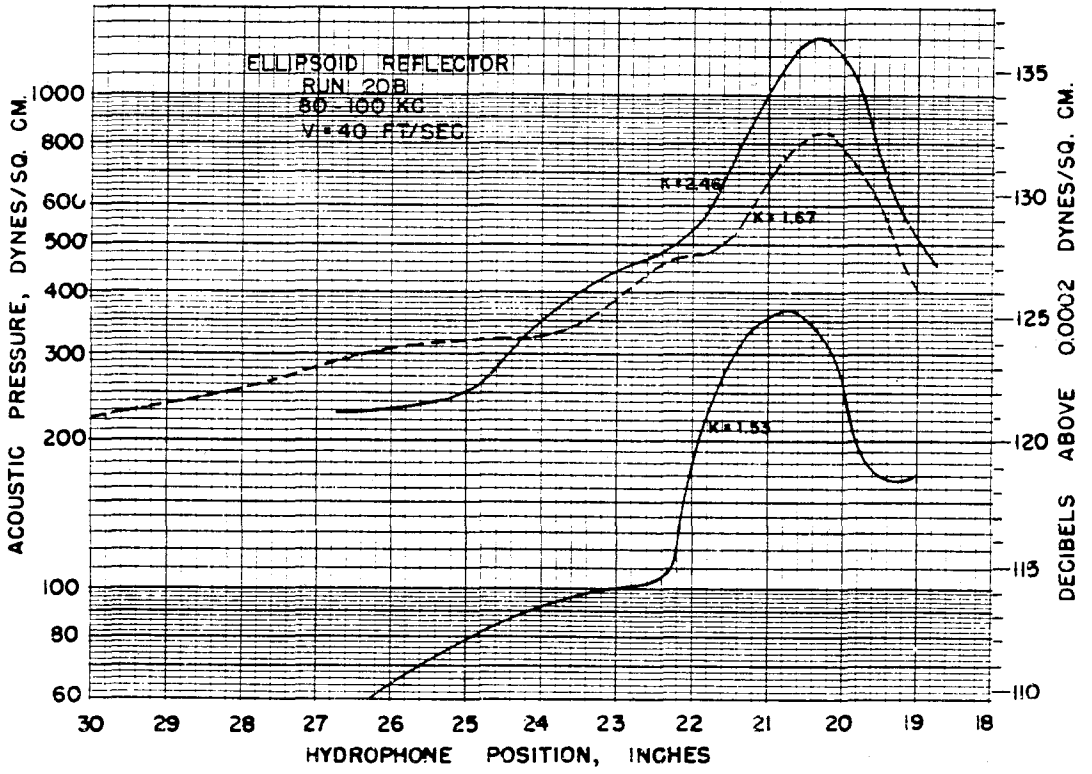

FIG. 41 MOVEMENT OF NOISE SOURCE WITH GROWTH OF CAVITATION ON THE TRUNCATED HEMISPHERE NOSE
Compare with Fig. 36 (a), (f)

the hydrophone in a fixed position. With the growth of the cavitation zone beyond the amount giving the maximum noise, the level measured by the fixed hydrophone is slightly low. This effect is small, however, being less than 2 db for the hemisphere nose at K = 0.56 or the truncated hemisphere at K = 1.51. Consequently, it does not alter the peculiar characteristics of the measurements shown nor change the conclusions already presented.

It is interesting to note that in Figures 40 to 42 the sound pressure location curves for the hemisphere nose and tail rudder showed more gradual reductions in noise on the side of the maximum which was toward the body of the model. This asymmetry became more pronounced at lower K values, while at high K's, as obtained with the cut hemisphere nose in Figure 41, no definite asymmetry is observed. Examination of the photographs in each figure shows that at the lowest K's, cavitation is occurring at the junction between the streamlined strut which supports the projectile and the cylindrical projectile body. It is thought that this secondary cavitation is contributing to the measured sound and is responsible for the asymmetry observed.

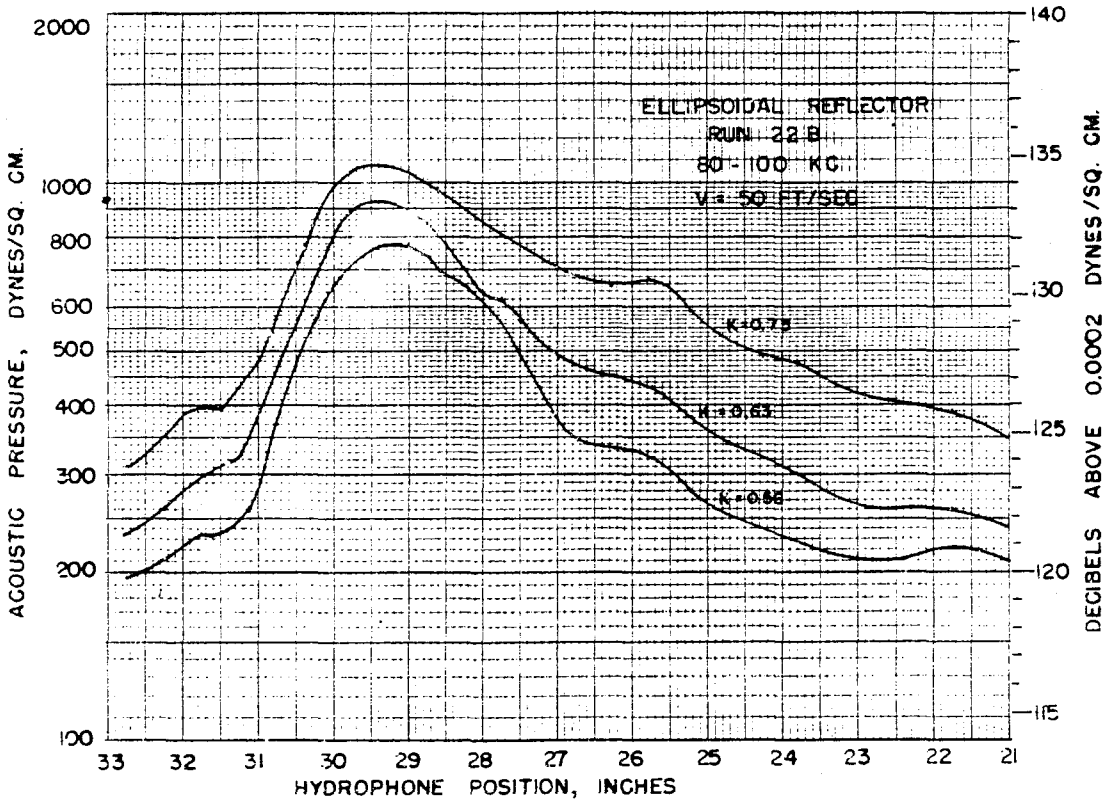

FIG. 42 MOVEMENT OF NOISE SOURCE WITH GROWTH OF CAVITATION ON UPTURNED RUDDER OF FIN TAIL
Compare with Figures 37 (h), (i), (j)

APPENDIX I

TEST EQUIPMENT AND PROCEDURES

The tests covered by this report were conducted in the High Speed Water Tunnel at the California Institute of Technology. The following paragraphs contain a brief description of the tunnel and the test procedures employed. A more detailed description of the High Speed Water Tunnel will be found in Reference (1).

Main Circuit

The water Tunnel is of the closed circuit, closed working section type. Figure A-1 shows a profile of the main flow circuit which consists essentially of the working section, the circulating pump, the stilling tank, and the necessary pipe connections. The cylindrical working section is 14" in diameter, 72" long, and is provided with three lucite windows. The propeller-type circulating pump is V-belt connected to a variable speed dynamometer. The speed of the dynamometer is automatically controlled and is held constant within ± 1 r.p.m., which corresponds to a maximum water velocity variation in the working section of 1/30 ft. per sec. Any water velocity between 10 and 72 ft. per sec. is easily obtainable.

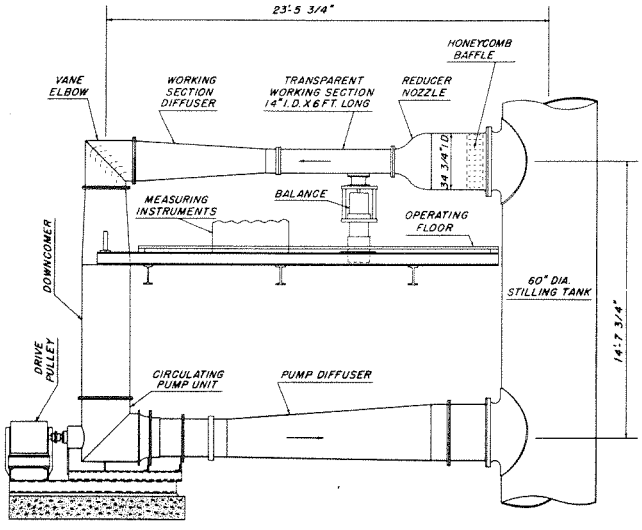

FIGURE A-1

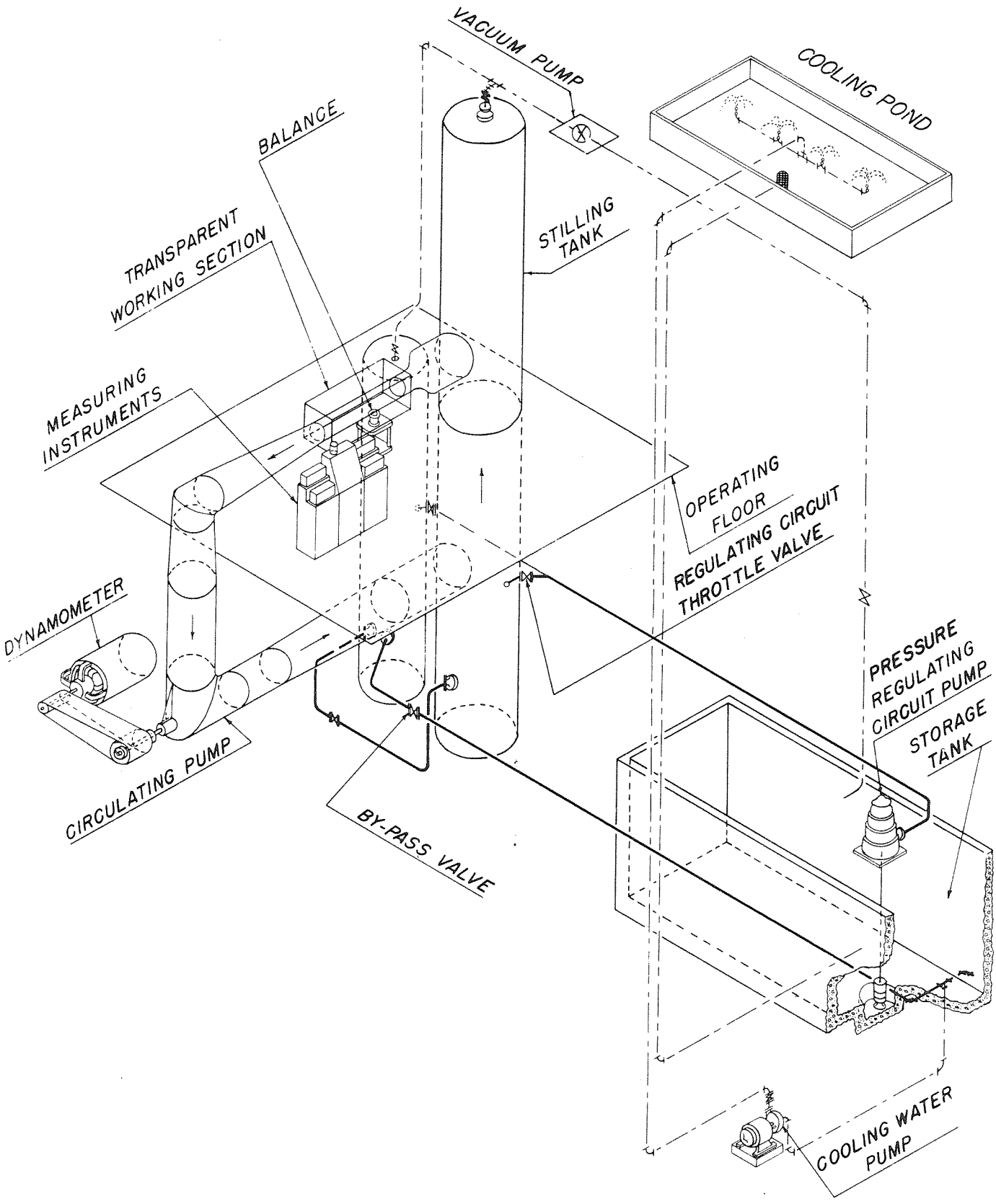
VACUUM PUMP
COOLING POND
BALANCE
TRANSPARENT WORKING SECTION
STILLING TANK
MEASURING INSTRUMENTS
OPERATING FLOOR
REGULATING CIRCUIT THROTTLE VALVE
DYNAMOMETER
PRESSURE REGULATING CIRCUIT PUMP
STORAGE TANK
CIRCULATING PUMP
BY-PASS VALVE
COOLING WATER PUMP

FIGURE A-2

Auxiliary Circuits

Two auxiliary water circuits, one for pressure control and one for temperature control, are used in conjunction with the main circuit. These circuits are shown in Figure A-2, which is an isometric diagram of the complete water tunnel installation.

To make it possible to induce or inhibit cavitation at will, it is necessary that the pressure in the working section be controllable independently of the velocity. This is accomplished by superimposing the pressure regulating circuit on the main circuit. A small flow of water from the sump is forced into the stilling tank by the regulating pump, and is returned to the sump through the by-pass valve. Since the main circuit is closed and completely filled, it is evident that the pressure in it may be controlled by varying the opening of the by-pass valve. A stripping pump (not shown in Figure A-2), in series with the by-pass valve, is used to remove air from the system so as to keep it full of water at all times.

The energy put into the water of the main circuit by the circulating pump (up to 250 HP) is all dissipated in heat. To prevent the temperature of the water from rising to undesirable values, it is necessary to remove this heat by cooling. Part of the water returned through the by-pass valve is picked up by the cooling water pump, circulated through the forced-draft cooling tower on the roof, and returned to the sump. By varying the quantity of water circulated through the cooling system, it is possible to maintain the water in the main circuit at a constant temperature.

Balance

The balance, shown schematically in Figure A-3, is designed to measure three components of the hydrodynamic forces acting on the model. These are the drag force parallel to the flow, the cross force normal to the flow, and the moment around the axis of support. The three forces to be measured are transmitted

hydrostatically to three self-balancing, weighing type pressure gages. These automatic gages, under glass covers, may be seen in Figure A-4, which is a view of the operating floor of the Water Tunnel. The fourth gage shown in this figure is a weighing type manometer used to determine the velocity in the working section by measuring the pressure drop across the reducing nozzle. The gages are responsive to a change in the drag or cross force acting on the model of 0.02 pounds, and a change of 0.04 inch-pounds in the moment.

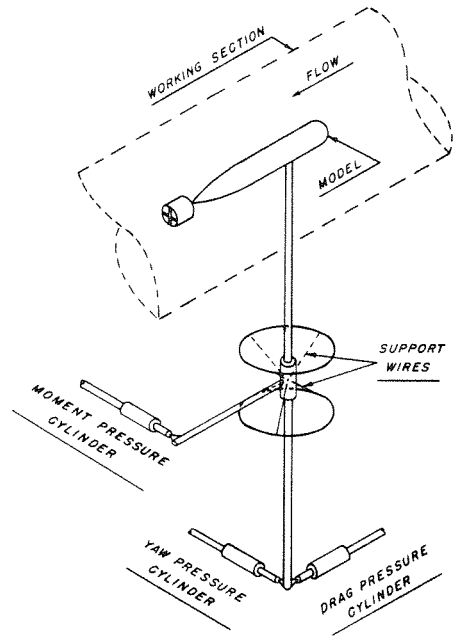

FIGURE A-3

The model is mounted on a shaft which forms the core of the vertical balance spindle shown in Figure A-3. By rotating this shaft within the spindle, it is possible to change the orientation of the model with respect to the direction of flow without altering the direction of the force components measured. Between adjustments, the spindle and shaft are held firmly together by a long, spring-loaded, tapered seat. To change the adjustment, the taper is unseated by an air diaphragm and the shaft is rotated through a worm and gear-sector by a small electric motor (not shown in the figure) mounted on the spindle. A Veeder counter on the worm gear shaft indicates the angle of attack to the nearest 1/10 degree. It should be noted that this whole system forms a part of the spindle assembly, which is pivoted about the point of intersection

of the support wires. Thus it does not affect the force measurements in any way.

To reduce the drag tare to a minimum, the portion of the spindle shaft which projects into the working section is protected from the flow by a streamlined shield which extends to within a few thousandths of an inch of the model.

Polarized Light Flume

The Polarized Light Flume is a separate piece of equipment used for studying the flow around submerged bodies. The fluid circulated is water containing 0.2 per cent by weight of Bentonite in suspension. Bentonite has the asymmetrical optical and physical properties required for the production of streaming double refraction. The flow to be studied is made visible by projecting a beam of light across it through a pair of polaroid plates which are oriented to produce a dark field when there is no flow. The observation section is a rectangular channel 6" wide and 12" deep, having glass sides and bottom.

The velocities used in this flume are necessarily lower than those employed in the High Speed Water Tunnel. However, this difference is not sufficient to affect the validity of the flow patterns observed. A knowledge of these flow patterns is found to be of assistance in the interpretation of the dynamic behavior of the projectiles studies. It is very helpful in investigating interference phenomena, the cause and location of separation or flow instabilities, and the behavior of the boundary layer. Care must be exercised in interpreting the observed patterns, both because the flow is three-dimensional, whereas the observed optical effect is an integration of the entire path of the light beam, and because the pattern produced is a shear pattern and not one of streamlines.

Test Procedures

The facilites of the High Speed Water Tunnel provide for

great flexibility in operation and test procedures. Individual test runs are usually made to determine the effect on the hydrodynamic forces of individual variables, although any of the variables may be changed at will independently of the others.

Constant-velocity tests runs are made to determine the variation of the hydrodynamic forces with changes in the orientation of the projectile with respect to the line of flow. The angle of attack is changed in steps of 1/2 or 1 degree, and the three force components are measured at each step.

To determine the cavitation characteristics of bodies, tests are made during which the pressure is varied while all the other factors are held constant. The inception and development of cavitation may be observed or photographed through the transparent windows of the working section, and the velocities and pressures at which cavitation begins on the various parts of the projectile are measured. Simultaneous measurements of the hydrodynamic forces can be made at any stage in the development.

For the investigation of the noise from cavitating projectiles, two types of sound measurements were made. One objective was to measure the sound pressure of the noise as cavitation developed. For this test the model was mounted in the tunnel and a constant velocity flow was established. A small amount of cavitation was produced by lowering the pressure in the working section and the hydrophone reflector assembly was positioned to give a maximum reading. Then the pressure in the tunnel was raised until cavitation disappeared completely. The water pressure was then reduced again by small steps, and cavitation developed. At each setting, the absolute water pressure and the sound pressure were measured. The water pressure was always reduced when data were taken in order to avoid a hysteresis effect in the formation and disappearance of cavitation which occurs for some conditions.[27] Flash photographs of about a 20 microsecond exposure were taken at each stage of the cavitation. Tests of this type were performed with various velocities, and sound pressure was measured in different frequency bands.

The second objective was to measure the variation in sound pressure along a line parallel to the axis of the tunnel for various degrees of cavitation on the nose, body, or tail of the model. During these experiments, water pressure and velocity were held constant, and the sound pressure was recorded as the hydrophone and sound reflector were moved parallel to the axis of the tunnel. The focused direction was held normal to this axis and, hence, normal to the lucite window of the working section. Tests of this type were performed for various values of water pressure, velocity, and also with different frequency channels.

In addition, in order to measure the background noise, tests of both types were performed without a model or a strut in the working section.

The amplifiers were calibrated before and after each test by introducing a known voltage in series with the hydrophone and measuring the output.

Sound pressure is the term used to describe the acoustic pressure in dynes per square centimeter of the noise produced by cavitation. Values of sound pressure measured by the hydrophone are stated in decibels above the standard reference level of 0.0002 dynes per square centimeter.

By plotting the measured acoustic pressure against the cavitation parameter, K, a semidimensionless representation of results is obtained. At any K along the abscissa, a cavitation zone having a characteristic overall geometry is described regardless of velocity and pressure. The magnitude of the sound pressure shown, however, holds only for the given velocity of test.

APPENDIX II

CORRECTIONS TO TEST DATA

The test data obtained from the water tunnel is in the form of forces and moments which indicate the actual hydrodynamic conditions to which the model is subjected in the tunnel working section. These in general, however, are not the conditions which would exist if the model were moving freely in an infinite body of water. Consequently, in reducing the data to coefficients applicable to the free-stream conditions, the following corrections are considered.

Support Shield Interference

In order to correct for the effects of interference with the flow around the model caused by the supporting spindle and its protecting shield, tests are normally made in pairs, one with and one without a dummy image shield on the side of the model opposite the support. The differences between the coefficients thus obtained from each pair of tests is subtracted from the run made without image shield.

For normal cavitation-free operation this procedure produces results believed to be a good approximation of free stream conditions. With the onset and development of cavitation, however, the shield and its image produce different results depending upon the degree of the cavitation obtained at various values of K. For very low K's the shield itself cavitates. As a result, the corrections determined by the above method vary in magnitude and, without doubt, in accuracy. For the full cavity stage corrections apparently are small. In general, for the material included in this thesis, the normal corrections were applied for all tests which covered the incipient or the early stages of development. For tests which included only the full cavity stage, no corrections were applied.

Tunnel Pressure Gradient

The tunnel pressure gradient correction to be applied to the measured drag for noncavitating or slightly cavitating conditions was evaluated by measuring the pressure gradient existing in the working section of the tunnel in the absence of the model. The pressure gradient dp/dx at each station was multiplied by the cross sectional area of the model at that station and the product was plotted against distance along model. The area under this curve gives

$$\int_0^L s \frac{dp}{dx}\, dx = \int_0^L S\,dp$$

where

S = cross sectional area of model at station where, in the absence of the model, the pressure would be p.

This gives the correction to be subtracted from the measured drag force.

For full cavity conditions the model is in contact with the water only over a small area and no pressure gradient corrections were applied.

Tare Drag

The streamlined shield surrounding the model support spindle reaches to within a few thousandths of an inch of the model. Thus the tare drag on the supporting spindle is reduced to a negligible quantity. Therefore, no tare drag corrections were applied.

APPENDIX III

DEFINITIONS

Pitch Angle

The angle in the vertical plane which the axis of the projectile makes with the direction of travel. Pitch angles are positive (+) when the nose is up, and negative (-) when the nose is down.

Yaw Angle

The angle in the horizontal plane which the axis of the projectile makes with the direction of travel. Looking down on the projectile and in the direction of travel, yaw angles to the right are positive (+), and to the left, negative (-).

Lift

The force, in pounds, exerted on the projectile in a direction normal to the line of travel and in the vertical plane, positive (+) when acting upward, and negative (-) when acting downward.

Cross Force

The force, in pounds, exerted on the projectile in a direction normal to the line of travel and in the horizontal plane. A positive cross force is defined as one acting in the same direction as the displacement of the projectile nose for a positive yaw angle.

Drag

The force, in pounds, exerted on the projectile in a direction parallel with the line of travel. The drag is positive when acting in a direction opposite to the direction of travel.

Moment

The torque tending to rotate the projectile about a transverse axis. A positive or clockwise moment tends to increase a positive

yaw or pitch angle. A moment, therefore, has a destabilizing effect when it has the same sign as the yaw or pitch angle, and a stabilizing effect when of opposite sign.

Coefficients

The force and moment coefficients are defined as follows:

Lift Coefficient, $$C_L = \frac{L}{1/2\ \rho\ V^2\ A}$$

Cross Force Coefficient, $$C_C = \frac{C}{1/2\ \rho\ V^2\ A}$$

Drag Coefficient, $$C_D = \frac{D}{1/2\ \rho\ V^2\ A}$$

Moment Coefficient, $$C_M = \frac{M}{1/2\ \rho\ V^2\ Al}$$

where

L = lift force, pounds

C = cross force, pounds

D = drag force, pounds

M = moment, foot-pounds

ρ = density of water, slugs per cu. ft.

V = velocity, feet per second

A = area of a cross section tak en normal to the longitudinal axis of the projectile at its maximum diameter, square feet

l = overall length of projectile, feet

Reynolds Number $$R_e = \frac{Vl\rho}{\mu} = \frac{Vl}{\nu}$$

where

V, l, and ρ are as defined above, and

μ = absolute viscosity of water, pound-second per square foot

$\nu = \frac{\mu}{\rho}$ = kinematic viscosity of water, square feet per second

Cavitation Parameter $K = \dfrac{P_o - P_B}{1/2\ \rho\ V^2}$

where

ρ and V are as defined above, and

P_o = absolute pressure in undisturbed water, pounds per square foot

P_B = pressure in the cavitation bubble (usually taken as the vapor pressure of the water), pounds per square foot

APPENDIX IV

BIBLIOGRAPHY

(1) "The High Speed Water Tunnel at the California Institute of Technology," by R. T. Knapp, V. A. Vanoni, and J. W. Daily, HML Report ND-1, June 29, 1942 (Confidential)

(2) "Measurements of Forces on Projectiles Enveloped in Cavitation Cavities," by James W. Daily, Proceedings of the Second Conference on Underwater Ballistics, January 29-31, 1945, P. 45 (Confidential)

(3) "Cavitation Noise from Underwater Projectiles," by James W. Daily and Howard Baller, HML Report No. ND-26, Section No. 6.1-sr207-1910, March 20, 1945 (Confidential)

(4) "The Tension Which Water Can Exert on a Steel Surface," by R. M. Davies, The Engineering Laboratory, Cambridge, December, 1944

(5) "Cavitation et Tension Superficielle" by F. K. Th.Van Iterson, Proceedings of the Royal Academy of Science, Amsterdam, Vol. 39, 1936

(6) "Concerning the Inception of Cavitation with Particular Reference to the Air Content of the Water", (German) by F. Numachi, Report of the Tokohu Imperial University, Vol. XII, No. 3, 1937

(7) "Experimentale und Theoretische Untersuchungen uber Hohlraumbildung im Wasser," by J. Ackeret, Report of the Kaiser Wilhelm Institute fur Stromungsforschung, Gottingen, January, 1930, Techn., Mechan., und Thermodynamik, pp 1-22, Vol. I

(8) "Hydrodynamics," by Horace Lamb, Sixth Edition, Cambridge University Press, 1932

(9) "Fluid Mechanics for Hydraulic Engineers," by Hunter Rouse, McGraw-Hill, 1938

(10) "Vorlesungen uber Mechanik," by G. Kirchhoff, 1876, p. 186

(11) "Pressure Distribution Measurements on the Mk 13-1, Mk 13-2, and Mk 13-2A Torpedoes," by R. T. Knapp and Joseph Levy, HML Rep. ND-15.3, Section No. 6.1-sr207-1643, June 23, 1944 (Confidential)

(12) Unpublished Pressure Distribution Measurements on the Mk 14 Torpedo in the High Speed Water Tunnel

(13) "Cavitation Tests on a Systematic Series of Torpedo Heads," by Hunter Rouse, J. S. McNown, and En-Yun-Hsu, a series of confidential reports numbered as follows:

Report No. 6.1-sr1353-2191, Feb. 28, 1945, Hemisphere
Report No. 6.1-sr1353-2192, Mar. 5, 1945, Blunt Head
Report No. 6.1-sr1353-2195, Mar. 20, 1945, 1 cal. Ogival Head
Report No. 6.1-sr1353-2196, Mar. 26, 1945, 2 cal. Ogival Head

(14) "Entrance and Cavitation Bubbles," by R. T. Knapp, HML Rep. No. ND-36, Section No. 6.1-sr207-1900, Dec. 27, 1944 (Confidential)

(15) "Nose Cavitation - Ogives and Spherogives," by R. T. Knapp and H. L. Doolittle, HML Rep. ND-31.1, Section No. 6.1-sr207-1906, January 18, 1945 (Confidential)

(16) "Force and Cavitation Characteristics of the NACA 4412 Hydrofoil," by R. T. Knapp and James W. Daily, HML Rep. ND-19, Section No. 6.1-sr207-1273, June 10, 1944 (Restricted)

(17) "Calculated and Measured Pressure Distributions over the Midspan Section of the NACA 4412 Airfoil," by R. M. Pinkerton, NACA, T.R., No. 586, 1936

(18) "Modern Developments in Fluid Mechanics", Vols. I and II, edited by S. Goldstein, Oxford University Press, 1938

(19) "Aerodynamic Theory," Vol. I to VI, edited by W. F. Durand, Julius Springer (Berlin), 1934

(20) "Applied Hydro- and Aeromechanics" by L. Prandtl and O. G. Tietjens, McGraw-Hill, 1934

(21) "Flow Diagrams of Projectile Components" by Garrett Van Pelt and Elizabeth A. Thorne, HML Rep. No. ND-36, Section No. 6.1-sr207-1649, September 15, 1945 (Confidential)

(22) "Centrifugal Pump Performance as Affected by Design Features," by R. T. Knapp, Trans. A.S.M.E., Vol 63, 1941, -- 251-260

(23) "Experimental Investigations of Design and Operating Features of Centrifugal Pumps with Reference to the Grand Coulee Irrigation Project," Part II, a report submitted by the Hydraulic Machinery Laboratory to the U. S. Bureau of Reclamation, 1942

(24) "Further Experiments on the Flow Around a Circular Cylinder," by A. Fage and V. M. Falkner, ARC Reports and Memoranda No. 1369, February, 1931

(25) "An Investigation of Fluid Flow in Two Dimensions," by A. Thom, A.R.C. Reports and Memoranda No. 1194, Nov. 1928

(26) "Underwater Trajectories and Ricochet Tendencies of Rockets," by I. S. Bowen, Proceedings of the Second Conference on Underwater Ballistics, January 29-31, p 39 (Confidential)

(27) "Measurements of the High Frequency Noise Produced by Cavitating Projectiles in the High Speed Water Tunnel," by R. T. Knapp, HML Report ND-8.2, Section No. 6.1-sr207-924, August 31, 1943

(28) "Measurements on a C11-A1 Hydrophone with an Ellipsoidal and a Spherical Reflector", a report prepared by the Calibration Group of the University of California Division of War Research, October 10, 1944, UCDWR No. C64